BEHAVIOUR OF CONTINUOUS CONCRETE BEAMS REINFORCED WITH HYBRID GFRP/STEEL BARS

A. M. A. A. ARABA

Submitted for the Degree of

Doctor of Philosophy

Faculty of Engineering and Informatics

University of Bradford

2017

PAPERS PRODUCED FROM THIS THESIS

1. A. Araba, A. F. Ashour and D. Lam ‘‘Hybrid GFRP-Steel Continuous Concrete Beams’’, Structural Faults & Repair Conference, 17th-19th May 2016, Edinburgh, Scotland.

2. Almahdi. M. Araba, A. F. Ashour and D. Lam ‘‘Flexural Performance of Hybrid GFRP-Steel Reinforced Concrete Continuous Beams’’, submitted for publication in the Composites for Construction, ASCE.

ABSTRACT

BEHAVIOUR OF CONTINUOUS CONCRETE BEAMS REINFORCED WITH HYBRID GFRP/STEEL BARS

ALMAHDI ARABA

University of Bradford, 2017

Keywords: Continuous members, Hybrid Reinforcement, GFRP Bars, Ductility, Moment redistribution.

An investigation on the application of hybrid glass fibre reinforced polymer (GFRP) and steel bars bars as longitudinal reinforcement for simple and continuous concrete beams is presented. Three simply and eleven multi-spans continuous reinforced concrete beams were constructed and tested to failure. Nine continuous and two simply supported beams were reinforced with a hybrid combination of both GFRP and steel re-bars at mid spans and internal support regions. In addition, two continuous concrete beams reinforced with either GFRP or steel bars and one simply supported beam reinforced with GFRP bars were tested as control beams. The beams were classified into two groups according to the reinforcement configurations. All specimens tested were 200 mm in width and 300 mm in depth. The continuous beams comprised of two equal spans, each of 2600 mm, while the simply supported beams had a span of 2600 mm.

Unlike GFRP reinforced concrete beams, the hybrid and steel reinforced concrete beams failed in a favourable ductile manner and demonstrated narrow cracks and smaller deflections compared to the GFRP-reinforced control beam. The lower stiffness and higher deflection of GFRP reinforced concrete beams can be controlled and improved by the use of steel reinforcement in combination with GFRP re-bars. However, the ratio of GFRP to steel reinforcement is a key factor to ensure sufficient ductility and stiffness beyond the first cracking stage. The experimental results showed that the extent of moment redistribution in hybrid reinforced continuous beams depends mainly on the amount of hybrid reinforcement ratio in critical sections. Similar area of steel and GFRP bars in critical sections leads to limited moment redistribution whereas different amount of steel and FRP bars in critical sections leads to a remarkable moment redistribution.

Design guidelines and formulas have been validated against experimental results of hybrid GFRP/steel reinforced concrete beams tested. The Yoon's equation reasonably predicted the deflections of the hybrid beams tested whereas Qu's model which is based on ACI 440.1R-15 underestimated the deflections of hybrid beams tested at all stage of loading after cracking. The ACI 440.2R-08 and Pang et al., (2015) equations reasonably predicted the sagging failure moment in most continuous hybrid reinforced concrete beams, whereas they underestimated the hogging flexural strength at failure of most hybrid continuous beams. On the other hand, the formulas proposed by Yinghao et al., (2013) was very conservative in predicting the failure moment at the critical sagging and hogging sections.

On the analytical side, a numerical technique consisting of sectional analyses has been developed to predict the moment–curvature relationship and moment capacity of hybrid FRP/ steel reinforced concrete members. The numerical technique has been validated against the experimental test results obtained from the current research and those reported in the literature. In addition, a two-dimensional nonlinear finite element model was proposed using ABAQUS package. The proposed model was validated against the experimental results of the beams tested in the present research.

DECLARATION

I hereby declare that this thesis entitled “Behaviour of Continuous Concrete Beams Reinforced with Hybrid GFRP/Steel Bars” is the result of my own work except where references have been made to the work related to others. This thesis has not been submitted anywhere for the application of another degree, diploma, or other qualification.

Almahdi Araba

DEDICATION

To My Late Father

Mohamed Abuham Araba**,** who died on 23 September 2017

I miss you every moment

ACKNOWLEDGEMENTS

All thanks are due to the Almighty ***ALLAH***, the Most-Gracious, and the Most-Merciful. Without his guidance and help, I would not be able to complete this work.

I would like to express my sincere appreciation and indebtedness to my supervisors **Prof. Ashraf Ashour and Prof. Dennis Lam** for their excellent supervision, constant encouragement and approachability throughout the period of this work. I deeply appreciate **Prof. Ashour** for his great support and help, especially throughout the difficult time course of the fighting in my country, Libya.

Special thanks go to the **Laboratory staff** who were always ready to help in times of needs. I would like to particularly thank **Steve Robinson**, **Owen Baines** and **Michael Procter** for their expert advice and help during the experimental investigation.

I am forever deeply grateful to **my late father.** He and **my mother** have given all my academic endeavours unwavering encouragement and in the pursuit of my study this support substantially contributed to its completion.

My great gratitude and my sincere thanks are to be dedicated towards **my wife and my son Mohamed, my daughter Mabrouka, my brothers and sisters** and all **my relatives** who supported me during the completion of this work.

I take the chance to thank and express my gratitude to all **my friends** for their encouragement, advice and understanding.

I do appreciate the grant and financial support provided by the Higher Education Institute in the **Libyan Government** needed to finish this research.

Finally, I would like to thank everybody who was involved in this work as well as expressing my apology to those I did not mention in this acknowledgment.

TABLE OF CONTENTS

LIST OF FIGURES

LIST OF TABLES

NOTATIONS

The following symbols are used in the present thesis:

a	The depth of each concrete segment in compression or tension
A_f	The area of tensile FRP reinforcement
A'_f	The area of compressive FRP reinforcements
A_s	The area of tensile steel reinforcement
A'_s	the area of compressive steel reinforcements
A_v	Shear reinforcement
b	Width of concrete beam
C_c	The total compressive forces in the concrete
C_{ci}	The compressive forces in segment i
C_{tj}	The tensile forces in segment j
d	Distance from extreme compression fibre to the centroid of the tension reinforcing zone
d_f	The bottom FRP reinforcement depth
d_s	The bottom steel reinforcement depth
d'_f	The top FRP reinforcement depth
d'_s	The top steel reinforcement depth
E_c	The elasticity modulus of concrete
E_{ela}	The elastic energy
E_f	The elasticity modulus of FRP
E_s	The elasticity modulus of steel
E_{tot}	The total energy
f_c	The stress in compressive concrete

f_c'	The cylinder compressive strength of concrete
f_{ci}	The concrete compressive stress in element number i
f_{cr}	Modulus of rupture of concrete
f_f	The stress of the FRP reinforcement.
f_f'	The stresses in compressive FRP bars
f_{fu}	The rupture tensile strength of the FRP reinforcement.
f_r	The ultimate tensile strength and corresponding tensile strain of concrete
f_s	The stress of the steel reinforcement.
f_s'	The stresses in compressive steel bars
f_t	The tensile stress in concrete
f_{tj}	The concrete tensile stress in element number j
f_y	The yield stress of the steel reinforcement.
h	Overall height of concrete beam
h_o	The tensile steel bars depth
h_1	The tensile FRP bars depth
I_{cr}	Moment of inertia of transformed crack section;
I_e	The effective moment of inertia
I_g	Gross moment of inertia
I_y	The moment of inertia after steel yields
K_C	the ratio of the second stress invariant on the tensile meridian to that on the compressive meridian
L	The span length
L_{ci}	The lever arm for the concrete compressive forces in segment i
L_{tj}	The lever arm for the concrete tensile forces in segment j

M	The bending moment
M_a	Maximum moment in the member at the current phase of deflection
M_{cr}	Cracking moment
M_e	The bending moment obtained from elastic analysis
M_m	The bending moment obtained from experiment
M_{pre}	The predicted ultimate moment
M_u	The section moment capacity
M_{us}	The moment capacity at mid span section at failure
M_{uh}	The moment capacity at middle support section at failure
M_y	The steel yielding moment
n_c	The number of concrete elements in compression
n_f	The modular ratio between the FRP reinforcement and the concrete
n_s	Elastic modulus ratio between steel reinforcement and concrete
n_t	The number of concrete elements in tension
P_{pre}	The predicted flexural load capacity at failure
Q	The summation of the internal forces
S	Spacing of shear reinforcement
T_c	The total tensile forces in the concrete
T_f	The forces of bottom FRP bars
T_S	The forces of bottom steel bars
T_f'	The forces of top FRP bars
T_s'	The forces of top steel bars
V_c	Shear strength of concrete
V_s	Shear strength of steel

V_{pred}	Predicted shear capacity
x	The value of the neutral axis depth
x_{ci}	The distance between the neutral axis and the mid depth of i segment
x_{tj}	The distance between the neutral axis and the mid depth of j segment
β	the amount moment redistribution ratio
β_1	The strength reduction factor
β_d	An empirical correction factor
γ	a factor which accounts for the length of the un-cracked regions of the member and for the change in stiffness in the cracked regions
γ_c	Partial factor for concrete
γ_s	Partial factor for steel
ϵ	Eccentricity
Δ	The immediate deflection
Δ_y	The mid span deflection at the second change in in slope caused by yielding of tensile steel
ε_c	The strain in compressive concrete
ε_{ci}	The concrete compressive at mid depth of i segment
ε_{co}	The strain of concrete corresponding to maximum stress
ε_{cu}	The ultimate strain of concrete
ε_f	The strain of the FRP reinforcement.
ε_f'	The strain in the top FRP bars
ε_{fu}	The rupture strain of the FRP reinforcement.
ε_r	The tensile strain of concrete corresponding to the ultimate tensile strength
ε_s	The strain of the steel reinforcement.
ε_s'	The strain in the top steel bars

ε_t	The tensile strain in concrete
ε_{tj}	The concrete tensile strain at mid depth of j segment
ε_y	The yield strain of the steel reinforcement.
ξ_n	The distance from the top of the beam to the neutral axis
θ	angle of inclination of the principal diagonal compressive stresses to the longitudinal axis of a member
μ	Viscosity parameter
$\mu_{\Delta 1}$	The deflection ductility index
$\mu_{\Delta 2}$	The displacement ratio
μ_{en}	The ductility index
υ	A strength reduction Factor for concrete cracked
ρ_{eff1}	The effective reinforcement ratio (FRP transformed into steel)
ρ_{eff2}	The effective reinforcement ratio (steel transformed into FRP)
$\rho_{\text{eff,b1}}$	The balanced reinforcement ratio of FRP concrete section
$\rho_{\text{eff,b2}}$	The balanced reinforcement ratio of RC section
ρ_f	The tensile FRP reinforcement ratio
ρ_s	The tensile steel reinforcement ratio
ρ_{sw}	Shear reinforcement ratio
σ_{bo}	the initial equi-biaxial compressive yield stress
σ_{co}	The initial uniaxial compressive yield stress
σ_{max}	The maximum principal stress
$\emptyset_c$	Resistance factor for concrete
$\emptyset_S$	Resistance factor for reinforcing bar
φ	The corresponding curvature

Ψ	Dilation angle

ABBREVIATIONS

The following abbreviations are used in the present thesis:

FE	Finite element
FRP	Fibre reinforced polymer
GFRP	Glass fibre reinforced polymer
RC	Reinforced concrete

CHAPTER ONE

INTRODUCTION

1.1 Background

Deterioration, reduced serviceability and failure of concrete structures reinforced with steel bars are inevitably the most common consequences of corrosion of steel reinforcement. Hence, this phenomenon has become a major concern in the construction industry due to a substantial increase of maintenance and repair costs. The use of fibre reinforced polymer (FRP) as an alternative reinforcement in concrete structures has emerged as an innovative solution owing to their non-corrosive and non-magnetic properties, making them an ideal reinforcement for severe environments and situations where magnetic transparency is required. However, due to the low modulus of elasticity of FRP, there is a noticeable reduction in the flexural stiffness of concrete members reinforced with FRP bars. This reduction occurs after cracking, which in return, causes a substantial increase in deformation under service conditions (ACI 440.1R-15).

Moreover, due to the linear-elastic behavior of FRP composite materials up to rupture, continuous concrete beams reinforced with FRP rebars generally exhibit less ability to redistribute stresses between critical sections compared to those reinforced with steel rebars (Habeeb and Ashour, 2008; Mahroug et al., 2014a; Mahroug et al., 2014b). As a result, a sudden failure is expected to occur with little or no warning. Therefore, there is a need for a new method of construction to avoid such problems; that is durable, cost effective, and exhibits some ductility. A number of methods have been suggested to improve

ductility, including hybridization of different types of fibrous material (Nanni et al., 1994; Tepfers et al., 1996; Somboonsong et al., 1998; Harris et al., 1998) and combining steel reinforcement with composite materials to make a rebar with an inner steel and an outer FRP (Saikia et al., 2005, Cheung and Tsang, 2010; Cui et al., 2008; Etman, 2010; Behnam and Eamon, 2013).These attempts were not practical to be implemented in the construction industry due to the high cost and complexity of manufacturing process. More practical solutions have been suggested such as; confinement of concrete in compression zone (Zhou et al., 2009), addition of fibres to concrete (Alsayed and Alhozaimy, 1999; Li and Wang, 2002; Wang and Belarbi, 2011) and use of a hybrid combination of FRP and steel re-bars (El Refai et al., 2015). Such hybrid reinforcement system shows improved serviceability and ductility, and enhancement of load-carrying capacity compared to traditional reinforcement (Aiello and Ombres. 2002; and Qu et al. 2009).

The research presented in this thesis highlights the structural performance of multi-span continuous concrete beams reinforced with hybrid GFRP/steel reinforcement. Thus, the knowledge gained from the experiments and the failure process in the continuous specimens are vital in order to add information which fundamentally benefits both the researchers and engineers.

1.2 Research significance

The hybrid combination of FRP and steel reinforcement was recently introduced in concrete structures to overcome the shortcomings of the individual use of a single type of reinforcement. In this hybrid reinforcement system, FRP rebars are placed near the outer surface of the tensile zone with a small cover thickness whereas steel bars are placed with relatively larger

concrete cover, achieving a better protection against corrosion. On the other hand, the brittle nature and low modulus of elasticity of FRP reinforcement can be compensated by the presence of steel bars that can enhance the structural performance in terms of crack width, deformability and ductility.

The literature shows testing of simply supported beams reinforced with hybrid FRP and steel reinforcement but none of the previous investigations was conducted on multi-span continuous hybrid reinforced concrete beams. However, the majority of concrete structures in practice are continuous members that behave differently from simply supported ones. For instance, it is not possible to investigate the ductility and consequent moment redistribution characteristics, changes in beam curvature from sagging to hogging and the actual combination of shear and flexure over supports in simply supported beams. The current research presents the first experimental study on continuous concrete beams reinforced with hybrid FRP and steel reinforcement. The test results show how brittle failure of continuous concrete beams reinforced with FRP bars could be avoided and a more ductile behaviour can be achieved. The test results would contribute to future development of design guidelines for continuous concrete beams reinforced with hybrid GFRP-steel bars.

1.3 Aims and Objectives Of the Research

This research aims to study in depth the behavior of multi-span continuous concrete beams reinforced with a hybrid combination of steel and GFRP bars. More specifically, the objectives of this research are:

- To experimentally study the structural behaviour of the simply and multi-span continuous hybrid reinforced concrete beams in comparison with concrete beams reinforced with either GFRP or steel bars.
- To develop an analytical technique for predicting the moment capacity and moment-curvature relationship of concrete sections reinforced with hybrid reinforcement.
- To study the extent of moment-redistribution in continuous concrete beams reinforced with hybrid reinforcement.
- To examine the applicability of the design guidelines available for FRP concrete structures and developed equations for hybrid sections against the experimental results of multi-span continuous hybrid GFRP/steel beams.
- To develop a two-dimensional nonlinear finite element model using ABAQUS to analyse the behaviour of continuous concrete beams reinforced with hybrid reinforcement and conduct a series of parametric studies. The proposed model will be evaluated against the present experimental results.

1.4 Research Methodology

To achieve the aims and objectives of this research, the following research strategy approaches have been employed:

- Nine continuously and two simply supported beams reinforced with a hybrid combination of both GFRP and steel re-bars at mid spans and internal support regions were constructed and tested to study various parameters such as the amount and configuration of longitudinal

reinforcement on the behaviour of hybrid continuous concrete beams including cracking load, load carrying capacity, strains in reinforcement, deflections and moment redistribution.

- The design methods proposed by researchers for the moment capacity and deflection of concrete sections reinforced with hybrid FRP/steel bars were assessed against the experimental results of simply and multi-span continuous hybrid beams.
- A sectional analysis technique was proposed for estimating the moment-curvature relationship and the flexural strength of sections reinforced with hybrid FRP-steel re-bars. The technique has been developed from the strain compatibility and equilibrium of forces. The moment capacities obtained by the developed technique have been compared with the experimental results obtained from the simply supported tested beams in this research and other researches.
- A two-dimensional nonlinear finite element model using ABAQUS software has been developed to analyse the effect of different parameters considered in this research on the behaviour of hybrid continuous concrete beams and conduct a series of parametric studies to explore the structural behaviour of multi-span continuous beams reinforced with hybrid FRP/steel bars with extended parameter variations, both within and outside the range of experiments.

1.5 Report Arrangement

This chapter presents a general introduction about the necessity to overcome the lack of ductility of FRP structures and serviceability governed design. It also summarizes the importance as well as the main aim and objectives of the

research. Chapter two presents the literature review investigating previous research on simply and continuously beams reinforced with FRP bars. Moreover, the literature review presents different methods used to overcome the drawback of using FRP as internal reinforcement for simple and continuous concrete beams. It also includes a general overview of the developed equations for predicting the moment capacity and deflection of concrete sections reinforced with hybrid FRP/steel bars.

The experimental program is described in chapter three. In this chapter, the cross-section dimensions and details of a total of eleven continuous concrete beams along with three simply supported beams reinforced with either GFRP bars, steel bars or hybrid GFRP/steel bars are described. Also, the reinforcement details for each beam are illustrated. Moreover, the properties of the used materials, details of instrumentations, test setup and procedure are provided in this chapter.

Chapter four presents the experimental results of simply and multi-span continuous beams reinforced with either GFRP bars, steel bars or hybrid GFRP/steel bars.

Chapter five presents the sectional analysis used in developed computer programmed for analyzing and predicting the behavior of simply and multi-span continuous reinforced concrete beams with hybrid FRP and steel bars. The mode of failure, ultimate moment capacity, and moment-curvature relationship along the length of beam can be predicted by means of the computer programme.

The main aim of chapter six is to evaluate the use of design codes of practice as well as the formulas suggested by researchers for moment capacity, deflections; and ductility of hybrid beams against the experimental results of simply and multi-span continuous hybrid GFRP-steel reinforced concrete beams tested.

A two-dimensional nonlinear finite element model using ABAQUS software is proposed in chapter seven to analyse the behaviour of continuous concrete beams reinforced with a hybrid combination of FRP and steel bars. The finite element model is verified using the experimental results of the current study.

Finally, chapter eight introduces the main conclusions of this research and presents recommendations and suggestions for future work.

CHAPTER TWO

LITERATURE REVIEW

2.1 Introduction

Reinforced concrete with steel reinforcement has performed well from structural and economic points of view except where structural members have been exposed to severe environmental conditions. Therefore, an ongoing basis maintenance and repair due to the corrosion of reinforcing steel are essential to extend the building life longer. The costly maintenance of structure members, generally, has raised the necessity to develop new materials to overcome the degradation of structures.

Fibre reinforced polymer (FRP) which mainly used in aerospace industry has appeared as a promise alternative to replace steel rebars due to the nature of the materials used in its fabrication. Their innovative properties such as, corrosion resistance, high tensile strength to weight ratio and electromagnetic transparency are the main attractive characteristics to construction industry and structural engineers specifically. In spite of these attractive features, the limit use of FRP in buildings and civil infrastructure has been noticeable. Achievement of ductility in FRP reinforced concrete structures, and consequently achievement of redistribution of stresses and moments in indeterminate concrete structures reinforced with FRP, requires further investigation because FRP materials are essentially linear elastic up to failure and thus lack ductility. In the other words, FRP reinforced concrete beams hardly exhibit any nonlinear moment-curvature response. Therefore, they fail without providing sufficient indication of impending failure and it is generally

believed that they lack the ability for any redistribution of stresses and moments.

The literature survey presented in this chapter will be divided into two main parts. The first part will describe the previous studies carried out on simply and multi-span continuous concrete members reinforced with FRP bars. The second part will focus on proposals suggested to overcome the lack of ductility and stresses redistribution between critical sections in concrete structures reinforced with FRP bars.

2.2 Historical Development and Use of FRP Composites in Construction Industry

Advanced polymer composite (APC) that referred to as fibre reinforced polymer (FRP) in civil engineering were mainly developed for aerospace industry. Due to the attractive engineering properties, the use of FRP in construction industry commenced during World War II to erect the Radomes to house electronic radar equipment (Hollaway, 2003). Their potential for use in reinforced concrete applications, however, was not fully recognized until the 1960's. Two FRP structures, a sandwich polymer composite skeletal dome structure and an all polymer composite roof structure were manufactured in the UK and shipped to Benghazi, Libya and Dubai, UAE in 1968 and 1972 respectively (Hollaway, 2003). Recently, FRP rebars started to become popular in bridge construction (Figure 2.1). In fact, in many countries, such as the United Kingdom, Germany, Canada and Switzerland, FRP reinforcement has been adopted for bridge deck construction.

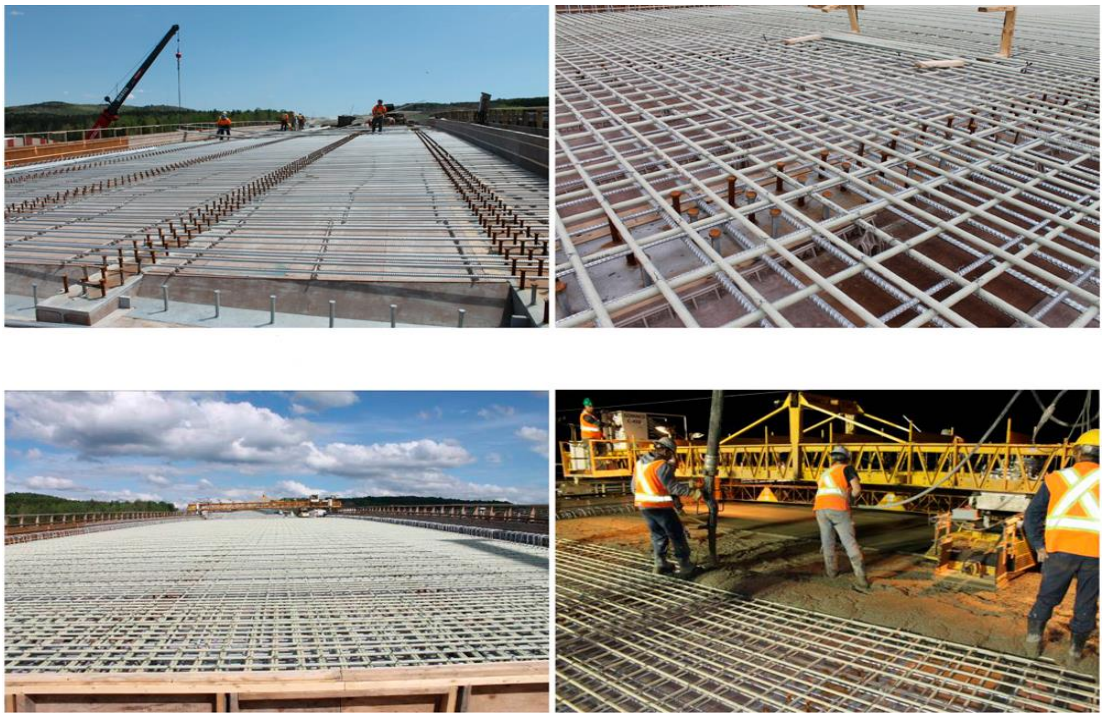

Figure 2.1 A recent application of GFRP bars in a bridge deck slab (Ahmed et al. 2014)

2.3 FRP as Internal Reinforcement

Many types of fibre-reinforced polymers such as, Glass, Aramid, Carbon and Basalt have been used as internal reinforcement for concrete structures. Figure 2.2 shows different types of FRP bars with various sizes, surface textures from different types of materials. FRP rebars, due to their non-corrodible nature, offers great performance in reinforced concrete construction under conditions in which conventional steel-reinforced concrete has yielded unacceptable service. Moreover, in structures supporting magnetic resonance imaging (MRI) units such as hospitals or other equipment sensitive to electromagnetic fields such as research laboratories the non-magnetic nature of FRP bars are unrivalled (Nanni et al., 2014).

Figure 2.2 Different types and sizes of FRP bars

2.3.1 Flexural Capacity and Modes of Failure

The behavior of FRP reinforced beams is different from that of reinforced with conventional steel reinforcement. The non-ductile behavior of FRP rebars due to linear stress-strain up to failure would form two modes of failure; either due to crushing (compression failure) of concrete or rupture (tension failure) of FRP reinforcement. The first one is more desirable as it gives some warning before failure while the latter should be avoided as the failure is sudden and catastrophic (ACI 440.1R-15). Several experimental and analytical studies (Theriault and Benmokrane, 1998; Vijay and GangaRao, 2001; Kara and Ashour, 2012; Mahroug et al., 2014) have been performed to understand the flexural behavior of concrete beams reinforced with FRP bars.

The nature of failure of the concrete member that is reinforced with FRP bars is much dependent on the FRP reinforcement ratio. Therefore, the effect of reinforcement ratio on the flexural behavior of simply and multi-span continuous concrete beams reinforced with FRP rebars has been investigated by many researchers (Theriault and Benmokrane, 1998; Vijay and GangaRao, 2001; Habeeb and Ashour ,2008; Ashour and Habeeb ,2008; Kassem et al.,

2011; Mahroug et al., 2014a and Mahroug et al., 2014b). Their tests showed that as reinforcement ratio increases, the ultimate moment capacity of concrete beams increases. However, this increase is limited by the concrete compressive failure strain of over-reinforced concrete beams (Theriault and Benmokrane, 1998). In addition, moment increase was not proportional to the increase in reinforcement percentage beyond a c/d ratio of 0.3 (Vijay and GangaRao, 2001). Habeeb and Ashour (2008) and Ashour and Habeeb (2008), reported that over-reinforcing the bottom layer of either the simply or multi-span continuous GFRP beams is a key factor in enhancing the load capacity of concrete beams.

Kassem et al., (2011) concluded that reinforcement ratio should be more than 1.4 of balanced reinforcement ratio to ensure compression failure which in agreement with ACI 440.1R-06.

Comparisons between the experimental results and those obtained from simplified methods proposed by the ACI 440 Committee show that ACI 440.1R-06 equations can reasonably estimate the load capacity of GFRP reinforced concrete beams under test (Habeeb and Ashour, 2008). Whereas Issa et al. (2011) indicated that ACI 440.1R-06 strongly underestimated the moment capacities of FRP RC beams.

The reinforcement ratio along the beam length might be different in the continuous concrete beams. In more recent study conducted by Mahroug et al., (2014a) to study the flexural behavior of continuous concrete slabs reinforced with CFRP. They observed from this study that increasing the bottom mid-span CFRP reinforcement of continuous slabs is more effective than the top over middle support CFRP reinforcement in improving the load

capacity. In general, a minimum practical reinforcement amount have to be maintained due to the sharp increase in reinforcement strains at cracking of over 3000 me (El-Nemr et al., 2013).

It is well known that concrete is a brittle material and raising its strength makes concrete even more brittle. Theriault and Benmokrane, (1998) concluded that the stiffness of the beam did not change much with the concrete strength, which means a slight reduction in deflection will occur. In addition, they found that as the concrete strength increases, the ultimate moment resistance increases, but this increase is limited by the concrete compressive failure strain. El-Nemr et al., (2013) concluded that using high strength concrete increased the cracking moment of the GFRP-RC beams compared to the normal strength concrete beams.

Kara and Ashour, (2012) proposed a numerical technique for estimating moment capacity of FRP reinforced concrete beams. Comparisons between the predicted resistance moments and experimental results show very good agreement.

2.3.2 Shear Capacity of FRP Reinforced Concrete Beams

The design of FRP reinforced concrete members for shear is generally more complicated than the flexural behavior. The applied shear stress could be resisted by a number of mechanisms; shear resistance in un-cracked compression concrete zone, aggregate interlock, dowel action of longitudinal reinforcement and residual tensile strength across the inclined crack as shown in Figure 2.3. However, to find out which mechanism of shear transfer will

contribute most to the shear resistance of the structural element is a complex issue.

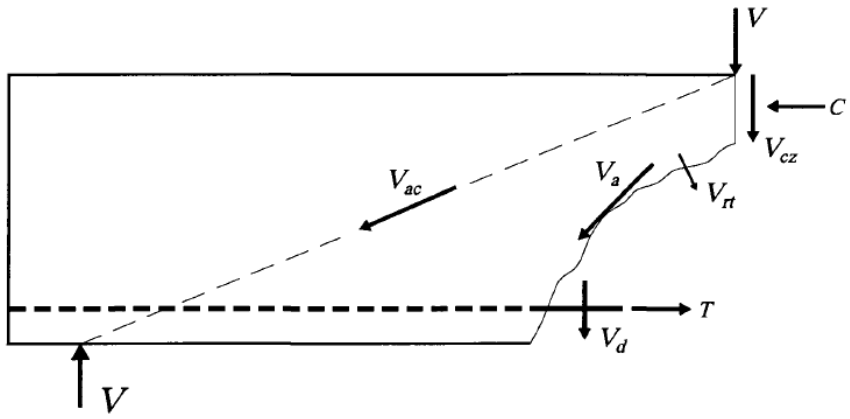

V_{cz}: Shear resisted y uncracked concrete
V_a : Shear transferred by aggregage interlock
V_d : Dowel action
V_{rt} : Residual tensile stresses across the crack
V_{ac}: Arch action (in deep members)

Figure 2.3 Shear transfer actions contributing to shear resistance

For equal amounts of flexural reinforcement, the lower modulus of elasticity of FRP results in a lower longitudinal FRP reinforcement stiffness than steel bars. In a flexural member reinforced with FRP bars, flexural cracks will penetrate deeper into the section, and wider cracks will form when compared to member reinforced with steel bars (with equal amount of tensile reinforcement). Deeper flexural cracks decrease the depth of the compression zone, thereby reducing the contribution of the un-cracked concrete to the shear strength. Wider cracks on the other hand, may result in reduction in the shear strength contribution for the aggregate interlock as well as from the residual tensile stresses. Additionally the relatively small transverse strength of FRP bars coupled with increased crack widths may result in the negligible effect of the dowel action. Eventually, the overall shear capacity of concrete members reinforced with

FRP bars as flexural reinforcement is lower than that the shear capacity of the concrete members with steel bars (with the same amount of reinforcement) (ACI 440.1R-15).

Many structural concrete members are constructed without transverse reinforcement such as slabs, footings, retaining walls and lightly stressed members. Ashour, (2006) reported test results of 12 simply supported rectangular-section concrete beams reinforced for flexure with GFRP bars and without shear reinforcement. Two modes of failure were observed, namely flexure and shear failure. The first mode of failure was mainly due the rupture of GFRP bars while the shear failure was initiated by a major diagonal crack within the beam shear span. In addition, the study presented a simplified method to estimate the shear capacity of a concrete section provided by the concrete without shear reinforcement.

In another study, El-Sayed et al., (2006) investigated the effect of shear strength of FRP reinforced concrete beams without transverse reinforcement. Three beams reinforced with glass FRP bars, three reinforced with carbon FRP bars, and three beams reinforced with conventional steel bars. All beams were tested in four-point bending. The test variables were the reinforcement ratio and the modulus of elasticity of the longitudinal reinforcing bars. The test results of this study revealed that the higher the reinforcement ratio or the modulus of elasticity of the reinforcing bars, the higher the obtained shear strength.

FRP can be moulded into different stirrup shapes similar to traditional steel stirrups. However, due to the difference in properties, FRP cannot be directly substituted for steel stirrups in design. Compared to steel, several issues need

to be taken into consideration in design of members reinforced with FRP for flexure and shear such as; bars have a lower dowel resistance; lower modulus of elasticity; tensile strength is decreased in bent bars. Ahmed et al., (2010) presented experimental results on shear strength of concrete beams reinforced with GFRP stirrups. Four large scale simply supported concrete beams with a T-shaped cross-section were tested under four-point bending till failure. The main investigated parameters were type and ratio of shear reinforcement. The study indicated that the presence of GFRP stirrups in the tested specimens, similar to steel stirrups, enhanced the concrete contribution after the formation of the first shear crack. It was observed that as the spacing was decreased, the shear resistance was enhanced due to the confinement, which improves the aggregates interlocking. Moreover, the study suggested that using FRP stirrups with strength of bend-to-straight portion ≥ 0.6 enables using the full capacity of the straight portion of the FRP stirrups, while lower ratios will cause the bend strength to govern the tensile strength of the stirrup.

El-Mogy et al., (2010) conducted an experimental study to investigate the effect of transverses reinforcement on the flexural performance of continuous concrete beams reinforced with GFRP bars. Results showed that the performance of the GFRP-reinforced beam provided with GFRP stirrups was similar to its counterpart reinforced with steel stirrups.

The effect of shear span-to-depth ratio (a/d) on the shear resistance of FRP-reinforced concrete members has been confirmed by many authors. It was conclude that all the available equations for calculating the concrete contribution to shear resistance predicted well the shear strength of the test beams with shear span-to-depth ratio > 2.5 while underestimated the shear

capacity of the beams with shear span-to-depth ratio < 2.5 (Razaqpur et al., 2010).

The shear strength increases with the increase in concrete tensile strength. Mahmoud and El-Salakawy, (2013) reported test results of 6 two-span continuous rectangular section concrete beams reinforced for flexural with GFRP bars. Four beams reinforced with minimum amount of transverse reinforcement as specified by the CSA-S806-12 (CSA 2012) whereas two without transverse reinforcement. The concrete strength of the test specimens were ranging from 39 to 81 MPa. They concluded that increasing the concrete strength from 39 to 69 MPa increased the shear capacity of continuous beams without shear reinforcement by approximately 12% and increased the shear capacity by approximately 56% beams with minimum transverse reinforcement. The results obtained compared with equations' results recommended by CSA-S6-06, CSA-S806-12 and the ACI 440.1R-06. It was found that, CSA-S806-12 overestimate the concrete contribution and underestimates the shear reinforcement contribution to shear strength. While the CSA-S6-06 and the ACI 440.1R-06 design equations, underestimate the concrete contribution and overestimate the shear-reinforcement contribution to shear strength.

2.4 Moment Redistribution in Continuous Beams Reinforced with FRP Materials

The current available design codes and recommendations for FRP-RC structures do not permit moment redistribution in statically indeterminate structures. This is due to the linear stress-strain behaviour of FRP bars up to

failure. However, research has been done to examine the moment redistribution in FRP-reinforced continuous concrete beams.

So far, unlike simply supported members, relatively few studies have experimentally been conducted to examine the flexural behaviour of multi-span continuous FRP reinforced concrete beams (Razaqpur and Mostofinejad, 1999; Ashour and Habeeb, 2008; Habeeb and Ashour, 2008; El-Mogy et al., 2010; Matos et al., 2012; Santos et al., 2013; Mahroug et al., 2014a; Mahroug et al., 2014b and Rahman et al., 2016). Razaqpur and Mostofinejad, (1999) studied experimentally the shear behavior of reinforced continuous beams. The shear reinforcement material (steel stirrups or a CFRP grid) and reinforcement ratio were the main variables in this experimental work. The research indicated that over reinforced sections with FRP bars exhibit a semi ductile behavior. This was noticed when middle support section reached its flexural capacity, however, tested beams did not fail. It should also be noticed that the performance of tested beams reinforced with a CFRP grid was analogous to that of steel stirrups. However, Habeeb and Ashour, (2008) and Ashour and Habeeb, (2008) through their experimental investigation found that, concrete crushing failure mode and bar rupture failure mode was experienced by beams with over and under reinforced section at mid span respectively. In addition, it was concluded that multi-span continuous GFRP-RC beams did not demonstrate any remarkable load redistribution.

El-Mogy et al., (2010) conducted a research study to evaluate the range of moment redistribution that could be achieved by continuous GFRP and CFRP reinforced concrete beams and their flexural behavior with different reinforcement configurations. According to the results of these studies, the

tested FRP-reinforced continuous beams exhibited higher deflections and wider cracks compared to the steel reinforced reference beam with similar flexural capacity. The GFRP reinforcement ratio at mid-span and middle support regions showed a strong influence on reducing mid-span deflections and improving load capacity. Moreover, the tested GFRP-reinforced continuous beam, with over-reinforced sections at mid-span and middle support, exhibited moment redistribution with different percentages. They also concluded that a reasonable agreement with the experimental results achieved when the correction factor proposed by Habeeb and Ashour, (2008) to the ACI 440-06 equation to calculate effective moment of inertia for GFRP-reinforced continuous concrete used.

Considering a linear elastic analysis with some redistribution of moments or a plastic analysis in a continuous concrete element reinforced longitudinally with FRP bars could be achieved by taking into account the non-linear response of concrete, which itself exhibits very limited material ductility. One possible way to increase such ductility is to confine the concrete material in critical cross-sections. Matos et al., (2012) conducted an experimental investigation about the flexural behavior of continuous beams reinforced with GFRP bars, namely their service and failure responses, and the effect of increasing concrete confinement in critical cross-sections. It was shown that the presence of sufficient stirrups increased the concrete confinement in critical zones and, consequently, enhanced the concrete compression ductility. Furthermore, Santos et al., (2013) studied the effect of increasing concrete confinement in critical zones by reducing the spacing between shear stirrups. Differently from the procedure adopted by Matos, additional stirrups used to increase concrete

confinement are positioned only in half of the height of the cross-section. The main parameters analyzed were the GFRP reinforcement ratio and the concrete confinement in a critical zone of the beams. It was concluded that the additional confinement of the concrete in compression at the central support used in beams did not result in a higher moment redistribution capacity.

Kara and Ashour, (2013) studied the moment redistribution in continuous concrete beams reinforced with FRP bars. The authors developed a numerical technique based on equilibrium of forces and full compatibility of strains to evaluate the moment-curvature relationships and moment capacities of FRP and steel sections. It was reported that the curvature of under reinforced FRP sections was large at FRP rupture but failure was sudden, that would not allow any moment redistribution. On the other hand, FRP over reinforced sections experienced higher curvature at failure than steel over reinforced sections because of the lower FRP modulus of elasticity.

Mahroug et al., (2014a) and Mahroug et al., (2014b) studied experimentally the flexural behavior of one-way continuous slabs reinforced with CFRP and BFRP rebars. It was observed that combined shear and flexural failure was the dominant mode of failure for all continuous CFRP and BFRP reinforced concrete slabs tested, indicating that shear in CFRP and BFRP reinforced concrete slabs may control the failure. In terms of improving the load capacity and reducing mid-span deflections, they found that increasing the bottom mid-span CFRP reinforcement of continuous slabs is more effective than the top over middle support CFRP reinforcement, consistent with the findings reported by El-Mogy et al., (2010). The test results showed signs of moment redistribution in continuous slabs with different percentages.

Recently, Rhaman et al., (2016) studied experimentally the behavior and possibility and the extent moment redistribution of large scale GFRP RC continuous beams with T- sections. It was concluded that all GFRP RC beams experienced crushing of concrete at the hogging moment regions; then the beams continuous to resist more loads until failure occurred due to either crushing of concrete in the sagging region or diagonal shear cracks near the middle support. The results showed that tested beams exhibited moment redistribution from the hogging to the sagging region in which the beams with close stirrup spacing or more lateral flange bars experienced high moment redistribution compared to their counterparts with larger spacing of lateral bars or stirrups.

2.5 Ductility and Deformability Improvement of FRP Reinforced Concrete Beams

Ductility permits a structure to undergo inelastic deformation which is considered as a precaution before failure of the structure, and to absorb and dissipate energy under seismic loads (Beeby, 1997). Moreover, in indeterminate structures, redistribution of stresses and moments between critical sections, and formation of plastic hinges will take place due to the ductile behavior of the structure. Therefore, steel reinforced concrete sections, where ductility is defined as the ratio of post-yield deformation to yield deformation, is recommended to be under-reinforced sections to ensure yielding of steel before the crushing of concrete. However, most guidelines recommend design to guarantee concrete crushing at ultimate limit states, instead of FRP rebars tensile failure owing to the brittle nature of the latter component of the cross-section, since it is more progressive and leads to a

less catastrophic failure with a higher degree of deformability. In addition, evaluating the ductility of FRP reinforced concrete sections cannot be obtained from the traditional definition of ductility, which is applied to the structures reinforced with steel reinforcement. Hence, different methods such as the energy-based method or the deformation-based method have been introduced to describe the ductility in FRP concrete structures (Wang and Belarbi, 2011).

A number of methods have been suggested to improve ductility, including provision of different type of FRP, combining two different reinforcement materials (e.g. FRP and steel), confinement of concrete in compression zone, addition of fibres to concrete and reinforcing concrete section with a hybrid combination of FRP and steel rebars.

2.5.1 Hybrid Reinforcing Rebars

Hybridization of different types of fibrous material was suggested as a solution for achieving ductility in FRP reinforced concrete beams. This has been reported in several publication such as (Nanni et al., 1994; Tepfers et al., 1996; Somboonsong et al., 1998; Harris et al., 1998). Tepfers et al., (1996) conducted a study on braided FRP wound around a thin cylindrical shell core made of GFRP. The main variables in specimens tested was the presence of core. They concluded that a ductile behavior could be achieved with braided FRP around core, although specimens without core accompanied by some decrease in the modulus of elasticity. However, a reduction in diameter, reducing rebar-concrete bond were the obvious drawbacks. Somboonsong et al., (1998) developed a hybrid FRP reinforcing bar using braided aramid around a carbon fibre core to increase the maximum elongation by reorienting portions of the fibres off axis of the rebar. Using carbon fibre in the core to

provide high rigidity and initial strength. They concluded that some specimens showed increasing in the maximum strain. Harris et al., (1998) used the new bars developed by Somboonsong et al., (1998) to reinforce simply concrete beams to achieve a similar behavior of that reinforced with traditional reinforcing bars. They concluded that, the beams were able to undergo large inelastic deformation and achieve a ductile behavior by giving ductility indexes which found to be very similar to those of a companion steel-reinforced beam.

Not only combining two or more different FRP composite materials was suggested to overcome the problem of the lack of ductility in FRP reinforcing bars, but also by using different materials with FRP composites to produce a hybrid reinforcement system. Nanni et al., (1994) presented a new system by producing a hybrid rod consisting of an AFRP skin with a steel core. The FRP skin is made of braided, epoxy-impregnated aramid or vinylon fibre. The steel core was protected by FRP skin which provides a structurl function. The tensile stress-strain behaviour of the hybrid rebars obtaind from the study displayed a bilinear relationship.

To evaluate the flexural behaviour of concrete beams reinforced with hybrid rebars, two concrete beams were tested by Saikia et al., (2005). The hybrid rebars used consisted of 2 mm-diameter GFRP strands,hellically wound on a 6 mm-diameter steel rebar. All beams were designed as under-reinforced sections similar to design principles employed for convintional steel reinforced concrete beams. They concluded that both beams failed at about 61% of designed load due to slip beween concrete and rebar. In another study done by Cheung and Tsang, (2010) to investigate the flexural behaviour of concrete beams reinforced with proposed hybrid FRP/steel fibre rebars which

developed by (Cui et al., 2008). The proposed hybrid rebars consisted of steel and glass fibres which were randomly dispersed across the cross section of the core while aramid and carbon fibres were placed within the shell to improve the elastic modulus as well as to serve as a shield for protecting the glass fibres from alkaline attack; and the steel fibres from moisture and chloride induced corrosion. The beams displayed some ductile behavior but still lower than that of steel reinforced concrete beams. Etman, (2010) examined the effect of core type and perimeter layer of hybrid rebars on the flexural behaviour of one way concrete slab. Ten simply supported concrete slabs reinforced with hybrid rebars and subjected to four-point loading were tested. The hybrid rebars consisted mainly of core reinforcement, which is made of mild steel or aluminium bars, surrounded by one or two perimeter layers of CFRP or GFRP. The experimental tests showed that hybrid rebars with aluminium core caused sudden brittle flexural failure while that with steel core exhibited flexural ductile failure. In addition, specimens reinforced with hybrid rebars where the perimeter layer were glass fibers exhibited higher deflection than those where the outer layer were carbon fibers. In more recent study, Behnam and Eamon, (2013) conducted a study to compare bar performance , in terms of ductility and cost for different hybrid rebars. They found that sections reinforced with continuous fiber hybrid ductile FRP bars required lower reinforcement ratio than beams reinforced with steel bars. Despite chopped fibre layer bars provided greatest ductility, they required twice the reinforcement ratio of the continuous bars, resulted in this bar type as a relatively costly option. It is possible to obtain ductility through a combination of different kinds of reinforcing fibres, such as carbon and glass fibres, together

with the adoption of appropriate manufacturing processes. However, a low modulus and a relatively high cost of hybrid rebars are still the problems faced by construction industry.

2.5.2 Confinement of Compression Concrete

The confinement of the compression zone is another possible method for achieving ductility in FRP reinforced concrete members. To confirm this, materials with higher compressive strain capacity are employed in the compression zone of the member. Zhou et al., (2009) placed a compression yielding (CY) block made of perforated SIFCON in the compression zone of the beam. The idea underlying CY is simple: the concrete in the compression zone of a plastic hinge is replaced with a strong, but more ductile material or mechanism, to ensure that the rotation of that hinge is achieved through compression yielding or deformation on the compression side, rather than through the yielding of the reinforcement on the tension side (Wu et al., 2010a). High ductility was acquired by developing a plastic hinge zone in the compression zone. However, the design of CY beams is very different from that of conventional reinforced concrete (RC) beams, and, therefore, a design method must be in place before the concept can be applied in practice (Wu et al., 2010b).

2.5.3 Concrete Mix Improvement

Another approach to enhance the ductility of beams reinforced with FRP rebars is to improve the property of concrete. Alsayed and Alhozaimy, (1999) carried out flexural tests on eighteen reinforced concrete beams to investigate the ductility enhancement of FRP beams due to the addition of crimped or

hooked steel fibres to the concrete mix. The main variables in the study were the type and volume fraction of the steel fibres. They found that the ductility index increased as much as 100% with the addition of 1% steel fibres. Moreover, replacing the brittle concrete matrix with a fibre reinforced cementations (FRC) composite with strain-hardening behavior was suggested by Li and Wang, (2002). They conducted a study to test sixteen beams reinforced with GFRP rebars in FRC using engineered cementations composite (ECC) material to investigate the flexural behaviour. Various GFRP longitudinal reinforcement ratios were used to reinforce the beams tested. The experimental tests results showed much better flexural behaviour of ECC beams. However, in order to translate the material ductility successfully into structural ductility, at the level of section, over-reinforced design is preferable. Recently, a total of twelve concrete beams reinforced either with GFRP or CFRP rebars, and containing polypropylene fibres, were tested by Wang and Belarbi, (2011). They observed that the ductility indices of the tested beams increased by more than 30% with addition of polypropylene fibres.

2.5.4 Hybrid FRP-Steel Reinforcement System

The use of such hybrid internal reinforcement is considered to be one of the current state of the art techniques that attracted many designers recently. An optimal solution can be achieved by placing FRP rebars near the outer surface of the tensile zone with small cover thickness and steel rebars at the inner level of the tensile zone, achieving larger cover and further corrosion protection (Tan, 1997; Aiello and Ombres, 2002; Leung and Balendran, 2003; Si-Larbi et al., 2006; Qu et al., 2009 ; Lau and Pam, 2010; Yoon et al., 2011; Yinghao; Yong, 2013 and Safan, 2013 and El-Refai et al., 2015). The presence of FRP

and steel bars would result in enhancing the ultimate load-carrying capacity and compensating for the brittleness nature of FRP rebars, respectively.

2.6 Flexural Behaviour of Concrete Beams Reinforced by Hybrid FRP/Steel Bars

The behavior of hybrid FRP/steel reinforced sections is different compared with sections either reinforced with traditional steel reinforcement or FRP bars. For concrete beams reinforced with either steel or FRP, the balanced reinforcement ratio is attained when the beam fails by crushing of concrete in compression and either yielding of steel or rupture of FRP in tension, simultaneously. As discussed earlier, a low amount of FRP reinforcement leads to the rupture of the bars prior to concrete crushing whereas a low amount of steel reinforcement leads to the yielding of the steel bars prior to concrete crushing. When high reinforcement ratios of either FRP or steel bars are used, concrete in compression crushes, while tensile stresses in FRP or steel bars remain below their ultimate and yield strength, respectively. However, a failure condition of hybrid FRP/steel reinforced concrete beams, in which crushing of concrete, yielding of steel and rupture of FRP simultaneously take place, is almost impossible to occur in practice. The steel reinforcement would have yielded long before rupture of FRP reinforcement as the steel yield strain is far much less than the FRP rupture strain (Kara et al., 2015). Hence, the balanced condition for hybrid FRP/steel reinforced concrete beams is proposed in a way such that concrete crushing in compression and rupture of FRP reinforcement simultaneously occur, while steel reinforcement would have already yielded (Lau and Pam, 2010).

2.6.1 Moment Capacity and Modes of Failure

To determine the ultimate moment capacity of hybrid FRP/steel RC beam, the key point is to understand the potential failure mechanisms of the hybrid reinforcing system. As explained earlier, unlike conventional under-reinforced RC beams, Hybrid FRP/steel RC beams may fail in different modes. These modes mainly include yielding of steel reinforcement followed by crushing of concrete, crushing of concrete before yielding of steel reinforcement (over-reinforced case) and tensile rupture of FRP bars (Kara et al., 2015). The best-case scenario for the failure mechanism is yielding of steel reinforcement followed by crushing of concrete without failure of FRP bars. This is because yielding of steel provides ductility and a warning of failure of the member (Pang et al., 2015). Fig 2.4 presents the strain distribution for various modes of failure as explained above.

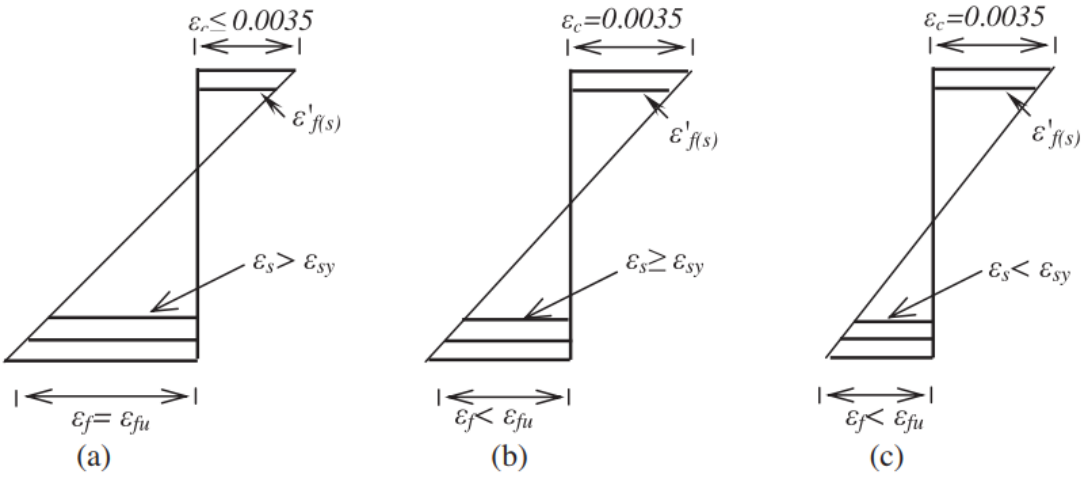

Figure 2.4 Strain distribution for various modes of failure (Kara et al., 2015)

Aiello and Ombres, (2002) tested four beams that reinforced with a hybrid combination of AFRP and steel bars. The beams were 3.0 m long with a rectangular of 150 mm width and 200 mm depth. The authors concluded that the use of a hybrid combination of AFRP and steel reinforcement in reinforcing

concrete beams would achieve desirable strength and ductility limits. In addition, they found that when the reinforcement ratio exceeded the balanced reinforcement ratio for FRP-reinforced concrete beams, the contribution of the steel reinforcement to the beams' flexural capacity was less than 15% even if the ratio between the tensile steel reinforcement and FRP reinforcement is high.

Leung and Balendran, (2003) demonstrated that increasing the amount of GFRP bars is a key factor in enhancing the load carrying capacity. Moreover, higher concrete strength led to an increase in flexural and shear capacities. Therefore, adequate shear reinforcement is needed to ensure a flexural failure mode.

Lau and Pam, (2010) also, performed research on hybrid GFRP/steel reinforced concrete beams. The ductility and ultimate strength were the two parameters key investigated. The longitudinal reinforcement in the beams comprised steel, GFRP bars or a combination of both, all arranged in one layer. They concluded that to prevent excessive elongation that causes rupture of FRP reinforcement, the amount of GFRP reinforcement should be larger than that of the steel reinforcement and should be also greater than the minimum FRP reinforcement content recommended by ACI 440.1R-06. In other words, the amount of hybrid reinforcement ratio should be chosen based on the assumption that yielding of steel occurs before crushing of concrete while the strain in FRP reinforcement is far much less than FRP rupture stain.

The arrangement of hybrid reinforcements in one or two layers plays an important role on the flexural performance of reinforced concrete beams. Recently, three Concrete beams with different arrangement of hybrid GFRP

and steel reinforcement were tested in four point bending by Yinghao and Yong, (2013). The flexural capacity, deflection and crack behavior of tested beams investigated experimentally. They concluded that the arrangement of steel and GFRP bars affect the flexural capacity of hybrid section. Among three different arrangements with the same amount of steel and GFRP bars as shown in Fig 2.5, it was found that placing GFRP and steel rebars both at the outer layer is the most effective on ultimate bending moment among other tensile reinforcement arrangement. However, from a durability point of view this arrangement does not avoid the corrosion of steel bars.

More recently, Safan, (2013) investigated the structural behavior of concrete beams reinforced with hybrid steel-GFRP reinforcement. The test parameters included the steel and GFRP reinforcement ratios and the configuration of the shear reinforcement to provide a practical solution for tying the hybrid reinforcement within the concrete section. The test results showed that higher GFRP-to-steel area ratios resulted in increasing the level of flexural capacity. This is due to the fact that any further increase in the ultimate load upon steel yielding is carried by the GFRP bars.

El-Refai et al., (2015) examined the effect of axial stiffness on the moment capacity of hybrid sections. The authors reported that the effective reinforcement ratio, ρ_{eff}, had more influence than the axial stiffness ratio, R, on the moment-carrying capacity of the hybrid reinforced beams. Increasing ρ_{eff} increased the moment capacities of the hybrid reinforced beams as shown in Fig 2.5. The same conclusion was reported by Qu et al., (2009).

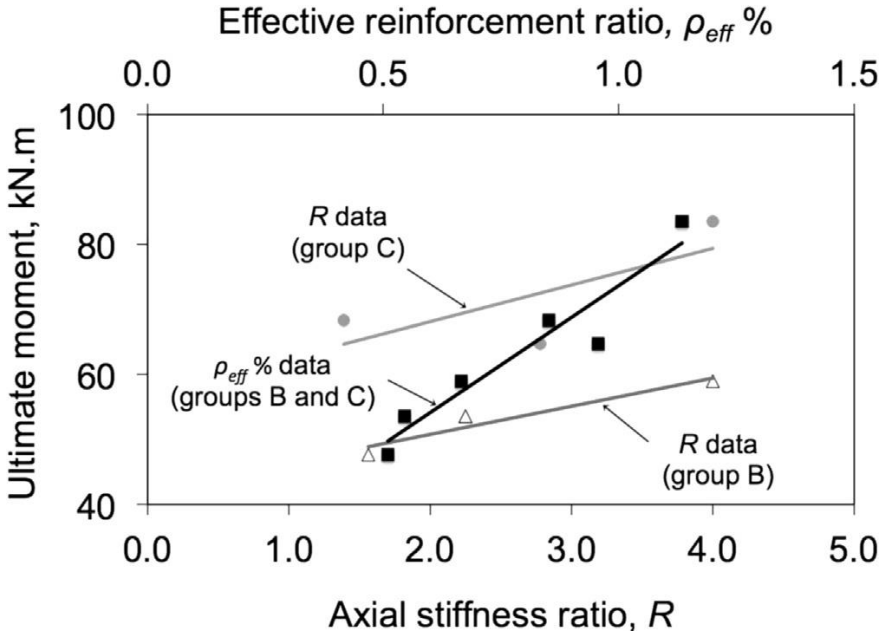

Figure 2.5 Effective reinforcement ratio, and axial stiffness ratio, versus ultimate moments in hybrid-reinforced beams (El-Refai et al., 2015)

El-Refai et al., (2015) reported that five hybrid beams failed by concrete crushing that followed by yielding of steel bars whereas none of GFRP bars ruptured. On the other hand, one hybrid beam exhibited a catastrophic failure after both steel and GFRP bars ruptured simultaneously with the concrete crushing.

On the other hand, short metallic fibre-reinforced high performance concrete (FRHPC) were combined with a mixture of carbon fibre-reinforced polymer (CFRP) and steel bars (Si-Larbi et al., 2006). The hybrid CFRP/steel-reinforced FRHPC beams had 50% more flexural capacity than beams with traditional steel reinforcement. The combination of hybrid CFRP/steel reinforcement and FRHPC effectively improved the flexural performance and lowered the weight of the beams by 48%.

Rafi and Nadjai, (2011) investigated the flexural performance of RC beams reinforced with CFRP and hybrid CFRP/steel bars at elevated temperatures.

Over-reinforced beams were tested under four-point load configuration in a furnace. The applied load was 40% of the nominal load capacity of the beams. All of the tested beams failed in flexure. The authors found that hybrid reinforced beams showed better strength and stiffness than those of steel or FRP reinforced beams. Hybrid-reinforced beams with one layer of bars showed better ductility than that with two layers of CFRP bars, with the later showing higher capacity.

Pang et al., 2015 proposed a theoretical model for predicting the moment capacity of hybrid FRP-steel concrete beams. The authors assumed plane cross-sections and perfect bond between concrete and reinforcement. The analysis of the section is based on the assumption that the flexural capacity of the hybrid-RC beams is governed by the yielding of the steel reinforcement followed by concrete crushing, while the tensile stress in the FRP bars is less than the ultimate strength. Comparisons with experimental results show that the proposed model can accurately estimate the moment capacity of under reinforced hybrid RC beams.

2.6.2 Deflection and Cracking of Hybrid FRP/Steel Reinforced Concrete Beams

FRP bars are known for their low modulus of elasticity as compared with steel bars. As a result, the serviceability requirements such as deflection and crack width are the main concern of in their behavior. Therefore, the design criterion of FRP reinforced concrete structures shift to serviceability limit states that check the structural behavior aspects instead of the strength to ensure functionality and safety during expected life of structures.

To address these problems, a combination of FRP and steel reinforcements has been proposed as a practical and effective solution for concrete structures. An optimal solution can be achieved by placing FRP rebars near the outer surface of the tensile zone with a small cover thickness and steel rebars at the inner level of the tensile zone, achieving larger cover and further corrosion protection. Consequently, the steel rebars within the cross section provide less contribution to the element capacity, while its contribution is more effective in terms of ductility and rigidity. The presence of steel reinforcement also reduces crack width and spacing.

Therefore, a combination of FRP and steel reinforcement offers improved serviceability and ductility compared to FRP reinforced concrete beams. limited experimental data and theoretical studies on the structural performance of hybrid FRP/steel reinforced concrete beams are available in the literature (Tan, 1997; Qu et al., 2009 ; and El-Refai et al., 2015).

Tan, 1997 tested concrete beams reinforced with hybrid aramid fibre reinforced polymer (AFRP) and steel bars. It was concluded that when the contribution from AFRP bars was no more than one-half of the total reinforcement, the hybrid AFRP/steel reinforced concrete beams had adequate serviceability.

Qu et al., 2009 carried out carried out an experimental investigation on six concrete beams reinforced with hybrid GFRP and steel bars. The amount of reinforcement and the ratio of GFRP to steel bars were the main parameters investigated. In addition, an analytical model was implemented to predict the flexural performance of the tested specimens.

The test results showed that the use of steel reinforcement in combination with GFRP bars improved the serviceability and ductility of the hybrid-reinforced beams. The flexural stiffness of hybrid GFRP-steel reinforced specimens was found to be higher when hybrid reinforcement ratio was increased. In addition, the authors concluded that there was a perfect bond between GFRP bars and surrounding concrete, which was demonstrated by experimental strain distribution results (Fig 2.6).

The developed theoretical load-deflection relationship was in good agreement with experimental results at loads up to the service load level for beams with medium hybrid reinforcement ratio. As for beams with low and high hybrid reinforcement ratio, however, the agreement was poor.

Moreover, it was concluded that using the equation for predicting crack widths proposed by ACI code is in good agreement with experimental results at the service load level.

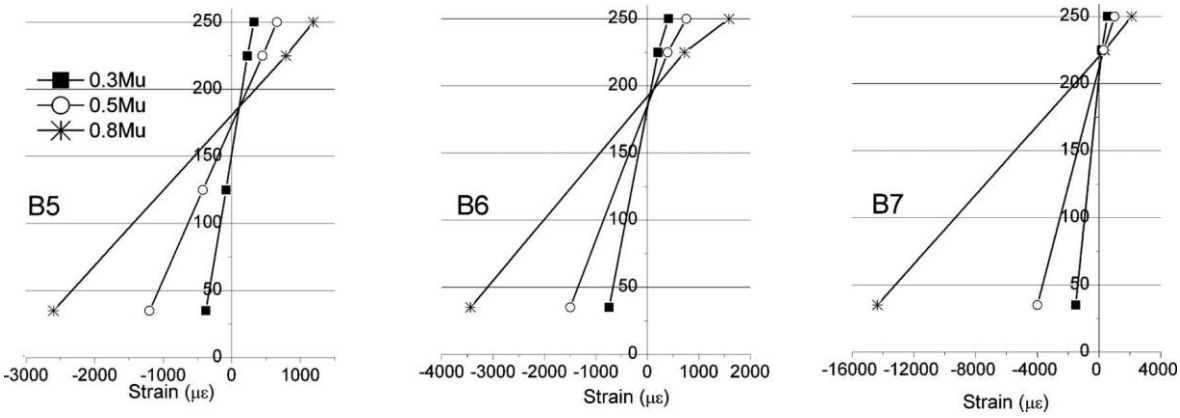

Figure 2.6 Strain distribution of tested beams (Qu et al., 2009)

Another experimental study was carried out by El-Refai et al., (2015) to investigate the flexural behavior and serviceability performance of hybrid concrete beams. The study presented the results of six full-size simply

supported concrete beams reinforced with hybrid GFRP-steel bars tested under four-point bending. These results were reported in terms of deflection and crack width. The main test parameters include the reinforcement ratio and the ratio of steel to GFRP bars used to reinforce the test beams. The study concluded that the enhancement in serviceability aspects was more pronounced at service loads prior to steel yielding. Crack widths were inversely proportional to the hybrid reinforcement ratio of the beam in which increasing the amount of reinforcement decreased the crack widths in all test beams. The presence of steel bars in hybrid system significantly decreased the crack widths at and beyond the service loads. Based on the test results, the authors proposed an equation to determine the bond coefficient for the hybrid-reinforced beams.

Furthermore, a few studies were dedicated to provide formulas to predict the load deflection response of hybrid FRP-steel reinforced concrete beams (Qu et al., 2009 and Yoon et al., 2011). The available formulas were based on Branson's equation to calculate the effective moment of inertia (I_e). As this equation was developed for steel-reinforced beams, modification factors were applied for the equation to be applicable with hybrid FRP-steel reinforced beams.

Branson's equation reflects two different phenomena: the variation of EI stiffness along the member and the effect of concrete tension stiffening (ACI 440-1R-06). ACI440.1R-06 proposed a modified Branson equation to predict the deflection for FRP-reinforced concrete beams, with an empirical correction factor β_d :

$$I_e = \left(\frac{M_{cr}}{M_a}\right)^3 \times \beta_d I_g + [1 - \left(\frac{M_{cr}}{M_a}\right)^3] \times I_{cr} \leq I_g \quad (2\text{-}1)$$

$$M_{cr} = 2\frac{f_{cr} I_g}{h} \quad (2\text{-}2)$$

The elastic analysis for FRP-reinforced concrete is similar to the analysis used for steel-reinforced concrete and is given by Eq. (2-3) and (2-4) with n_f as the modular ratio between the FRP reinforcement and the concrete

$$I_{cr} = \frac{bd^3}{3} k^3 + n_f A_f d^2 (1-k)^2 \quad (2\text{-}3)$$

$$k = \sqrt{2\rho_f n_f + (\rho_f n_f)^2} - \rho_f n_f \quad (2\text{-}4)$$

In addition, Bischoff, (2007) recommended a new expression for the effective moment of inertia I_e that showed a good agreement with test results for both steel and FRP reinforced concrete beams.

$$I_e = \frac{I_{cr}}{1 - \eta(\frac{M_{cr}}{M_a})^2} \leq I_g \quad (2\text{-}5)$$

$$\eta = 1 - \frac{I_{cr}}{I_g} \quad (2\text{-}6)$$

Where; I_{cr} is moment of inertia of transformed crack section; I_g $(= \frac{bh^3}{12})$ is gross moment of inertia; $M_{cr} (= 2\frac{f_{cr} I_g}{h})$ is cracking moment; $f_{cr} (= 0.62\sqrt{f_c'})$ is modulus of rupture of concrete; M_a is maximum moment in the member at the current phase of deflection; and *h* is overall height of concrete beam.

The deflection behavior of the hybrid reinforced beams with steel changes after the yielding of steel. Moreover, both of them were empirically derived from test results of only steel- or only FRP-reinforced concrete beams. Therefore, neither the modified Branson's method (ACI440.1R-06) nor Bischoff's

approach could be used directly to predict the short-term deflection of hybrid FRP/steel-reinforced concrete beams at service load levels.

Qu et al., (2009) adopted Eqs (2-5) and (2-6) to predict the short-term deflection of hybrid GFRP/steel-reinforced concrete beams at service load levels, with I_{cr} calculated for the combined GFRP and steel reinforcements by following Equations:

$$I_{cr} = \frac{bd^3}{3}k^3 + (n_f A_f + n_s A_s)\, d^2(1-k)^2 \tag{2-7}$$

$$k = \sqrt{(\rho')^2 + 2\rho'} - \rho' \tag{2-8}$$

$$\rho' = \rho_f n_f + \rho_s n_s \tag{2-9}$$

where; $n_f \left(= \frac{E_f}{E_c}\right)$ is elastic modulus ratio between GFRP reinforcement and concrete; $n_s \left(= \frac{E_s}{E_c}\right)$ is elastic modulus ratio between steel reinforcement and concrete and *d* is distance from extreme compression fibre to the centroid of the tension reinforcing zone.

Yoon et al., (2011) suggested an effective moment of inertia after steel yields based on Bischoff's equation as the following:

$$I_e = \frac{I_{cr}}{\frac{I_{cr}}{I_y} + \frac{M_y}{M_a}\left(1 - \frac{I_{cr}}{I_y}\right) - \left(\frac{M_y}{M_a}\right)^2\left(1 - \frac{I_{cr}}{I_y}\right)} \leq I_g \tag{2-10}$$

where M_y is the steel yielding moment and I_y is the moment of inertia after steel yields.

$$I_{cr} = \frac{bd^3}{3}k^3 + (n_f A_f + n_s A_s)\, d^2(1-k)^2 \tag{2-11}$$

$$I_y = \frac{bd^3}{3}k^3 + (n_f A_f)\, d^2(1-k)^2 \tag{2-12}$$

As mention earlier, at the service load level, the model of effective moment of inertia proposed by Qu et al., (2009) provides good predictions of the deflection of hybrid GFRP/steel-reinforced concrete beams; however, the prediction errors became large when the load exceeded the service load level.

Yinghao and Yong, (2013) implementd Yoon's model to examine the applicability of this method to predict deflections of hybrid reinforced beams tested in their study. They found that deflections experimental results and prediction results by Yoon's model were in a good agreement.

2.6.3 Numerical and Analytical Studies on Hybrid FRP-steel Concrete Beams

The use of finite element method (FEM) as an analytical model to predict the behaviour of RC structures is not a straightforward process. The behaviour of RC is very complicated because it consists of completely two different materials in terms of physical and mechanical characteristics. The steel/ FRP reinforcement is a homogenous material which can be easily defined whereas concrete is a heterogeneous material and is difficult to model. Moreover, the behaviour of RC is nonlinear even when subjected to small loads and it has a continuous variation under load increment because of the appearance of cracks. Furthermore, the interaction between concrete and reinforcement is very complex due to the bond slip. In addition, there are many other factors which affect the behaviour of concrete such as creep and shrinkage. The accuracy of FE method relies on the selection of the finite elements to precisely represent the behaviour of concrete, reinforcement and the bond between concrete and reinforcement.

Although several finite element models have been developed to simulate the behaviour of reinforced concrete beams, limited finite element models had been conducted on simulating the response of simply supported concrete beams reinforced with hybrid FRP/steel bars (Hawileh, 2015; Bencardino et al., 2016 and Qin et al., 2017).

Hawileh, (2015) used ANSYS, a general-purpose finite element program, to develop 3D finite element models of the specimens tested by Aiello and Ombers (2002). The longitudinal bond-slip behaviour between the reinforcement bars and surrounding concrete were simulated using spring elements. The developed FE models managed to accurately predict the load-deflection response of the tested specimens with a deviation less than 10%. The FE study also showed that assuming full compatibility of coincident nodes between the reinforcing bars and concrete elements (perfect bond) yielded good correlation with experimental data.

In another study, Bencardino et al., 2016 and Qin et al., 2017 used ABAQUS, a general-purpose finite element program, to model simply supported beams reinforced with hybrid FRP/steel bars. Two-dimensional (2D) and three-dimensional (3D) models were adopted, respectively. Perfect bond between the reinforcement and surrounding concrete was assumed. The proposed FE models were solved using a dynamic approach in order to overcome convergence difficulties due to strain softening; and to perform a quasi-static analysis of RC beams. It was found that the proposed FE models was capable to predict the overall structural performance of hybrid simply supported beams (Bencardino et al., 2016).

Qin et al., (2017) carried out a parametric study of hybrid reinforcement ratio to investigate the contribution of FRP and steel reinforcement to the overall structural performance of hybrid beams. The authors concluded that the hybrid reinforcement ratio should be designed in range of 1-2.5 to provide enough post-elastic strength and stiffness for meeting the ductility requirement.

In chapter seven, a two-dimensional nonlinear FE model using ABAQUS software is proposed in order to analyze and predict the behavior of multi-span continuous concrete beams reinforced with hybrid GFRP/steel bars. The model will be verified against the experimental results of continuous beams tested in the current research investigation. In addition, the proposed FE model will be used to conduct a parametric study with the aim of exploring the structural behaviour of continuous concrete beams reinforced with hybrid GFRP/steel bars with extended range of parameters.

On the analytical side, Kara et al., (2015) developed an iterative technique to determine the moment-curvature relationship of a concrete cross section reinforced with a hybrid combination of FRP and steel bars. This iterative technique is based on equilibrium of forces and full compatibility of strains. The strains in the constituent materials, i.e. the concrete, the internal steel and FRP reinforcements, are calculated from the strain profile using the linear interpolation method. From the cross section dimensions and the calculated stresses in the constituent materials, the internal forces applying on the cross section can be determined. Accordingly, the bending moment and the corresponding curvature can be evaluated. Comparison between experimental results and predicted curvature and moment capacity of hybrid FRP/steel reinforced concrete beams showed good agreement.

Further details of this technique are given in chapter five because this technique has been used for the sectional analysis part of a computer program developed by the author.

2.7 Experimental Investigation on Hybrid FRP/Steel Continuous Members

As presented earlier, several studies investigated the flexural behaviour of simply supported beams reinforced with hybrid FRP/steel bars. However, to date, unlike simply supported members, only one study has experimentally examined the flexural behaviour of multi-span continuous slabs reinforced with hybrid basalt fibre-reinforced polymers (BFRP)/steel reinforcing bars (Akiel, 2016).

Akiel, (2016) tested twelve two-span concrete slabs, six of which were reinforced only with BFRP reinforcing bars while the other six were reinforced with hybrid BFRP/steel bars in both the sagging and the hogging regions. The main variables of the test program were the amount of reinforcement in the sagging region and the hogging-to- sagging nominal capacity ratio.

It is important to mention that both BFRP and steel bars were placed at the same level. This reinforcement arrangement is not effective from a durability point of view because it does not avoid the corrosion of steel bars.

The design concept of sections reinforced with hybrid BFRP/steel reinforcement was based on the nominal moment capacity of the sagging and hogging sections in specimens reinforced with BFRP bars only. The nominal moment capacity of the sagging and hogging sections in specimens reinforced with hybrid BFRP/steel bars were similar to those of their counterpart specimens reinforced with BFRP bars only.

The hybrid specimens were divided into two groups, three over reinforced and three under reinforced specimens. Over reinforced specimens and under reinforced specimens were corresponding to their counterpart specimens reinforced with only BFRP bras.

Throughout the experimental tests two different modes of failure were observed. These two modes of failure were: concrete crushing after yielding of the steel reinforcement in both hogging and sagging regions and steel yielding in both sagging and hogging regions followed by progressive BFRP rupture in the hogging region. The first type of failure was demonstrated by over reinforced specimens while the second type of failure was demonstrated by under reinforced specimens.

The study concluded that specimens reinforced with hybrid steel-BFRP bars exhibited less deflections and smaller crack widths at service load than those of their counterparts with BFRP bars only. The deflection at service load for the hybrid specimens was approximately 50% lower than that of the BFRP specimens. The crack widths in the hogging regions of specimens reinforced with the hybrid reinforcement were 57%-78% lower than those of their counterparts with BFRP bars only.

Although the use of hybrid reinforcement improved the serviceability of the specimens, it had no noticeable effect on the deflection at ultimate load. The specimens reinforced with hybrid steel-BFRP bars reached their ultimate loads at deflection values comparable to those of their counterparts reinforced with BFRP bars only.

The inclusion of steel bars in the hybrid-reinforced specimens restricted growth of cracks prior to yielding and reduced the difference in flexural rigidity between the sagging and hogging regions. Accordingly, the hybrid-reinforced specimens tended to exhibit moment redistribution ratios lower than those of their counterparts reinforced with BFRP bars only.

2.8 Concluding Remarks

The review of literature shows that many of the issues related to ductility and moment redistribution in FRP reinforced concrete members remain unresolved. In addition, concrete beams reinforced with FRP bars tend to experience larger deflections and wider cracks compared to that with steel reinforcement. However, the above literature review indicates that

- Previous studies show that the behavior and structural performance of hybrid FRP/steel reinforced concrete members is significantly different to those of steel or FRP reinforced members. This necessitated the need for developing new design code provisions for the properties of FRP and steel materials.
- The hybrid reinforcement system could improve the structural performance of FRP reinforced concrete beams. The use of such hybrid internal reinforcement is considered to be one of the current state of art technique that attracted many researches recently.
- The literature shows that the moment redistribution occurred in FRP RC continuous beams in a similar manner to that of their counterparts reinforced with steel. However, because the FRP bars do not exhibit yielding, moment redistribution occurs due to the variation in flexural

stiffness, the inelasticity of concrete, the ability of FRP bars to withstand large deformations, and the bond-slip characteristics of the FRP bars.

- Based on the previous studies, existing developed approaches to estimate deflection, moment capacity of hybrid structure members reinforced with FRP/steel bars appear in general to give a reasonable result in comparison with experimental data.
- The literature shows that there several studies investigated the flexural behaviour of simply supported beams reinforced with hybrid FRP/steel bars. However, no experimental investigations have been conducted regarding the flexural behaviour of multi-span continuous concrete beams reinforced with hybrid FRP/steel reinforcement.
- A numerical technique is essential to predict the full behaviour of continuous concrete beams reinforced with hybrid FRP/steel bars. The linear analysis can predict the behaviour of hybrid continuous beams before cracking. However, after cracking, a major redistribution of stresses occurs and therefore, a nonlinear finite element model is required.

CHAPTER THREE:

EXPERIMENTAL PROGRAM

3.1 Introduction

This chapter describes the main experimental program, which was developed to investigate the behavior of hybrid GFRP-steel reinforced concrete continuous beams. The main objective of the experimental program was to investigate the structural behaviour of continuous concrete beams reinforced with hybrid GFRP-steel bars compared to counterparts reinforced with either steel or GFRP bars. Design concept of the hybrid GFRP-steel section and specimen details are given; material property tests for GFRP, steel and concrete are described; test setup, instrumentation and test procedure are provided. The results of testing these beams will be presented and discussed in Chapter 4.

3.2 Test Specimens

Three simply and eleven multi-span continuous reinforced concrete beams were tested in flexure. All specimens tested were 200 mm in width and 300 mm in depth. The continuous beams comprised of two equal spans, each of 2600 mm, while the simply supported beams had a span of 2600 mm, as shown in Figs 3.1 and 3.2, respectively.

Nine continuous and two simply supported beams were reinforced with a hybrid combination of both GFRP and steel re-bars at mid spans and internal support regions. In addition, two continuous concrete beams reinforced with either GFRP or steel bars and one simply supported beam reinforced with

GFRP bars were tested as control beams as shown in Figs 3.1 and 3.2, respectively.

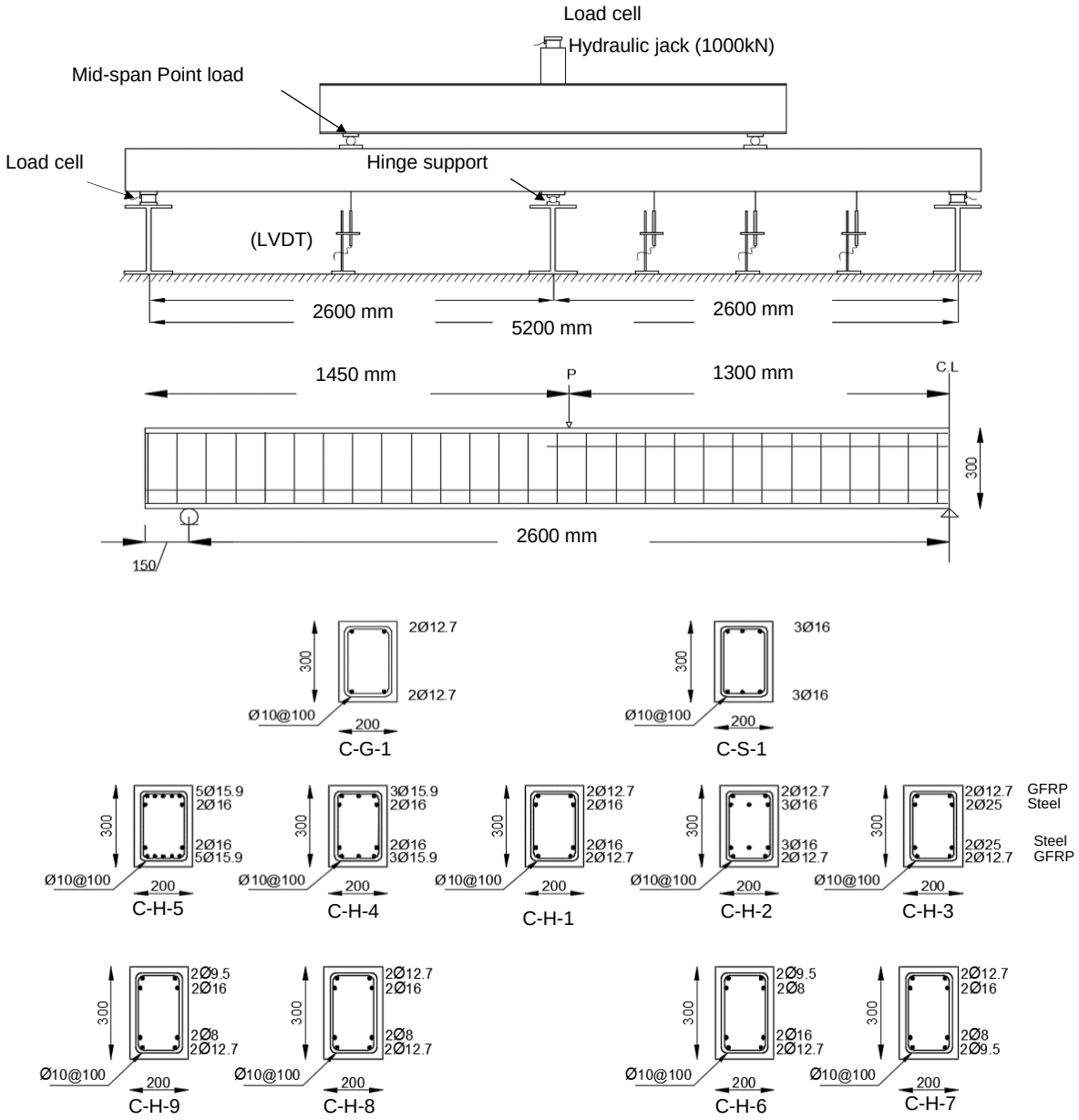

Figure 3.1 Experimental setup and details of continuous beams

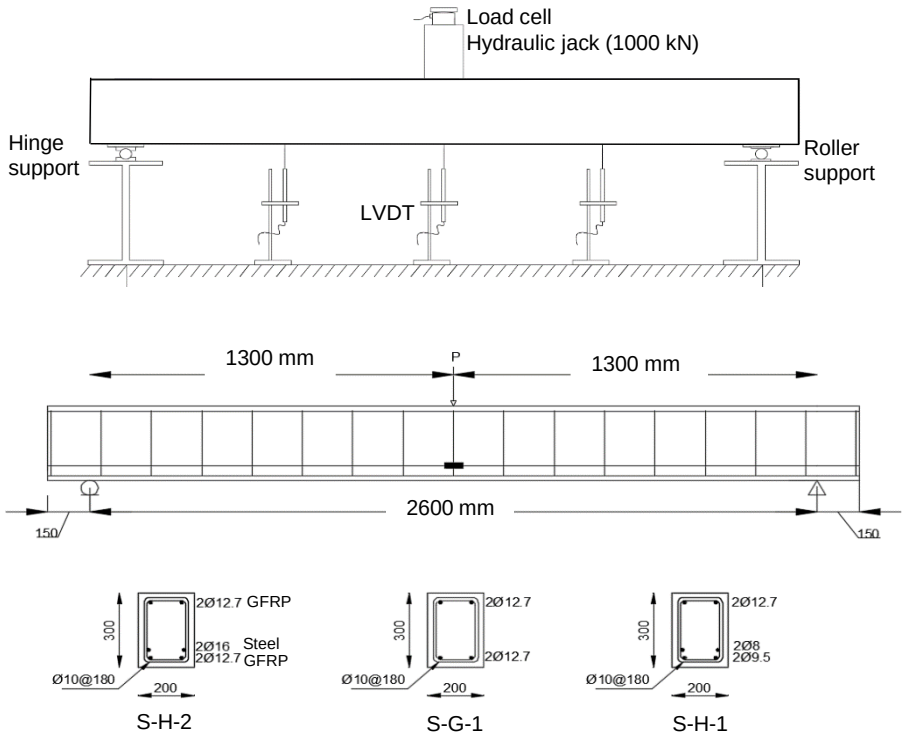

Figure 3.2 Experimental setup and details of simple beams

3.3 Design of Test Specimens

The design of GFRP reinforced concrete continuous beam C-G-1 was chosen to fail in compression (concrete crushing) at mid span and over support sections as recommended by ACI 440.1R-15. Therefore, it was reinforced with two GFRP bars of 12.7mm diameter. On the other hand, the steel-reinforcement (3 bars of 16mm. diameter) of the continuous beam C-S-1 was selected to achieve tensile capacity of 330kN, equivalent to that of two GFRP of 12.7mm diameter, used at the bottom layer of beam C-G-1.

For the continuous beams with hybrid reinforcements, the design of hybrid GFRP-steel sections was based on the assumption that failure mode is governed by yield of tensile steel reinforcing bars before rupture of GFRP bars or concrete crushing. The ratio of GFRP and steel reinforcements were, then,

chosen as shown in Figs 3.3 and 3.4. The design chart shown in Figs 3.3 and 3.4 were obtained by studying the effect of the tensile steel reinforcement ratio and GFRP reinforcement ratio on the failure mode of a hybrid section (will be discussed in detail in Chapter 5) with material properties given in Tables 3.2 and 3.3. The dotted and solid lines represent the boundaries of different flexural modes for cylinder compressive strength of concrete of 40 MPa and 70 MPa, respectively. The hybrid reinforced concrete beams were reinforced with five different longitudinal reinforcement combinations as summarized in Table 3.1.

The beam C-H-1 was reinforced with two GFRP longitudinal bars of 12.7 mm diameter and two steel longitudinal bars of 16 mm diameter on the bottom and top sides as shown in Figs 3.1 and 3.3. The beam C-H-1 is considered as a control beam to measure the effect of reinforcements ratio change.

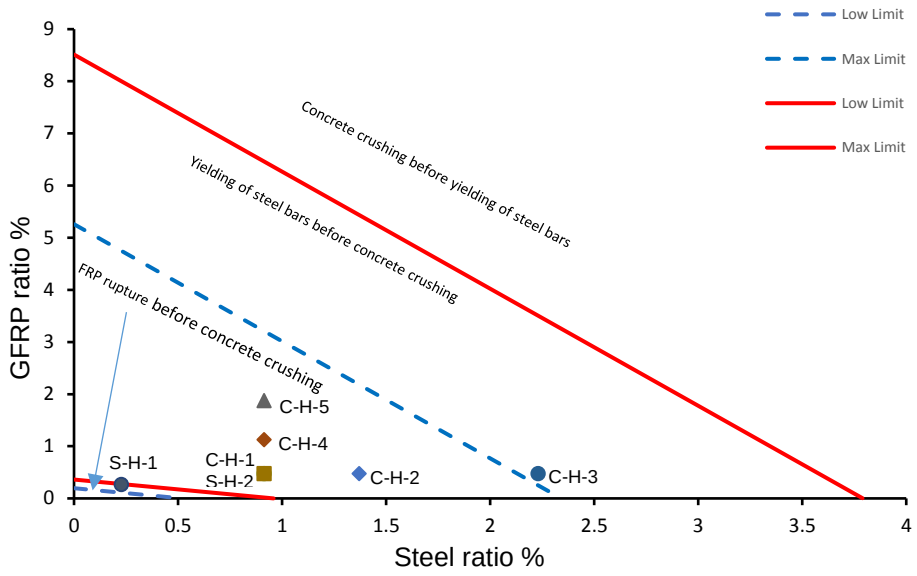

Figure 3.3 GFRP reinforcement ratio vs steel reinforcement ratio, indicating the different flexural failures

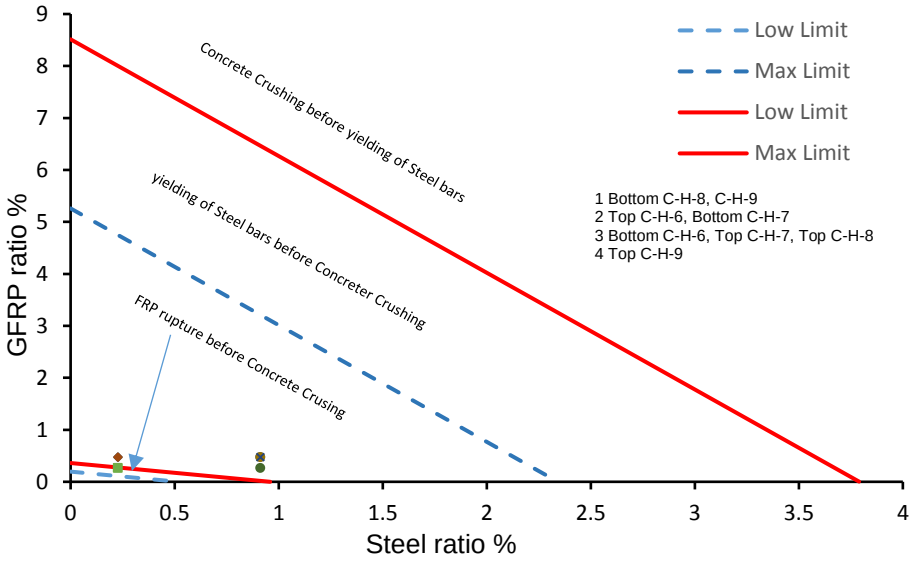

Figure 3.4 GFRP reinforcement ratio vs steel reinforcement ratio, indicating the different flexural failures

3.3.1 Reinforcement Ratios of Beam of Series I

As for beams C-H-2 and C-H-3, three steel bars of 16 mm diameter and 2 steel bars of 25 mm diameter with similar GFRP reinforcement ratio of that of

C-H-1 were used in C-H-2 and C-H-3 beams, respectively, as shown in Figs 3.1 and 3.3.

As depicted in Figs 3.1 and 3.3, for beams C-H-4 and C-H-5, three GFRP bars of 15.9 mm diameter and five GFRP bars of 15.9 mm diameter GFRP reinforcement ratio with similar steel reinforcement ratio of that of C-H-1 were used in C-H-4 and C-H-5 beams, respectively.

3.3.2 Reinforcement Ratios of Beam of Series II

The beam C-H-6 was reinforced with two GFRP longitudinal bars of 12.7 mm and two steel bars of 16 mm on the bottom side and with two GFRP longitudinal bars of 9.5 mm and two steel bars of 8 mm on the top side, whereas beam C-H-7 was reinforced with an opposite arrangement of longitudinal GFRP and steel bars as shown in Figs 3.1 and 3.4.

The top reinforcement of beam C-H-8 was the same as the top reinforcement of beam C-H-7. While the bottom side of beams C-H-8 and C-H-9 was reinforced with two GFRP bars of 12.7 and two steel bars of 8 mm. The hybrid combination at top layer of beam C-H-9 was two GFRP bars of 9.5mm and two steel bars of 16 mm as shown in Figs 3.1 and 3.4.

The simply supported beams S-G-1, S-H-1 and S-H-2, were reinforced with two GFRP bars of 12.7 mm diameter (over reinforced), two GFRP bars of 9.5 mm diameter and two steel bars of 8 mm diameter, and two GFRP bars of 12.7 mm diameter and two steel bars of 16 mm diameter, respectively.

The bottom longitudinal steel bars were elevated, whereas the top longitudinal steel bars were lowered to increase the protecting concrete cover and in return improves the durability. The concrete cover to the centre of the bottom and top

main steel bars was 80 mm. All continuous and simply supported beams were provided with 10-mm diameter steel stirrups spaced at 100 mm and 180 mm, respectively, all over the entire length to prevent shear failure. It should be mentioned that negative moment reinforcement were curtailed beyond the mid-span point load except those at top corners used as stirrup hangers along the beam span, whereas bottom bars continued throughout the beam length as shown in Fig 3.1. As for simply supported beams, bottom and top bars continued throughout the beam length as shown in Fig 3.2.

The beam notation was defined according to the type of reinforcement and support system. The first letter in the notation indicates the type of supporting system, ‘C’ for multi-span continuous beams and ‘S’ for simply supported beams. The second letter corresponds to the type of reinforcement, either ‘S’,’G’ or ‘H’ for steel, GFRP and hybrid GFRP/steel, respectively, followed by a number indicating the beam number.

Table 3-1 Concrete and reinforcement details

Beam notation	Bottom bars at mid-span				Top bars at central support			
	No		Diameter, mm		No		Diameter, mm	
	Steel	GFRP	Steel	GFRP	Steel	GFRP	Steel	GFRP
C-S-1	3	-	16	-	3	-	16	-
C-G-1	-	2	-	12.7	-	2	-	12.7
C-H-1	2	2	16	12.7	2	2	16	12.7
C-H-2	3	2	16	12.7	3	2	16	12.7
C-H-3	2	2	25	12.7	2	2	25	12.7
C-H-4	2	3	16	15.9	2	3	16	15.9
C-H-5	2	5	16	15.9	2	5	16	15.9
C-H-6	2	2	16	12.7	2	2	8	9.5
C-H-7	2	2	8	9.5	2	2	16	12.7
C-H-8	2	2	8	12.7	2	2	16	12.7
C-H-9	2	2	8	12.7	2	2	16	9.5
S-G-1	-	2	-	12.7	-	2	-	12.7
S-H-1	2	2	16	12.7	-	2	-	12.7
S-H-2	2	2	8	9.5	-	2	-	12.7

3.4 Material properties

3.4.1 GFRP and Steel Reinforcement

The GFRP bars used in this study had a sand-coated surface to enhance their bond with concrete and load transfer. The bars were made of continuous longitudinal fibres impregnated in a thermosetting vinyl-ester resin with a fibre content of 81% by weight (Pultrall Inc. 2015). Deformed steel bars, were used in the flexural and shear reinforcement of the tested beams.

Standard characteristics tests were conducted on three specimens of each bar diameter in accordance to ACI 440.3R-04 in the laboratory to obtain the actual mechanical properties of the used reinforcement as applicable. The GFRP specimen ends were embedded into steel pipes filled with expansive grout to avoid premature failure of GFRP bars at the steel jaws of the testing machine as shown in Fig 3.5. Specimens were tested using a 500 kN -capacity, universal machine as shown in Fig 3.5a. A tensile test machine with an extensometer attached on the backside of the sample was used to measure

the modulus of elasticity as shown in Fig 3.5b. In addition, the cross-sectional area and equivalent diameter of each bar were determined by immersion testing in accordance with ACI 440.3R-04. Table 3.2 details the mechanical properties of the entire bar reinforcement used in the beams tested.

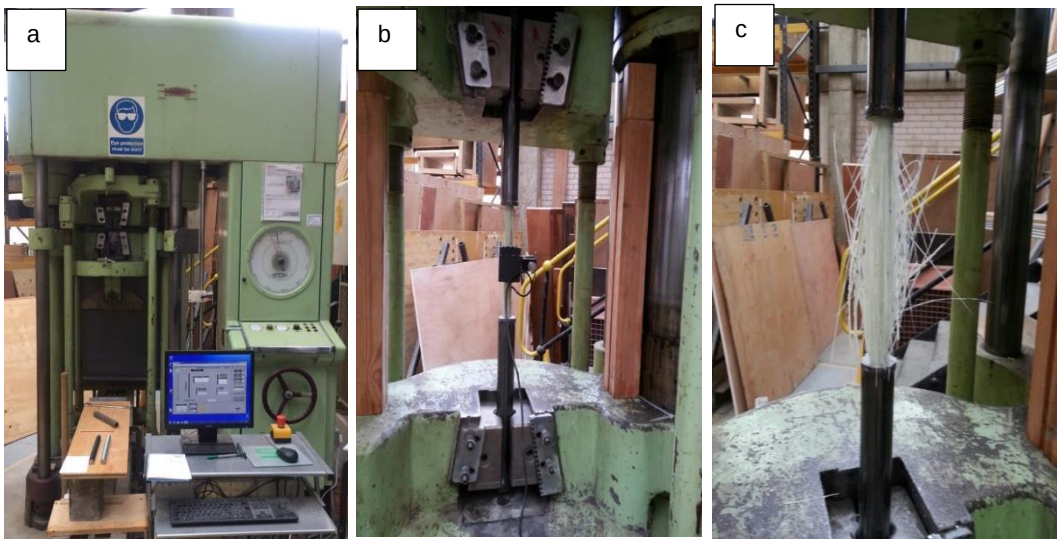

Figure 3.5 Tensile test of the GFRP bar: (a) tensile test rig for bar testing, (b) during GFRP bar testing, (c) after rupture

Table 3-2 Properties of GFRP and steel reinforcements used in the tested beams

Type of bars	Bar diameter: mm	Modulus of elasticity: (GPa)	Tensile strength : (MPa)	Yield strength (MPa)	Rupture strain	Yield strain
Longitudinal GFRP	9.5	51	1225	N/A	0.024	N/A
	12.7	51	1175	N/A	0.023	N/A
	15.9	52	1210	N/A	0.023	N/A
Longitudinal Steel	8	200	N/A	580	N/A	0.0029
	16	200	N/A	580	N/A	0.0029
	25	200	N/A	580	N/A	0.0029
Steel stirrups	10	200	N/A	580	N/A	0.0029

3.4.2 Concrete Strength

The average values of the cube compressive strength, f_{cu}, and splitting tensile strength, f_{ct} , were obtained by testing three 100 mm cubes and three 150mm diameter by 300mm high cylinders immediately after testing of each specimen. In addition, two 100x100x500 mm prisms were also tested for each group of beams to obtain the modulus of rupture, f_r, as shown in Fig 3.6 and listed in Table 3-3.

Figure 3.6 Concrete cubes, cylinders and prisms for compressive and tensile strength; and modulus of rupture

Table 3-3 Characteristics of concrete

Series No	Beam notation	Concrete properties		
		$f_{cu}: MPa$	$f_{ct}: MPa$	$f_r: MPa$
I	C-S-1	50.5	2.8	3.3
	C-G-1	48	3.3	
	C-H-1	50.7	3.1	
	C-H-2	54	2.7	
	C-H-3	54.6	2.9	
II	C-H-4	70.6	3.6	4.2
	C-H-5	75	3.6	
	C-H-6	69.5	3.6	
	C-H-7	69.6	3.8	
	S-G-1	72	3.6	
III	C-H-8	62.2	3.4	4.0
	C-H-9	66.6	3.5	
	S-H-1	66.6	3.4	
	S-H-2	63.2	3.4	

3.5 Test Preparations

All relevant experimental activities, including specimens' preparation and casting, were conducted in the heavy structural lab at the University of Bradford. First of all, five continuous formworks made of plywood were prepared to accommodate the required reinforcement cages as shown in Figure 3.7. This was followed by preparation of reinforcement cage stage. The longitudinal steel bars, prior to placing the reinforcement cages inside the wooden mould, were equipped with three electronic strain gauges in which two strain gauges at the maximum sagging section of each span and one strain gauge at the maximum hogging region. The reinforcement cage assembled and very carefully placed in the plywood forms after brushing the inside with oil to facilitate the beam removal after casting and curing of the concrete. The reinforcement cages rested on concrete spacers to maintain a 20mm clear concrete cover to an outer surface of the steel stirrups.

The wooden moulds, prior to casting, were reinforced at the top against the fresh pressure to avoid distortion in the beam width and resist vibrations resulting during construction as shown in Figure 3.8a. Ready-mix concrete of 20-mm maximum aggregate size was used to construct all test specimens and the exposed surface was carefully leveled and manually finished as shown in 3.8a. Casting of the concrete beams was performed in three consecutive series where three deliveries of concrete from two different batches of concrete were supplied. The first series were C-S-1, C-G-1, C-H-1, C-H2 and C-H-3. While the second series were C-H-4, C-H-5, C-H-6, C-H-7 and S-G-1. The last series were C-H-8, C-H-9, S-H-1 and S-H-2. After concrete casting, all specimens were stored under the same condition and covered by polyethylene sheets to keep down moisture loss at all times during the period of curing until the day of first specimen testing of each group as shown in Fig 3.8b and listed in Table 3.3. Each beam, prior to testing, was painted white in order to trace the crack patterns during testing.

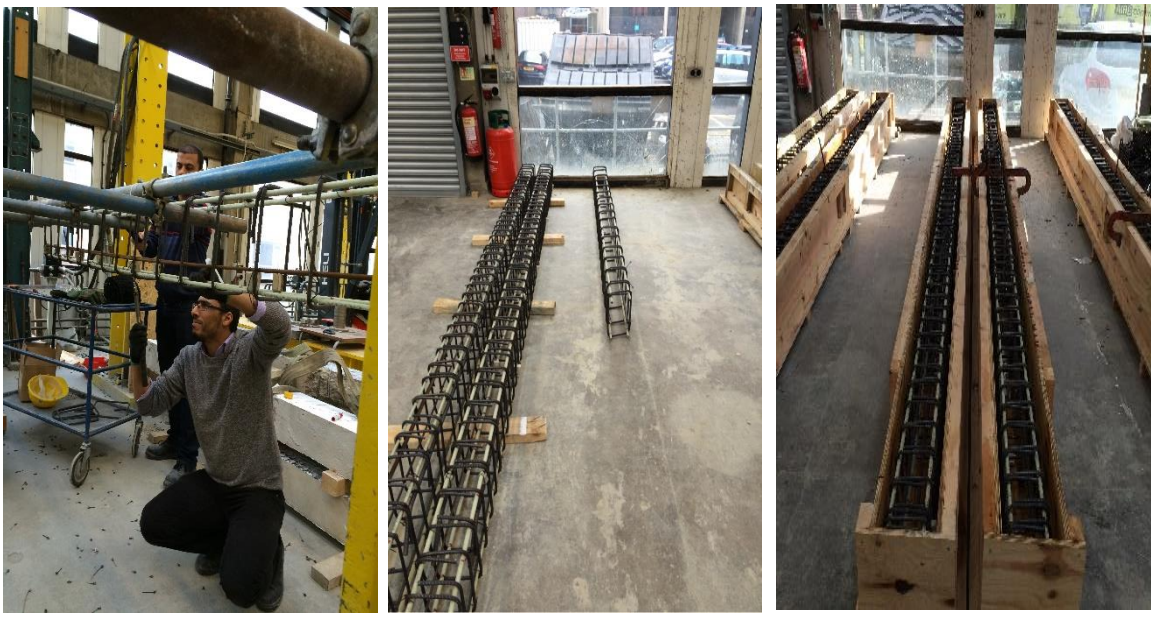

Figure 3.7 Reinforcement work and cage positioning

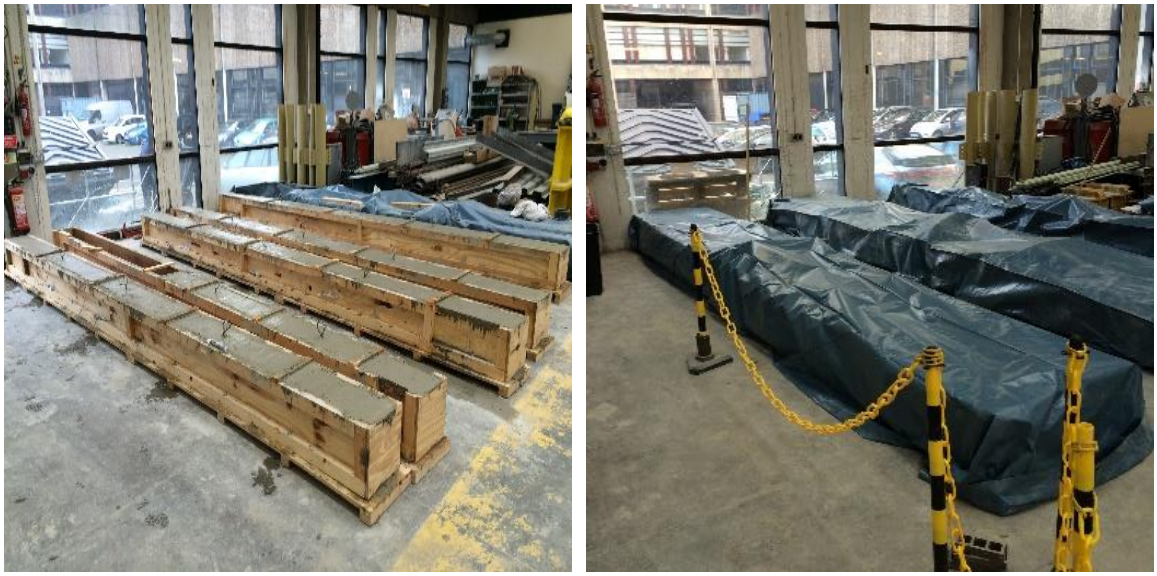

a) Test specimens after casting

b) Typical view of concrete beams while curing

Figure 3.8 Construction stages of test specimens

3.6 Test Set Up

Each continuous reinforced concrete beam comprised two equal spans supported on two end rollers and one middle hinge support. Each span was loaded at its mid-point as shown in Fig 3.9 via a 1000 kN hydraulic actuator with the use of a top spreader beam. The simply supported beams were

similarly loaded at its mid-span and supported on a roller support at one end and on hinge support at the other end as shown in Fig 3.2. To avoid concrete bearing failure at the load application points, steel plates were used between the supports and the test specimens. The two end steel plates had a width of 100 mm while the middle and loading steel plates had a width of 150 mm. All the steel plates had a minimum length of 200 mm to cover the full width of the beam and a thickness of 15 mm except for the loading plates which were 25 mm thick. Plaster was used, where required, between the beam and the supports or load application points to ensure a uniform load distribution and avoid uneven loading of the specimen. In all tests, a load-controlled rate of 10 kN/min was used to apply equal loads to the two spans. After the formation of the first flexural crack, the loading was put on hold after each load increment to visually inspect the beam in order to monitor crack propagation on one face of the beam.

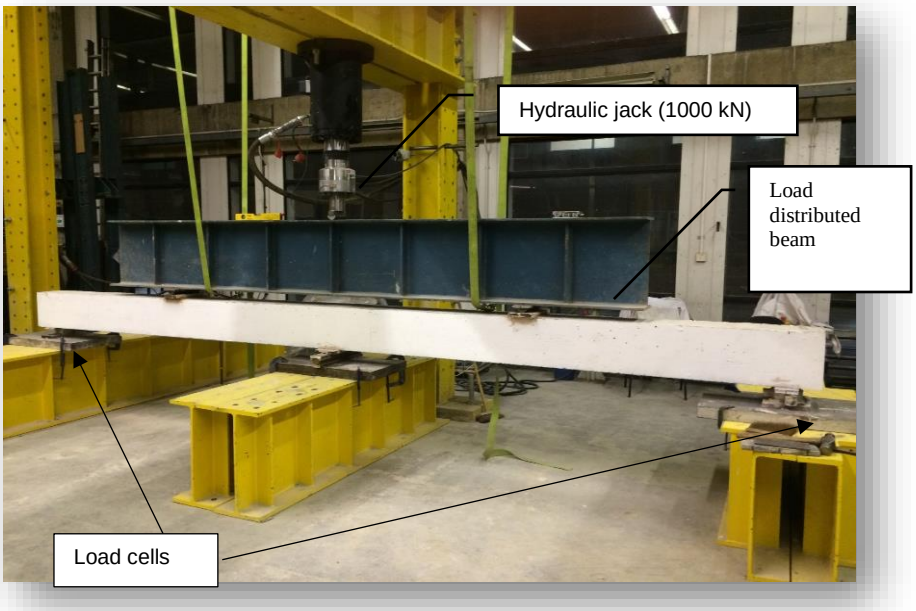

Figure 3.9 Test setup

3.7 Instrumentation

Three load cells were utilised to measure the reactions at the two end supports and the main applied load from the hydraulic ram. Moreover, each continuous beam was instrumented with seven linear variable differential transducer (LVDTs) to measure the deflections at different locations as shown in Fig 3.10. Two LVDTs at the two mid-spans of multi-span continuous beams were used to record the vertical movement of each specimen. Additional two LVDTs were located at equal spacing of $L/4$ on one span of the continuous beams to measure the deflections at these locations, where L is the span length. The last three additional LVDTs were installed at the end and middle supports to measure any movement at supports. Three electrical strain gauges of 5 mm length were also mounted on the tensile longitudinal steel bars at mid spans and internal support to monitor the strain variation during loading as shown in Fig 3.11. All load cells, LVDTs and strain gauges readings were automatically registered at each load increment using a data logger. In addition, digital

image correlation (DIC) was carried out using a digital single lens reflex (DSLR) to monitor deflection profile of the beams tested. The camera was mounted on a tripod with its axis perpendicular to the area of interest (mid-span region). A good variation of the specimens' texture was achieved by applying a random speckled black/white pattern (as shown in Fig 3.12) to one side of the beams. Images were taken at 5 kN load increments at first stage of loading (before first cracking), then at 10kN load increments.

Figure 3.10 Position of LVDTs and cameras for test specimens

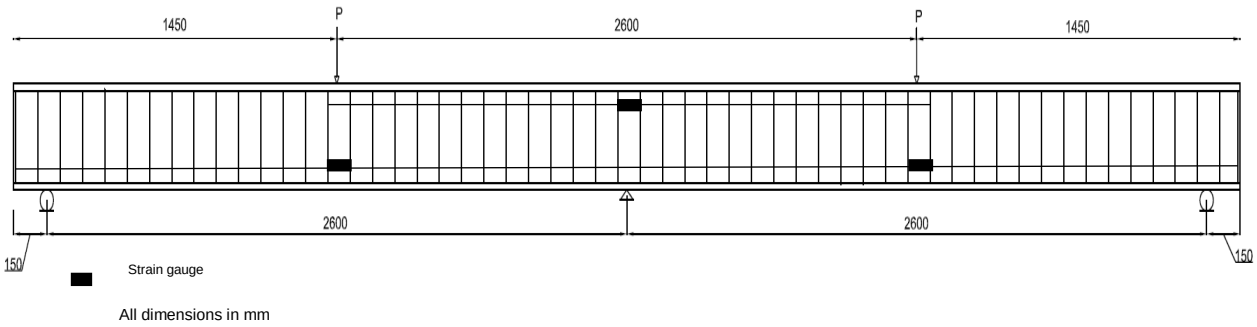

Figure 3.11 Position of strain gauges for test specimens

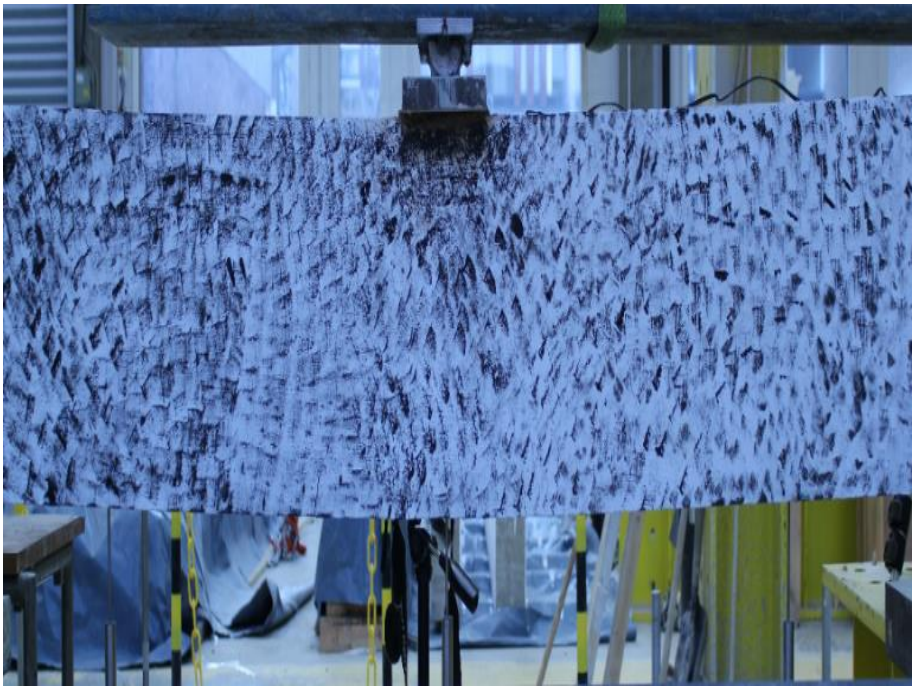

Figure 3.12 The random speckled pattern used for DIC analysis

3.8 Summary

An experimental programme has been presented in detail in this chapter, including designed specimens of hybrid GFRP-steel beams, material property tests GFRP and steel bars, test up and instrumentation, and the full procedures of the experimental tests. The main aim of the experiments is to investigate the complete behaviour of continuous concrete beams reinforced with hybrid GFRP-steel bars experimentally and to be able to conduct a parametric study by analytical model and finite element model which will be presented in the chapters 5 and 7, respectively.

In the following chapter, the results and observations from the beam tests are provided in detail. These include the failure load and mode, flexural performance, load-deflection curves, strain variation on the steel bars surface, cracking patterns, and the level of moment redistribution for each beam.

CHAPTER FOUR

RESULTS AND DISCUSSIONS

4.1 Introduction

This chapter presents the experimental results of tested specimens. As previously described in chapter three, nine continuously and two simply supported concrete beams reinforced with a combination of GFRP and steel bars were tested. Additionally, two continuous concrete beams reinforced with either GFRP or steel bars and one simply supported beam reinforced with GFRP bars were tested as control beams. The behaviour of the tested beams during the test was carefully observed. The displacement at different locations, the strains of steel reinforcement, the reactions at the end supports, and crack width at mid-span were recorded using an automatic data acquisition system. The experimental results including the deflection, ultimate load and strains would be used in chapter five, six and seven for validation purposes.

For the sake of clarity of the reported results, the tested beams are divided into two series. Series I is related to beams investigating the effect of increasing either the steel or GFRP longitudinal reinforcement ratio in sagging and hogging regions with same ratio, while Series II investigates the effect of different hybrid reinforcement ratios in critical sections. Series I consists of ten beams, C-S-1, C-G-1, C-H-1, C-H-2, C-H-3, C-H-4, C-H-5, S-G-1, S-H-1 and S-H-2, whereas series II consists of four beams, C-H-6, C-H-7, C-H-8, and C-H-9, in addition to beam C-H-1, C-S-1 and C-G-1 from the previous group for comparison purposes.

4.2 Results and Discussion of Beams of Series I

4.2.1 Crack Propagation and Reinforcement Strains

Crack propagation was monitored and manually marked throughout the beams testing. The crack patterns in the multi-span continuous reinforced concrete beams at failure were sketched in Fig. 4.1. The first visible cracking load of each beam tested is presented in Table 4.1. Generally, cracks were initially observed in the maximum moment regions below the point loads and over the internal support but propagated towards the compressed concrete zone with the load increase. At later stage of loading, more cracks appeared outside the maximum moment regions along the beams as shown in Fig. 4.1. The concrete beam reinforced with only steel bars exhibited a higher first cracking load than that reinforced with only GFRP bars due to the higher axial stiffness of steel bars than that of GFRP bars. On the other hand, the first crack of hybrid GFRP/steel beams occurred at a higher load than that of the steel beam C-S-1, except hybrid beam C-H-1. This is attributed to the fact that the axial stiffness (*EA*) of the provided hybrid reinforcement at critical sections was higher than that of beam C-S-1. The crack lengths in the hybrid specimens and steel beam C-S-1 were smaller in comparison to that in GFRP beam C-G-1. This indicates that the presence of steel bars in hybrid beams can restrain the fast and deep propagation of cracks observed in the GFRP reinforced concrete beam. In addition, for beams with hybrid reinforcement, the crack spacing is lower and the number of cracks is higher than that in the GFRP beam as shown in Fig. 4.1. As the load increased, shear stresses had a profound effect and led to inclined cracks in beams C-H-2, C-H-4 and C-H-5. These cracks diagonally propagated towards the vicinity of load points on the compressive

side of these beams. However, beam C-H-3 exhibited a major horizontal crack in compression zone of sagging section at later stage of loading (near to failure) followed by a diagonal crack towards the intermediate support. Horizontal cracks were observed in Beams S-G-1 and S-H-1 at the bottom reinforcement level indicating deboning between GFRP bars and concrete. This can be attributed to the high deformation experienced by the aforementioned beams, which led to the slippage between GFRP bars and surrounding concrete.

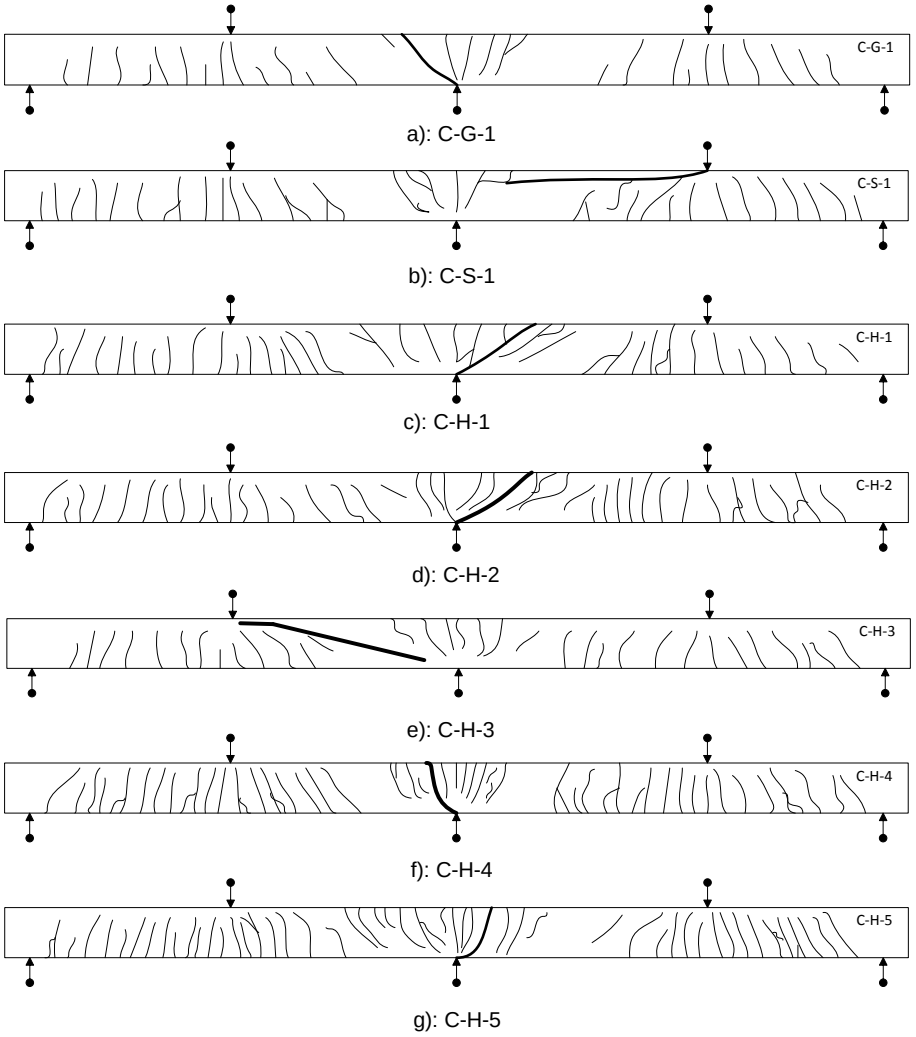

Figure 4.1 Crack patterns at failure of continuous concrete beams tested

Table 4-1 First cracking and total experimental failure loads of beams tested

Beam notation	First cracking loads (kN)		Failure loads(kN)	Observed failure mode
	Sagging	Hogging		
C-S-1	47	45	511	Flexure-tension failure at both mid-span and middle support
C-G-1	33	30	309	Concrete crushing
C-H-1	43	40	465	Flexure-tension failure at both mid-span and middle support
C-H-2	52	50	571	Flexure-shear failure at middle support
C-H-3	57	55	589	Flexure-tension failure at both mid-span and middle support
C-H-4	63	60	665	Flexure-shear failure at middle support
C-H-5	68	65	781	Flexure-shear failure at middle support
S-G-1	10	N/A	118	GFRP bar rupture at mid span
S-H-1	9	N/A	94	Flexure-tension failure at mid-span
S-H-2	15	N/A	169	Flexure-tension failure at mid-span

Note that the first cracking and failure loads are the total loads acting on each beam tested, i.e. the sum of the two mid-span point loads in case of continuous beams and the mid-span point load in case of simply supported ones.

The relation between the total applied load and the width of flexural cracks at the sagging moment region is shown in Figs 4.2 and 4.3. The results were obtained by recording the width of cracks using high quality digital cameras. Two cameras were used to capture the flexural crack of sagging zone at mid-spans. The images of cracks at mid-spans were processed by Image-Pro Plus software version 6.0. As for continuous concrete beams, only one side flexural crack is presented in Fig 4.2 due to the similarity in crack widths between the two spans. It can be observed that increasing the amount of longitudinal GFRP or steel re-bars had a clear effect on flexural crack widths. However, the addition of steel reinforcement had a more significant effect on reducing the crack width than GFRP reinforcement.

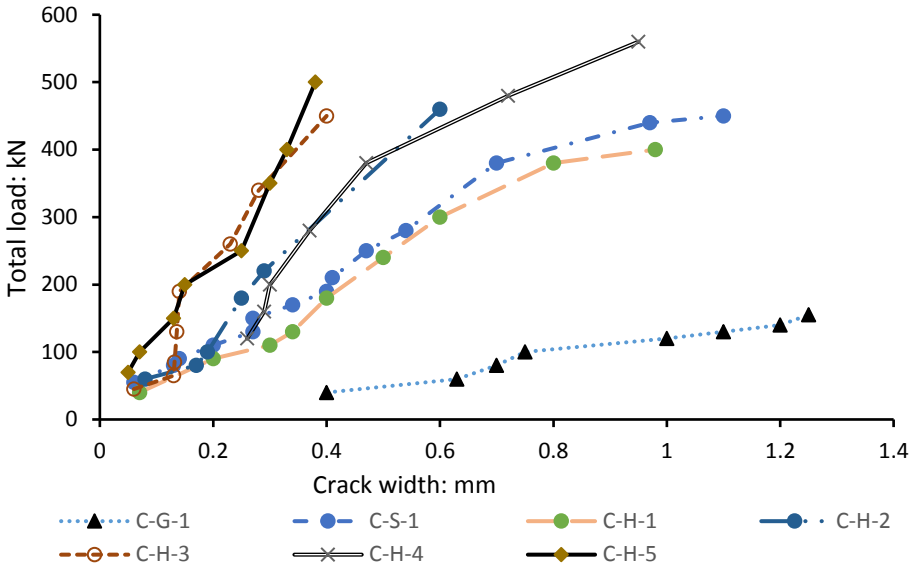

Figure 4.2 Mid-span crack width of continuously supported beams tested

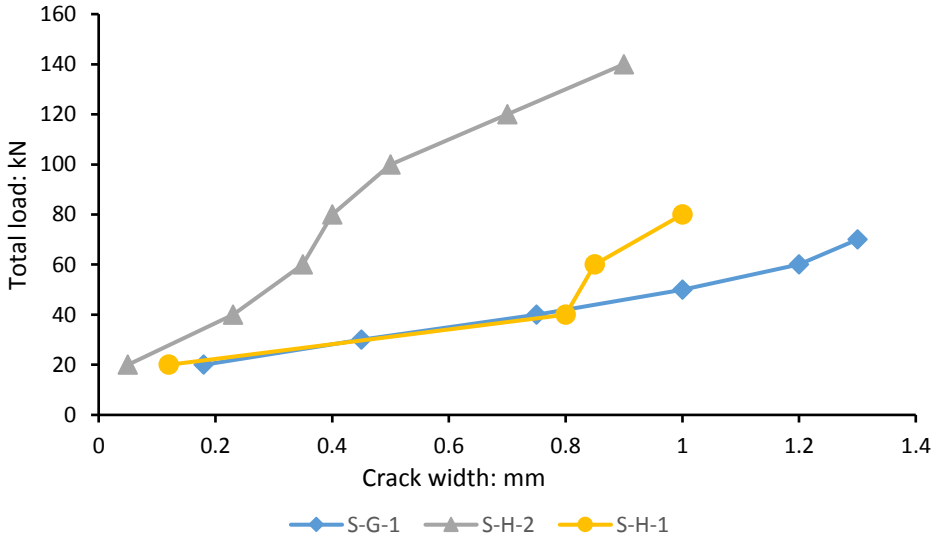

Figure 4.3 Mid-span crack width of simply supported beams tested

Figures 4.4 and 4.5 present the tensile strains in the bottom steel reinforcement at the mid-span and top steel reinforcement at the internal support against the total applied load for the multi-span continuous beams tested, respectively. After the first crack, the steel strains increased at an almost a constant rate until yielding occurred at either the sagging or hogging

region. In general, all hybrid GFRP/steel beams exhibited their first steel yielding in the hogging regions as shown in Figs. 4.4 and 4.5 as the hogging region is exposed to higher stresses than sagging zone for the same total applied load. On the other hand, for specimen C-S-1, yielding of tensile steel in the sagging and hogging regions occurred at very similar loads as shown in Figs. 4.4 and 4.5, respectively. This is attributed to the difference in flexural rigidity between the mid-span and over-support sections as the steel reinforcement ratio in compression zone at hogging region is higher than that of sagging region. Generally, the results show that increasing either GFRP reinforcement ratio (C-H-5) or steel reinforcement ratio (C-H-3) delayed the yielding of tensile steel, hence increased the yielding and ultimate loads of beams tested.

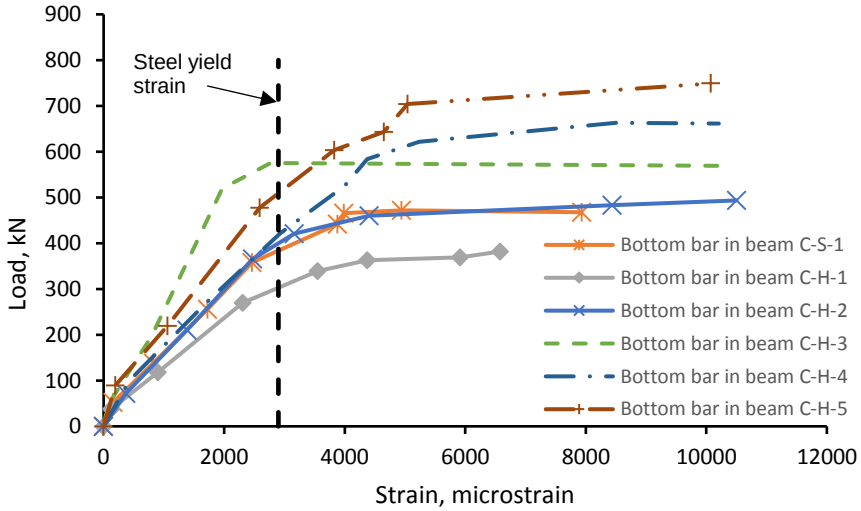

Figure 4.4 Total applied load versus tensile steel strains at mid-span of continuous beams tested

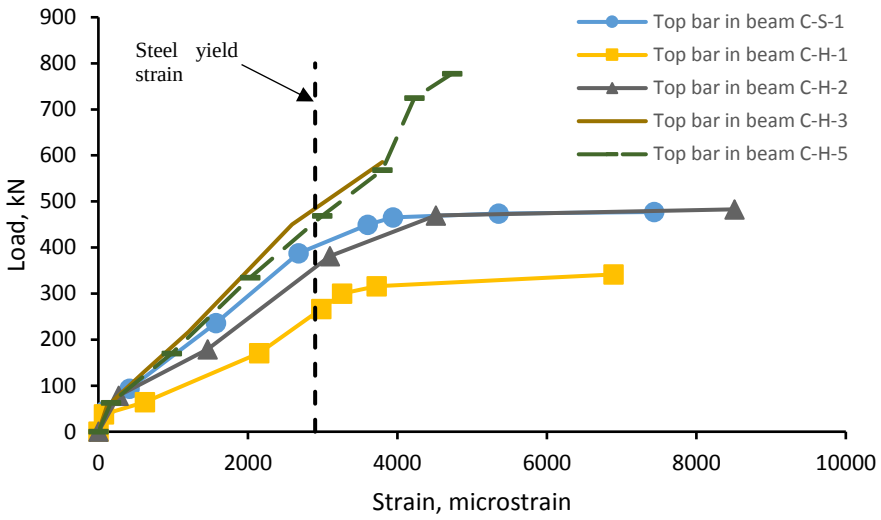

Figure 4.5 Total applied load versus tensile steel strains at middle support of continuous beams tested

4.2.2 Failure modes

Four different failure modes were observed in the experimental tests as shown in Fig. 4.6, summarized in Table 4.1 and explained below.

Mode 1: Conventional Ductile Flexural Failure

This mode was demonstrated by the continuous concrete beam C-S-1, that reinforced only with steel bars. The failure of C-S-1 eventually occurred due to yielding of tensile steel reinforcement at both middle support and mid-span sections followed by concrete crushing as shown in Fig. 4.6-A.

Mode 2: Bar Rupture

This mode was illustrated by beams S-G-1 and S-H-1 as shown in Figs. 4.6-B and 4.6-C. As for beam S-G-1, it was designed to have reinforcement ratio of GFRP at the bottom layer higher than the balanced reinforcement ratio (ρ_b). Owing to the reinforcement ratio, it was expected that strains in GFRP reinforcement would not reach its rupture limit before the full exhaustion of the

ultimate concrete strain. Such anticipation has not been exhibited by beam S-G-1. This is mainly due to the difference between the assumed concrete compressive strength ($f_{cu} = 40MPa$) that used to find the balanced reinforcement ratio (ρ_b) and the actual compressive strength ($f_{cu} = 72\ MPa$) of concrete used in casting such beam. This difference resulted in increasing the balanced reinforcement ratio from 0.17 to 0.32.

For beam S-H-1, rupture of GFRP bars occurred post the yield of steel reinforcement. The beam experienced this mode of failure due to the concrete compressive strength increase as the concrete section was mainly designed for compressive strength ($f_{cu} = 40MPa$). This increase resulted in change of the failure mode from steel yielding before concrete crushing to GFRP rupture before concrete crushing.

Mode 3: Yielding of Steel Reinforcement Followed by Crushing of Concrete

Hybrid beams C-H-1, C-H-3 and S-H-2 exhibited this mode of failure as shown in Figs 4.6-D, 4.6-F and 4.6-J. The failure of beam C-H-1 was in a ductile manner due to crushing of concrete in the compressive zone after yielding of steel bars. The failure in beam C-H-3 was compression failure at both sagging and hogging regions, followed by a major horizontal crack propagated towards the compression side of the middle support, causing a complete loss of load capacity of beam C-H-3. Failure of specimen S-H-2 was initiated by crushing of concrete at sagging zone after yielding of the steel reinforcement took place in the tension zone.

Mode 4: Concrete Crushing Combined with Shear Failure

This type of failure was observed in hybrid beams C-H-2, C-H-4, C-H-5 and GFRP beam C-G-1. The presence of high reinforcement ratio in compressive zone at middle support sections of beams C-H-2, C-H-4 and C-H-5 increased the compression resistance of the failed section. Such increase in compression force allowed the shear force to have a profound effect on the failure process as shown in Figs. 4.6-E, 4.6-G and 4.6-H, respectively.

Beam C-G-1 which was reinforced with an over reinforcement ratio of GFRP bars at the bottom and top layers experienced this mode of failure (see Fig. 4.6-I). At a late stage of loading, wide cracks appeared over the intermediate support section, indicating bond-slip between GFRP bars and concrete. A diagonal shear crack emerged immediately after the flexural concrete crushing at the middle support region.

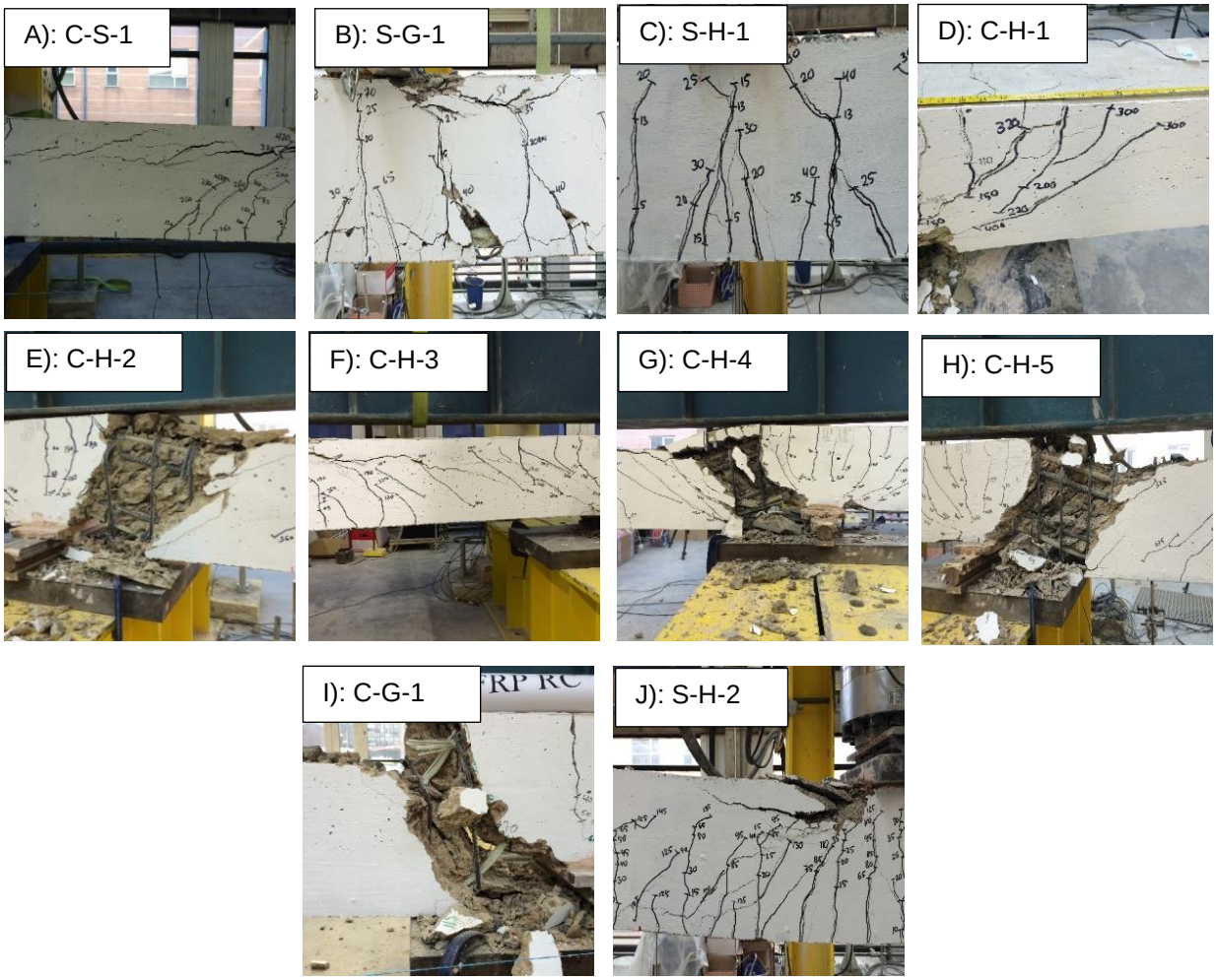

Figure 4.6 Failure modes of tested beams

4.2.3 Load Capacity

Table 4.1 and Figure 4.7 present the failure loads of the beams tested. The failure loads of simply supported beams S-G-1 and S-H-2, respectively, were around 77% and 73% of the total failure loads of beams C-G-1 and C-H-1, respectively. This comparison between the failure loads of the simply supported beams S-G-1 and S-H-2; and that of the continuous hybrid C-G-1 and C-H-1 beams is due to the fact that each compared set of beams were reinforced with the same area of reinforcement. In comparison with beam C-H-1, beam C-H-5 that was reinforced with higher reinforcement ratio of GFRP

bars tolerated more loads than beam C-H-3 that was reinforced with higher reinforcement of steel bars. This is attributed to the fact that GFRP bars play an important role to resist loading after yielding of steel reinforcement. In addition, the high compressive strength of beam C-G-5 contributed in load capacity increase. The results show that the load capacities of hybrid reinforced concrete continuous beams C-H-2, C-H-3, C-H-4 and C-H-5 were, respectively, around 1.2, 1.26, 1.4 and 1.7 times that of the control beam C-H-1. This confirms that GFRP reinforcement is mainly responsible for enhancement of load capacity. Although the steel reinforcement ratio used to reinforce the critical sections of beam C-S-1 had similar strength of that used in beam C-G-1, beam C-S-1 exhibited a higher load capacity than that of beam reinforced with pure GFRP bars. This is due the fact that the bond strength of GFRP bars is lower (60-90%) than that of steel bars (Benmokrane and Tighiouart, 1996).

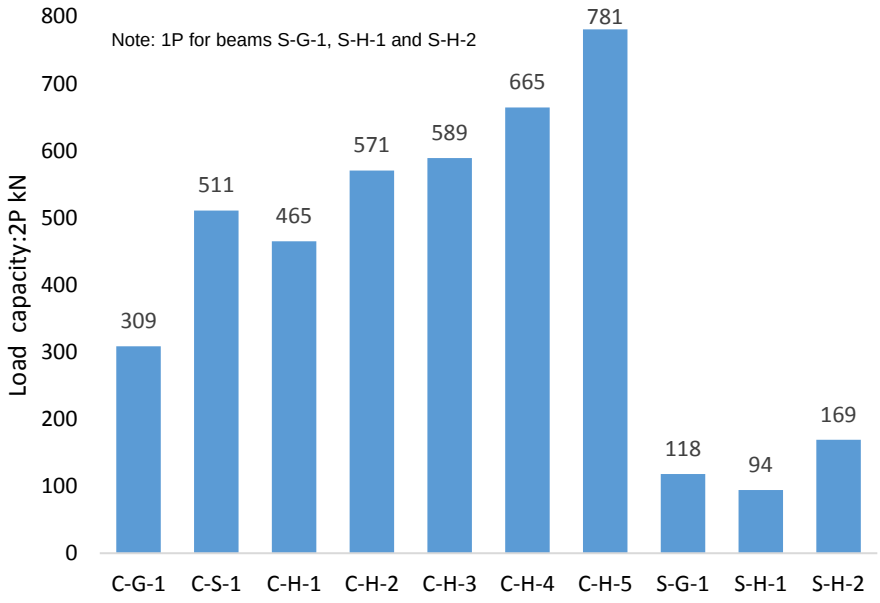

Figure 4.7 Experimental load capacities of tested beams

4.2.4 Load Deflection Response

The relationship between the total applied load, *2P* and the recorded deflection at mid-span is shown in Fig. 4.8. There was no noticeable measured movement at the end and middle supports; therefore not presented. Due to the similarity in the recorded vertical movement in the two spans of each beam, only one side mid-span deflection is presented. All beams demonstrated linear load-deflection behaviour up to the cracking load. After the linear phase is reached its limit by concrete cracking, the beam stiffness is controlled by reinforcing bars which play a significant role in post cracking stage. However, there is a remarkable variation between tested beams in terms of reduction in stiffness, which resulted in the difference in cracking behaviour among tested beams. This is mainly due to the difference in reinforcement ratios used to reinforce concrete sections. The flexural stiffness after cracking is the highest for steel, followed by hybrid GFRP/steel with high reinforcement ratio, then hybrid GFRP/steel beams with low reinforcement ratio, followed by pure GFRP beam. It could be noticed that the load-deflection curves of hybrid-beams showed three different regions as follows; pre-cracking, post cracking, and yielding of steel. Whereas the GFRP beam exhibited bilinear curve in both un-cracked and cracked stages. For hybrid GFRP/steel reinforced concrete beams, yielding of tensile steel reinforcement further reduces the beam stiffness to a similar level of pure GFRP beam stiffness. While the stiffness of hybrid GFRP/steel reinforced concrete beams C-H-1, C-H-2 and C-H-4 lies between these of their counterpart steel and GFRP reinforced concrete beams, the flexural rigidity of beams C-H-3 and C-H-5 is similar to that of beam C-S-1 up to the yielding load of steel control beam. Overall, the amount

of GFRP and steel reinforcements used is a key factor in enhancing the flexural stiffness and, consequently, reducing deflections of the beams tested. As seen in Fig. 4.8, the stiffness of hybrid beams increased with either the increase of steel or GFRP reinforcement after the first cracking; the higher the ratio of hybrid reinforcement, the higher the stiffness. On the other hand, due to the elastic and brittle nature of GFRP reinforcement, the ductility of the hybrid beam specimens reinforced with larger GFRP reinforcement ratio was reduced as shown in Fig. 4.8. It is important to mention that this result could be beneficial for establishing a guide line to determine a suitable reinforcement ratio for hybrid GFRP/steel reinforced concrete beams, so that the achieved stiffness behaviour of hybrid beams can be according to the serviceability limit state requirements. The allowable deflection according to Canadian Standard Association (CSA) (2002) ranges from 5.5-15 mm (L/480-L/180, where L is the beam span) based on the type and function of the structure. It can be noticed that the maximum deflections corresponding to the calculated service loads for hybrid beams C-H-1, C-H-2 and C-H-3 were 5, 5.4, 4.5 mm, respectively, while hybrid beams C-H-4 and C-H-5 did not satisfy the low serviceability limit for certain structural applications in which the deflections corresponding to the service loads were 6.5 and 6.3 mm, respectively.

In all hybrid beams tested, the presence of steel reinforcement had a profound effect on enhancement of the beam stiffness and load capacity after cracking. While GFRP bars showed an important role in resisting load after yielding of steel. An improvement in terms of deformability and ductility can also be observed for hybrid beams in comparison with the C-G-1 and C-S-1 reference beams.

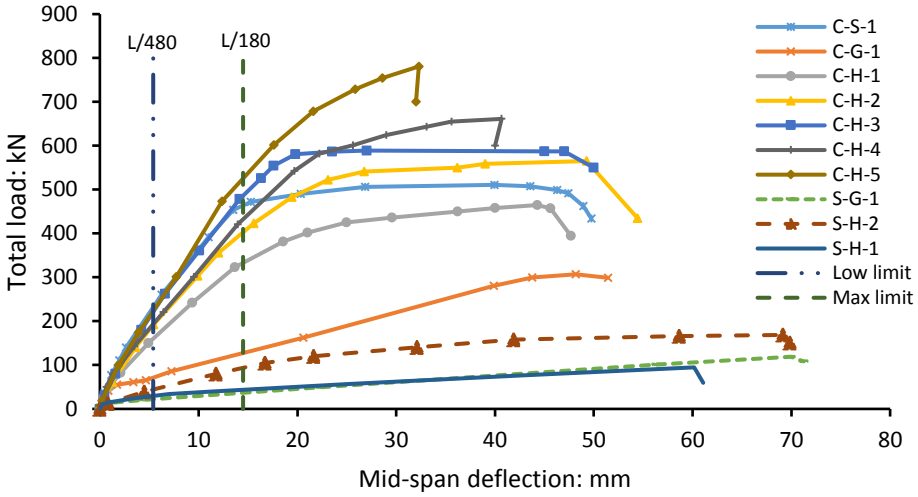

Figure 4.8 Load-deflection response of the tested beams

4.2.5 Redistribution of Support Reactions and Bending Moments

Two load cells were used at the end supports to measure the reactions. As the beams were statically indeterminate, the measured end support reactions, *R*, were used to calculate the actual internal forces, mainly bending moments, at any location along the length of the specimens.

Figure 4.9 shows the load transferred to the end support against the total applied load for each multi-span continuous beam tested. To assess the amount of load redistribution, the calculated end support reaction obtained from elastic analysis (R=0.312P), was also plotted in Fig. 4.9. As expected, before concrete cracking, the measured end support reaction of all multi-span continuous beams was very close to that obtained from the elastic analysis as shown in Fig. 4.10. Similar load redistribution behaviour was observed for all beams. Due to the brittle behaviour of GFRP bars and ductile behaviour of steel bars, it was expected that distinctive load redistribution would be shown by beam C-S-1 in comparison to beam C-G-1 reinforced with only GFRP bars. As can be seen in Figs. 4.9 and 4.10, such anticipation has not been exhibited

by beam C-S-1. This is accredited to the small difference between the sagging and hogging moments produced by the loading system used in the experiments; and the similar amount of steel reinforcement (three bars of 16 mm diameter) at the sagging and hogging regions of the steel reinforced concrete beam tested. As the amount was the same, strains in the top and bottom bars were similar and consequently, the yielding point for the top and bottom steel reinforcement was near enough to be compatible as shown in Figs. 4.4 and 4.5.

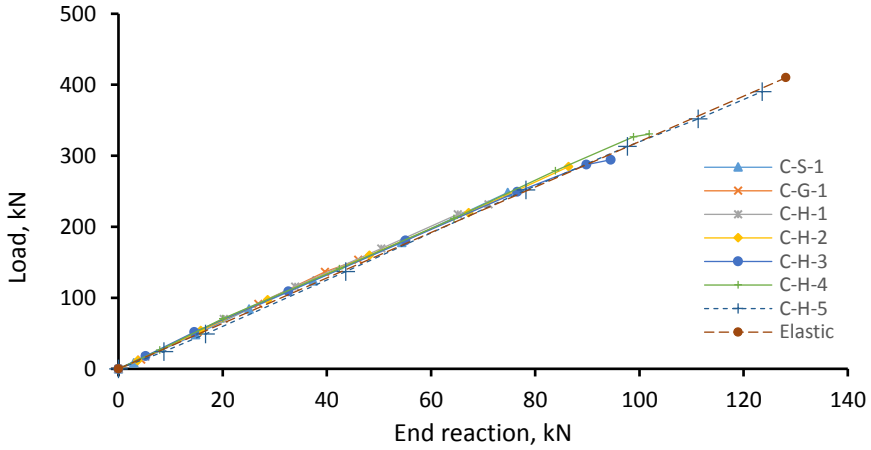

Figure 4.9 Load-end reactions relationship for the tested beams

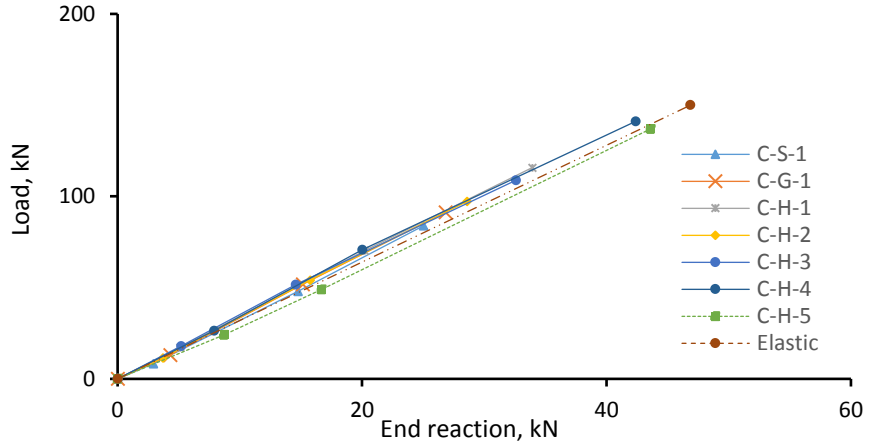

Figure 4.10 End reactions - Loads below 180kN relationship for the tested beams

All continuous hybrid GFRP/steel reinforced concrete beams tested exhibited a similar trend of end support reactions. They failed, however, at different loads.

For evaluating the amount of moment redistribution, β, in the beams tested, the measured sagging and hogging bending moments; and the elastic bending moment at critical sections along the hybrid continuous beam span at failure are presented in Fig. 4.11. The moment redistribution ratio for the mid-span and over support sections, which are given in Fig.4.11, can be obtained by comparing the actual and elastic bending moments as given by Eq (4.1).

A positive value of β indicate that the region has gained a moment greater than the elastic moment, whereas a negative value indicate the opposite.

$$\beta = \left(\frac{M_m - M_e}{M_e}\right) \times 100\% \quad (4\text{-}1)$$

where M_m is the bending moment obtained from experiments using the measured end support reaction and mid-span load and M_e is the bending moment calculated from elastic analysis at failure load.

Figure 4.11 shows the experimental and elastic bending moment distribution at failure along the continuous beam span. The hybrid beams tested showed similar limited moment redistribution behaviour to beam C-S-1.

For example, the maximum recorded end reaction of beam C-H-1 corresponding to the failure load, $P = 232.4\ kN$, was around $71\ kN$. While the maximum calculated (based on elastic analysis) end reaction was $75\ kN$. Therefore, as shown in Fig 4.11, the bending moment at mid-span section, calculated from the measured end support reaction of beam C-H-1, was $92.3\ kNm$, which represents 97.5% of the calculated elastic moment of $94.5\ kNm$ at the failure load $P = 232.4\ kN$. This would be mainly attributed to the same reinforcement ratio at the top and the bottom along the beam length in which leads to similar stiffness of the beams cross sections at middle support and mid-span regions.

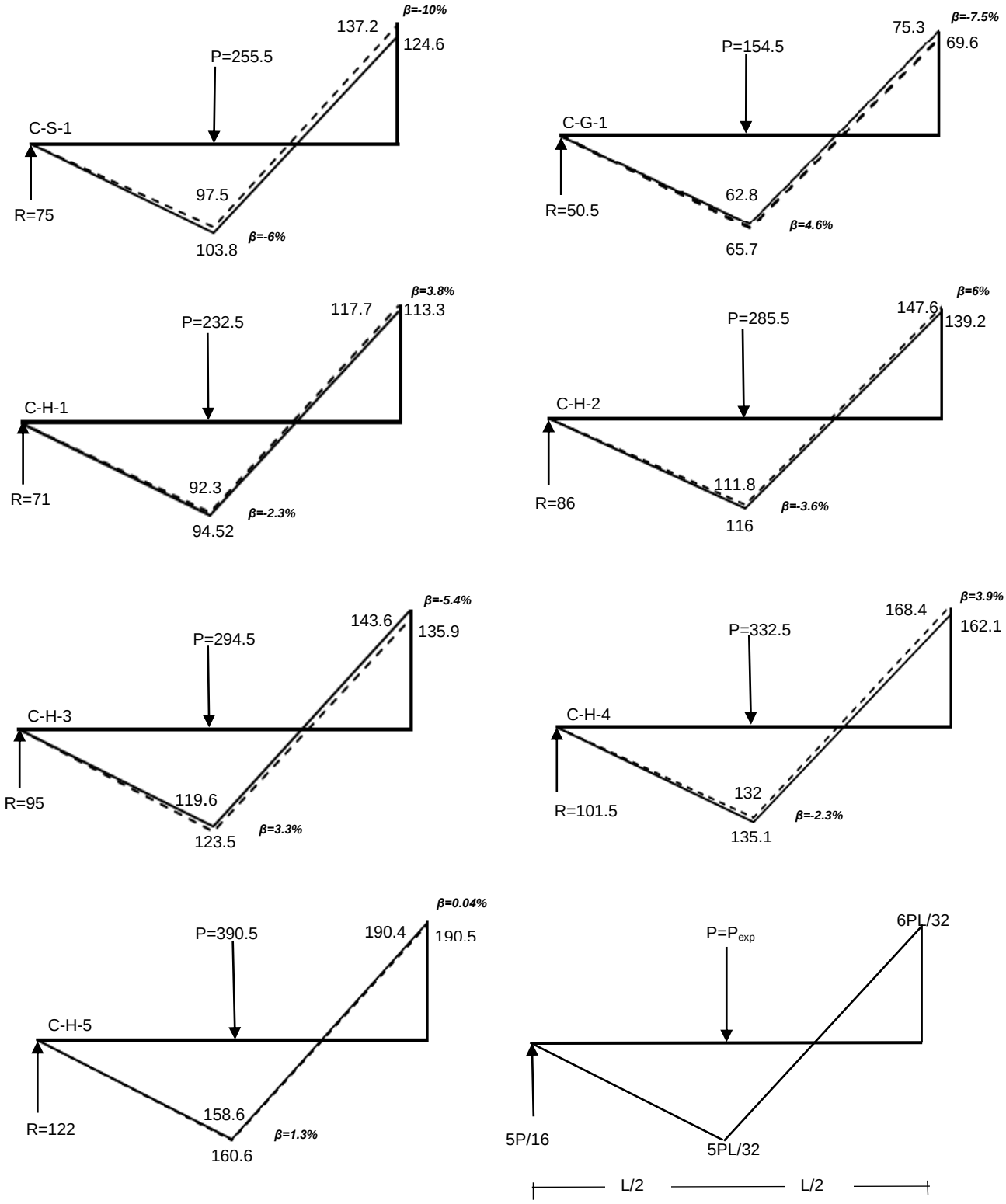

Figure 4.11 Actual versus elastic bending moment at failure

4.3 RESULTS AND DISCUSSION OF BEAMS OF SERIES II

This section presents the experimental results of four tested beams that mainly investigate the effect of longitudinal hybrid reinforcement ratio in sagging and hogging regions on the behaviour of continuous beams reinforced with hybrid GFRP-steel bars. In addition, the test results of the control beams (C-S-1, C-G-1 and C-H-1) are presented for comparison purposes. The main investigated parameter in this section was the hybrid reinforcement ratio in sagging and hogging regions.

4.3.1 Crack Propagation and Reinforcement Strains

Figure 4.12 shows the crack patterns in series II of multi-span continuous hybrid reinforced concrete beams at failure. Generally, the cracking pattern of beams C-H-6, C-H-7, C-H-8 and C-H-9 was similar. Table 4-2 presents the first visible cracking load of all beams in this series. Generally, cracks were first observed at the hogging region for beam C-H-6 and at sagging region for beam C-H-7 at a load of 40 kN, respectively, followed by a crack in the opposite region region at a load of 45 kN and 35 kN, respectively. The number of cracks at the middle support in the hogging region of beam C-H-7 is higher than those in beam C-H-6; whereas the opposite in the sagging region as shown in Fig 4-12.

For beam C-H-8, the first crack was observed simultaneously at mid-span and over middle support at a load of 35 kN. The cracking behavior at the middle support was similar to beam C-H-7 in the hogging region. This might be attributed to the similarity in hybrid reinforcement at the tension zone of the middle support.

For beam C-H-9, the first visible crack occurred at the middle support at a load of 25 kN followed by a crack in the sagging zone at a load of 30 kN. Due to similarity in hybrid reinforcement ratio in beam C-H-8 and C-H-9 at mid-span sections, the cracking behavior in the vicinity of the mid-span region was similar. Comparison between beam C-H-9 and beam C-H-6 showed that at a total applied load of 240 kN, the effect of increasing steel reinforcement ratio in the hogging zone resulted in a larger number of cracks. This might be attributed to low bond strength of steel bars in beam C-H-6 due to high stresses and small surface area.

Table 4-2 First cracking and total experimental failure load of beams tested

Beam notation	First cracking loads,$2P_{cr}$ (kN)		Total experimental failure load $2P$: (kN)	Observed failure mode
	Sagging	Hogging		
C-H- 6	45	40	452	Flexure-tension failure at both mid-span and middle support
C-H- 7	40	35	364	Flexure-tension failure at both mid-span and middle support
C-H- 8	35	35	450	Flexure-tension failure at both mid-span and middle support
C-H- 9	30	25	423	Flexure-tension failure at both mid-span and middle support

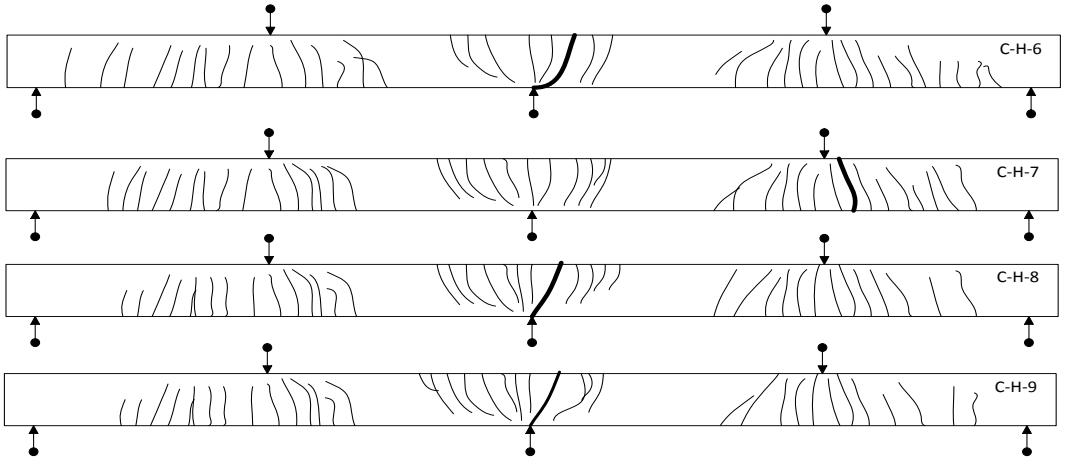

Figure 4.12 Crack patterns at failure of continuous concrete beams tested

The relation between the total applied load and the width of flexural cracks at the sagging moment region is shown in Fig 4.13. The results were obtained by recording the width of cracks through high quality digital cameras. Two cameras were used to capture the flexural crack of sagging zone at mid-spans. The images of cracks at mid-spans were processed by Image-Pro Plus software version 6.0. It can be observed that increasing the amount of longitudinal hybrid GFRP- steel re-bars had a clear effect on flexural crack widths. In comparison with hybrid beam C-H-1, beam C-H-6 which reinforced with similar reinforcement ratio at mid span section, it exhibited less crack width at same level of loading. This is attributed to the high compressive strength of concrete C-H-6.

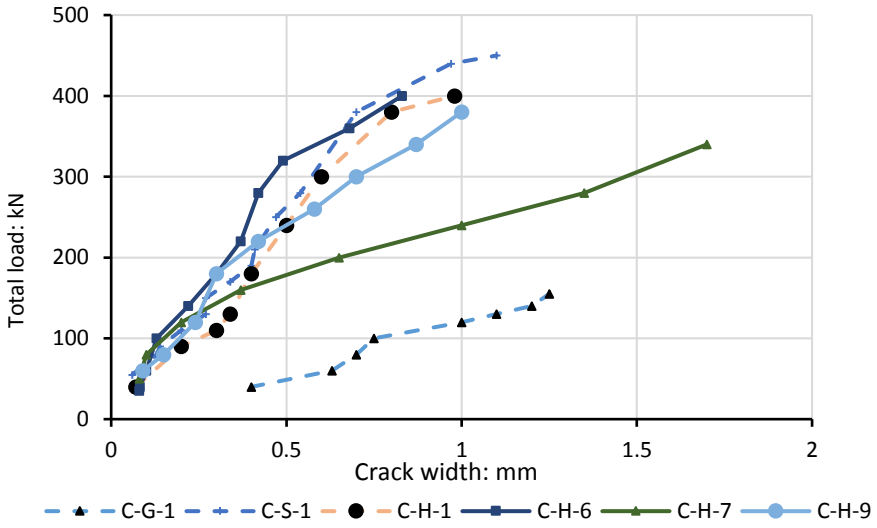

Figure 4.13 Mid-span crack width of simply supported beams tested

Figures 4.14 and 4.15 present the tensile strains in the bottom steel reinforcement at the mid-span and top steel reinforcement at the internal support against the total applied load for the multi-span continuous hybrid beams tested, respectively. Generally, specimens exhibited a tri-linear steel strain response. The tensile strain in tensile longitudinal steel bars were very small prior to the cracking stage. Once crack formed, a sudden increase of strain in the tensile steel reinforcement was noticed at the sagging and hogging regions. For specimen C-H-6, the steel yielded first in the hogging region. Conversely, the tensile steel reinforcement in the sagging zone yielded first in beam C-H-7. This is due to the fact that the hybrid reinforcement ratio provided, especially the area of steel bars, at mid span and middle support sections in beam C-H-7 and C-H-6, respectively, is less than that at mid span and middle support sections in the aforementioned beams, respectively.

For hybrid beams C-H-8 and C-H-9, the tensile steel bars in the sagging regions yielded almost at the same load level. This is ascribed to the similarity

in the hybrid reinforcement ratio that provided in both sections. In specimens C-H-6 and C-H-9, the experimental tensile steel strain response at hogging and sagging zones, respectively, was incomplete due to malfunction of the corresponding strain gauges.

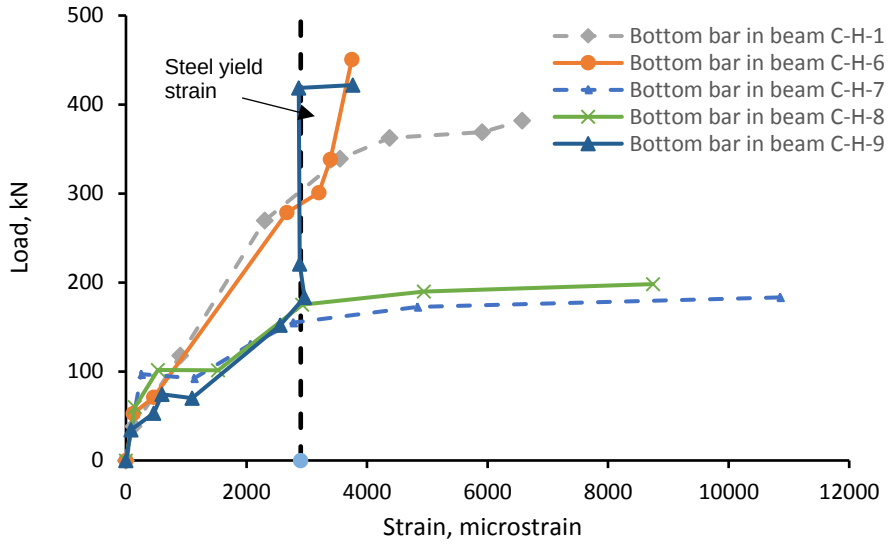

Figure 4.14 Total applied load versus tensile steel strains at mid-span of continuous beams tested

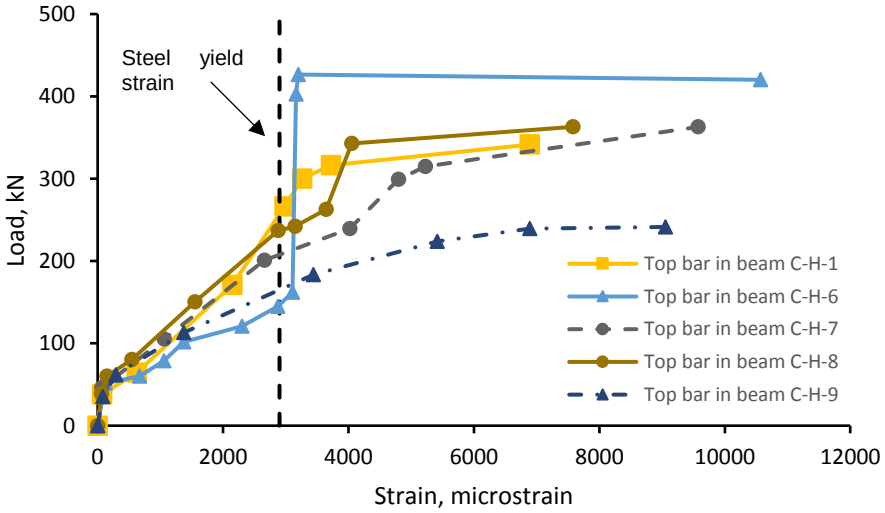

Figure 4.15 Total applied load versus tensile steel response at middle support of continuous beams tested

4.3.2 Failure Modes

All specimens failed in a ductile manner due to yielding of the tensile steel occurred in both sagging and hogging regions followed by concrete crushing at the mid-span sections and over the intermediate support as shown in Fig. 4.16.

In the continuous hybrid beam C-H-6, hogging flexural failure was observed as yielding of the tensile steel reinforcement took place at the hogging region followed by yielding of the tensile steel reinforcement at the sagging region as shown in Fig 4.16-A. As illustrated in Fig 4.16-B, on the other hand, beam C-H-7 exhibited sagging flexural failure due to yielding of the steel bars at tension zone of mid-span region earlier than that at the central support. In addition, the over support and mid span sections, respectively, experienced wide cracks indicating that bond slip would have been occurred as depicted in Figs 4.16A and 4.16B.

Failure of specimen C-H-6 was initiated by crushing of concrete in the hogging region followed by concrete crushing in the sagging region. Conversely, concrete crushing was observed at the beam mid span for beam C-H-7 before occurred at the intermediate support. As for hybrid beams C-H-8 and C-H-9, the failure of the specimens was initiated by concrete crushing in middle support section followed by concrete crushing in mid-span section; and wide cracks at the middle support section.

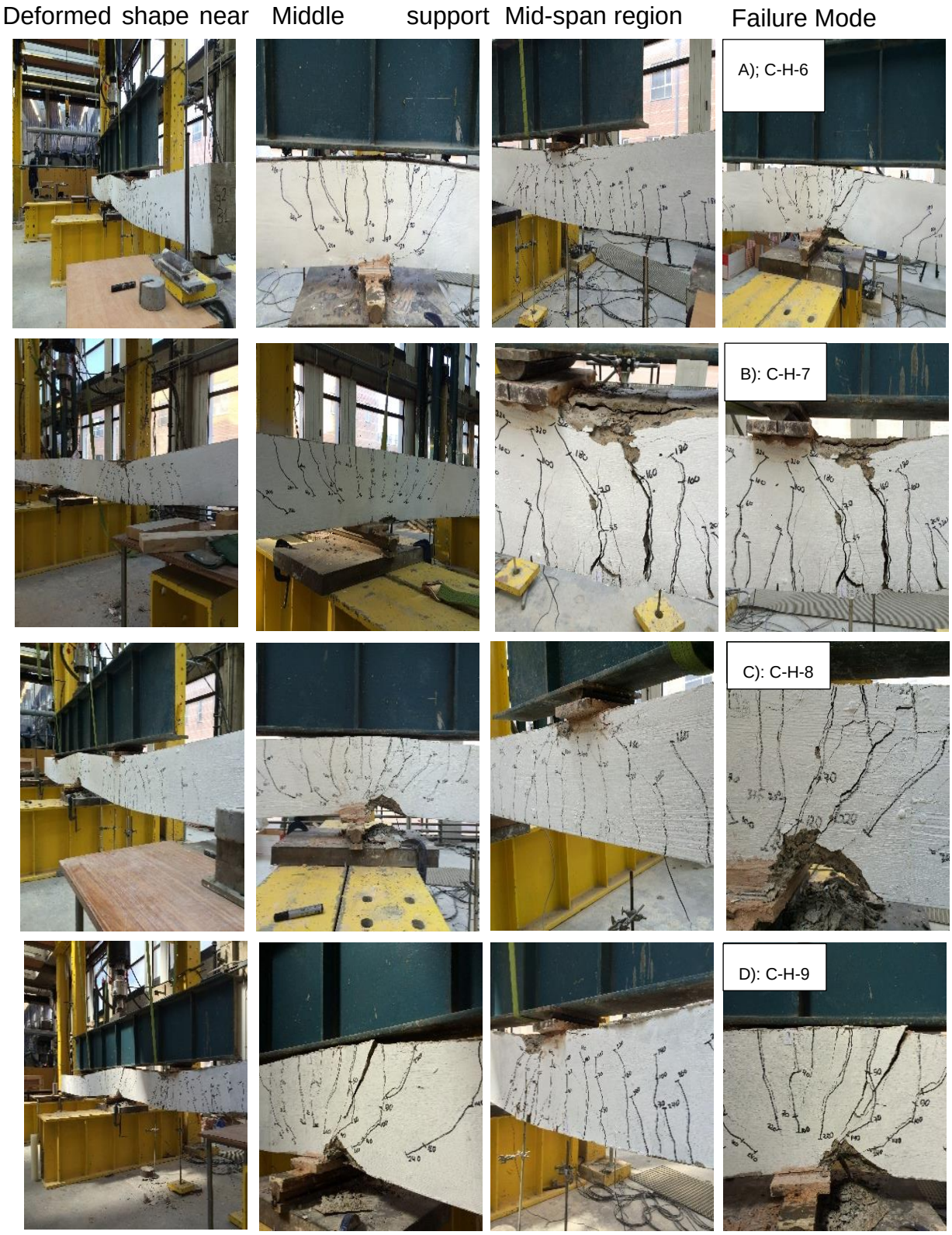

Figure 4.16 Failure modes of tested beams (series II)

4.3.3 Load Capacity

Table 4.2 and Figure 4.17 present the failure loads of the beams tested in group II. For hybrid beams reinforced with different hybrid reinforcement ratios at the sagging and hogging regions, these beams accomplished lower load capacity than hybrid beams reinforced with similar hybrid reinforcement ratio at the mid-span and over mid-support zones.

Figure 4.17 shows that the failure load of beam C-H-6 was higher by approximately 19.5% than that resisted by the beam C-H-7 having an opposite hybrid reinforcement arrangement. In addition, the effect of hybrid reinforcement ratio at the sagging section on load capacity can be seen by comparing results of beams C-H-6 and C-H-7 against results of beam C-H-1. It is clear that there is no noticeable difference between load capacity of beam C-H-6 and C-H-1 as both beams were reinforced with similar hybrid reinforcements in mid-span section. While beam C-H-7 accomplished lower load capacity than beam C-H-1 as beam C-H-7 was reinforced with lower hybrid reinforcement ratio at sagging section than that in beam C-H-1.

In terms of the effect of GFRP reinforcement ratio on load capacity, Fig 4.17 shows that even though the GFRP reinforcement ratio used in beam C-H-8 at hogging section was approximately two times more than that used in beam C-H-9, the failure load accomplished by beam C-H-8 was only higher by approximately 6% than that of C-H-9. This would indicate that the GFRP top reinforcement was ineffective in enhancing the beam load capacity. On the other hand, increasing the bottom GFRP reinforcement ratio has more effect on load capacity increase as exhibited by beam C-H-8 in comparison with C-

H-7, in which both beams having similar hybrid reinforcement at the hogging zone and similar area of steel bars at mid-span section.

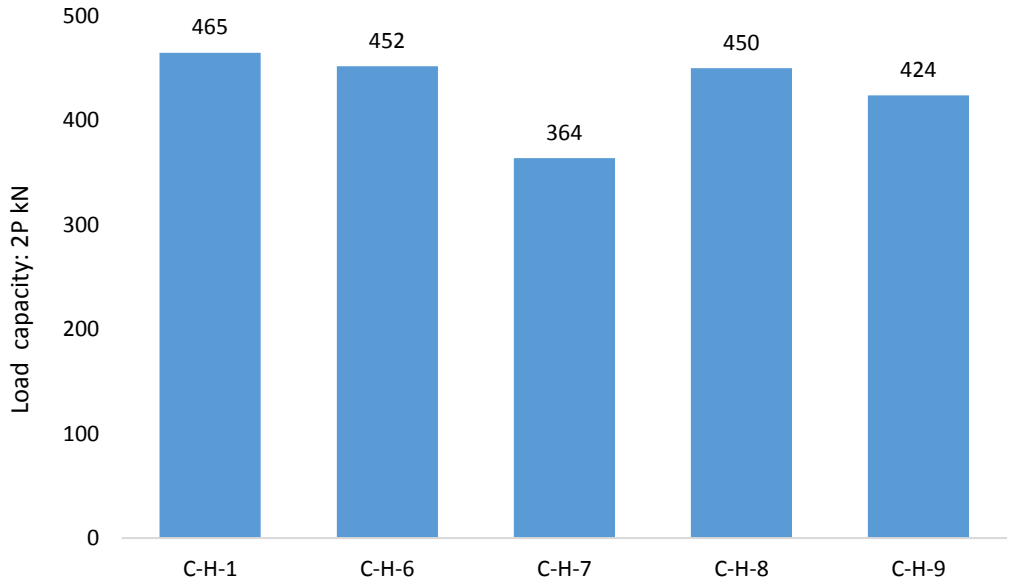

Figure 4.17 Experimental load capacities of tested beams

4.3.4 Load Deflection Response

The deflection responses of specimens C-H-6, C-H-7, C-H-8 and C-H-9 are depicted in Fig. 4.18 in addition of specimens C-H-1, C-S-1 and C-G-1 for comparison purposes. There was no noticeable measured movement at the end and middle supports; therefore, not presented. Due to the similarity in the recorded vertical deflections in the two spans of each beam, only one side mid-span deflection is presented. All beams demonstrated linear load-deflection behavior up to the cracking load. Following cracking, the results showed that the flexural rigidity of mid-span section has a profound effect on the stiffness reduction the beams tested as shown in Fig. 4.18. Generally, the amount of hybrid GFRP-steel reinforcement at mid-span section is a key factor in enhancing the flexural stiffness, and, consequently, reducing deflections of the beams tested. It could be noticed that beam C-H-7 demonstrated higher

deflection than C-H-6 at the same level of loading. This is due to the fact that the mid-span flexural stiffness of C-H-6 is higher than that of C-H-7.

In terms of the effect of area of GFRP bars at hogging section on load-deflection response, Fig 4.18 shows that, even though the sagging zone of beams C-H-8 and C-H-9 were reinforced with the same hybrid reinforcement ratio, beam C-H-8 was slightly stiffer than beam C-H-9 beyond a load value of approximately 350 kN. This attributed to the difference in the top area of GFRP reinforcement at the hogging zone. On the other hand, the effect of GFRP reinforcement ratio at sagging section on load-deflection behaviour can be seen by comparing between beams C-H-7 and C-H-8. Both beams were reinforced with similar hybrid reinforcement ratio and steel reinforcement ratio at middle support and mid-span sections, respectively. Beam C-H-8 exhibited a higher flexural stiffness than that of beam C-H-7 at a failure load of beam C-H-7, the recorded deflection of beam C-H-7 was approximately twice that of beam C-H-8.

The allowable deflection according to Canadian Standard Association (CSA) (2002) ranges from 5.5-15 mm (L/480-L/180, where L is the beam span) based on the type and function of the structure. It can be noticed that the maximum deflections corresponding to the calculated service loads (67% of ultimate load) for hybrid beams C-H-6, C-H-7, C-H-8 and C-H-9 were 20, 16, 20 and 18 mm, respectively, in which the deflections corresponding to the service loads did not satisfy the max serviceability limit for certain structural applications. This result could be beneficial for establishing a guideline to determine a suitable hybrid reinforcement ratio, so the achieved stiffness behaviour of hybrid beams can be according to the serviceability limit state requirements.

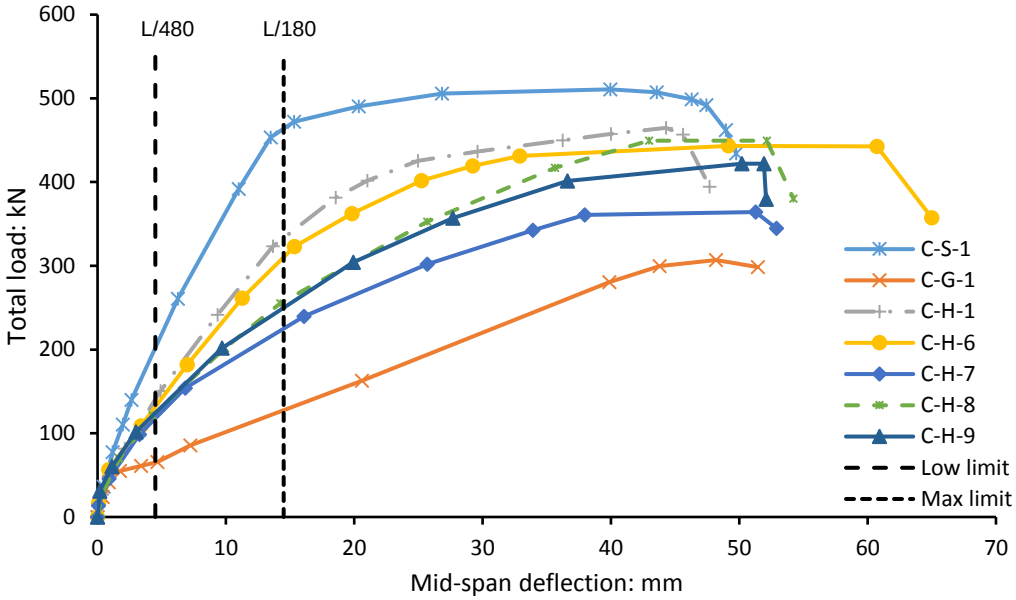

Figure 4.18 Load-deflection response of the tested beams (Series II)

4.3.5 Redistribution of Support Reactions and Bending Moments

Reactions recorded at end supports for each continuous beam are presented in Figure 4.19. To assess the amount of load redistribution, the calculated end reaction obtained from elastic analysis, was also plotted in Fig. 4.19. As expected, before concrete reached its tensile strength, the measured end support reaction of all multi-span continuous beams was very close to that obtained from the elastic analysis due to the linear elastic characteristic of concrete, GFRP bars and steel bars before reaching the cracking load. Unlike the series I, the hybrid beams of series II demonstrated a remarkable load redistribution behavior indicating signs of moment redistribution between the sagging and hogging regions. The end support reaction of beam C-H-6 was slightly larger than the elastic reaction, indication signs of load redistribution from the middle support region to the mid-span region due to the higher stiffness at mid-span region. Conversely, beam C-H-7 demonstrated an

opposite reaction response to bema C-H-6, that is attributed to the reverse reinforcement arrangement of beam C-H-7 in comparison with beam C-H-6. Beams C-H-8 and C-H-9 demonstrated similar load redistribution behaviour up to a load level of 150 kN where beam C-H-8 exhibited larger moment redistribution than that of beam C-H-9 until failure. This is attributed to higher GFRP reinforcement ratio at hogging section in beam C-H-8 than that of beam C-H-9.

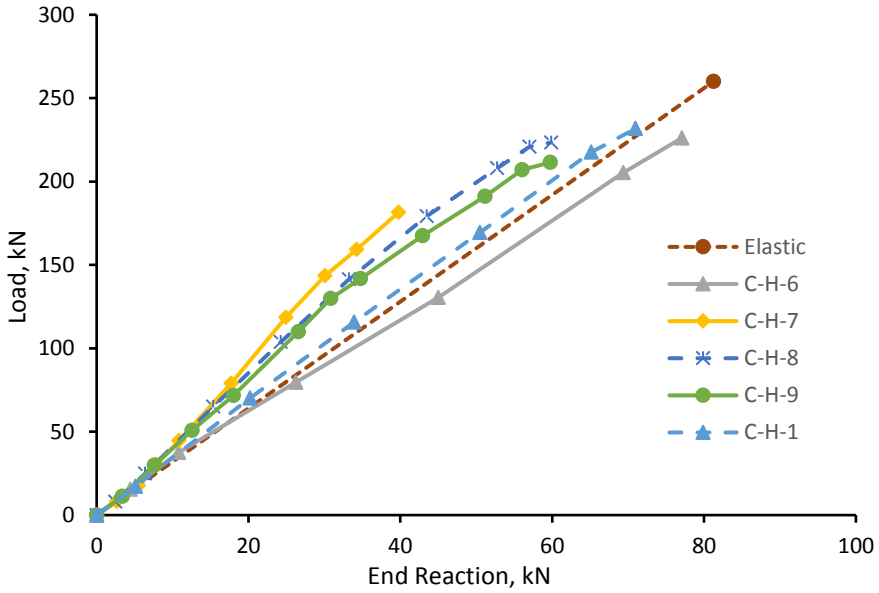

Figure 4.19 Load-end reactions relationship for the tested beams (Series II)

For evaluating the amount of moment redistribution, β, in the beams tested, the measured sagging and hogging bending moments; and the elastic bending moment at critical sections along the hybrid continuous beam span at failure are presented in Fig 4.20. The moment redistribution ratio for the mid-span and over support sections, which are given in Fig 4.20, can be obtained by comparing the actual and elastic bending moments (see Eq. 4-1).

In comparison with hybrid beam C-H-1, Figure 4.20 indicates that the experimental bending moment distribution at failure is significantly different from that obtained from linear elastic analysis for the failure load for the beams tested, especially for beam C-H-7 as depicted in Fig 4.20. The value of β at the hogging section is always larger than that of sagging sections for all hybrid continuous beams tested.

Furthermore, redistribution from sagging to hogging regions occurred in hybrid beams C-H-7, C-H-8, and C-H-9 as shown in Figs 4.20-C, 4.20-D and 4.20-E, respectively, whereas redistribution of moment from the hogging to sagging zones took place in hybrid beam C-H-6 as shown in Fig 4.20-B. For the latter, this is attributed to the higher stiffness at mid-span span section provided by the higher hybrid reinforcement ratio as compared to the middle support section. The results show that the area and arrangement of the steel reinforcement had a profound effect on the moment redistribution ratio. The small area of hybrid reinforcement at the sagging region of a continuous beam, the high moment redistribution ratio, as shown by comparing beams C-H-6 and C-H-7 which depicted in Figs 4.20-B and 4.20-C, respectively. However, it is important to mention that increasing the area of GFRP bars at the bottom side resulted in decreasing the moment redistribution ratio as noticed by comparing between hybrid beams C-H-7 and C-H-8. This is ascribed to that the high GFRP reinforcement ratio restricted the propagation and growth of flexural cracks and hence reduced the moment redistribution ratio. Moreover, the increase of GFRP area in hogging section resulted in less moment redistribution in sagging section as seen by the experimental results obtained from beams C-H-8 and C-H-9.

Comparing the actual and elastic bending moment in each beam at failure, it can be seen from Fig 4.20-B that beam C-H-6 redistributed up to 15% of hogging bending moment whereas beams C-H-7, C-H-8 and C-H-9 redistributed up to 43%, 19% and 18% of sagging bending moment as shown in Figs 4.20-C-4.20-E, respectively,

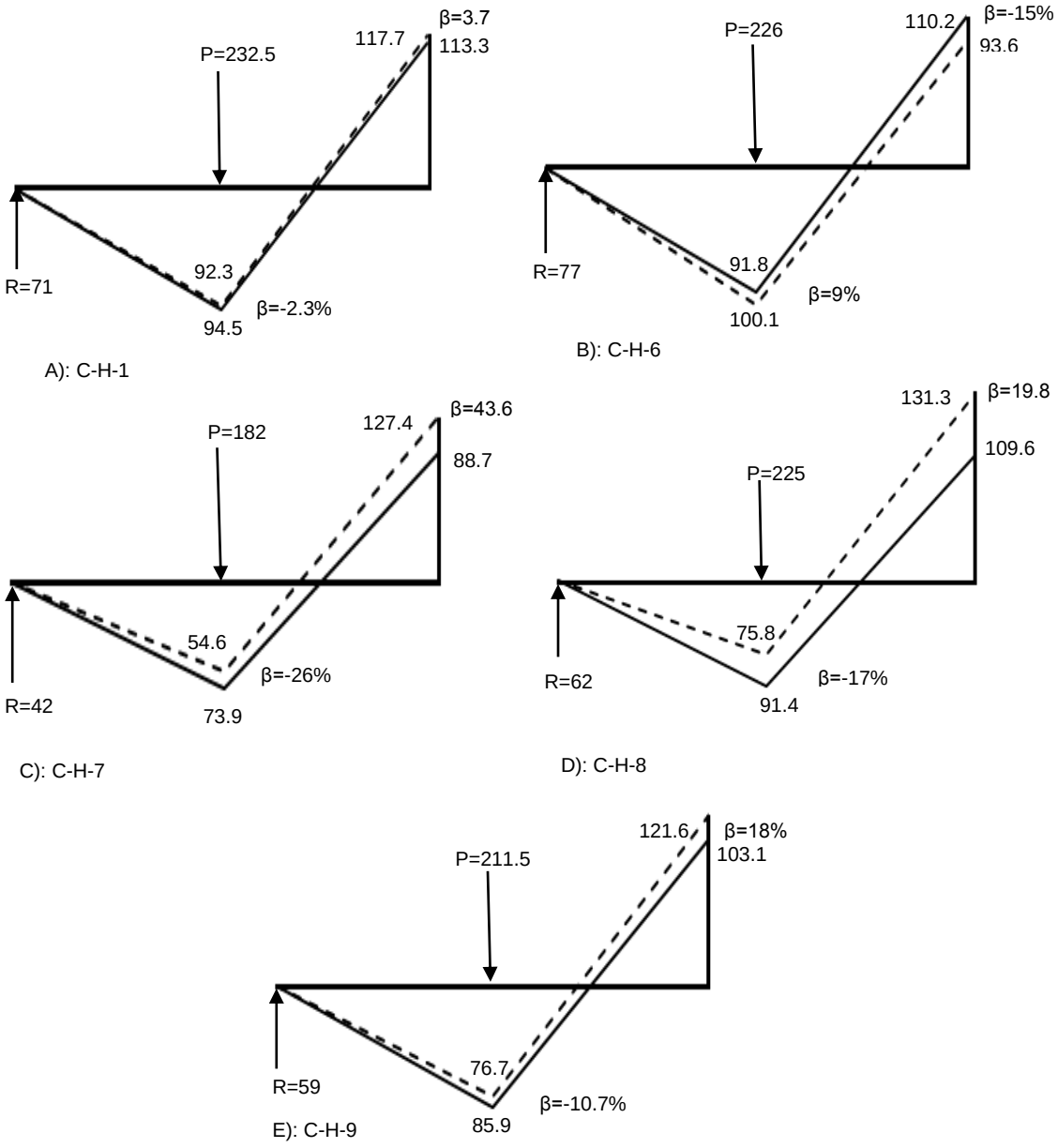

Experimental bending moment ($kN.m$)

Elastic bending moment ($kN.m$)

P Load at failure (kN)

R End reaction at failure (kN)

Figure 4.20 Actual versus elastic bending moment at failure

4.4 Digital Image Correlation (DIC)

As mentioned in chapter three, a digital image correlation analysis was undertaken for the beams. The results provided by this technique allowed for comparison between the experimental displacements (recorded by LVDTs) and those calculated through numerical interpolation by DIC analysis.

Figure 4.21 illustrates the correlation between the test results and DIC results in continuous beams, related to the position of the concentrated load. The good comparison observed in Figure 4.21 indicate that the DIC analysis can be relied on for displacement. It is important to mention that for some specimens, cameras were removed before the actual test finished. Therefore, there are some differences between the maximum deflection obtained experimentally and that obtained by DIC analysis.

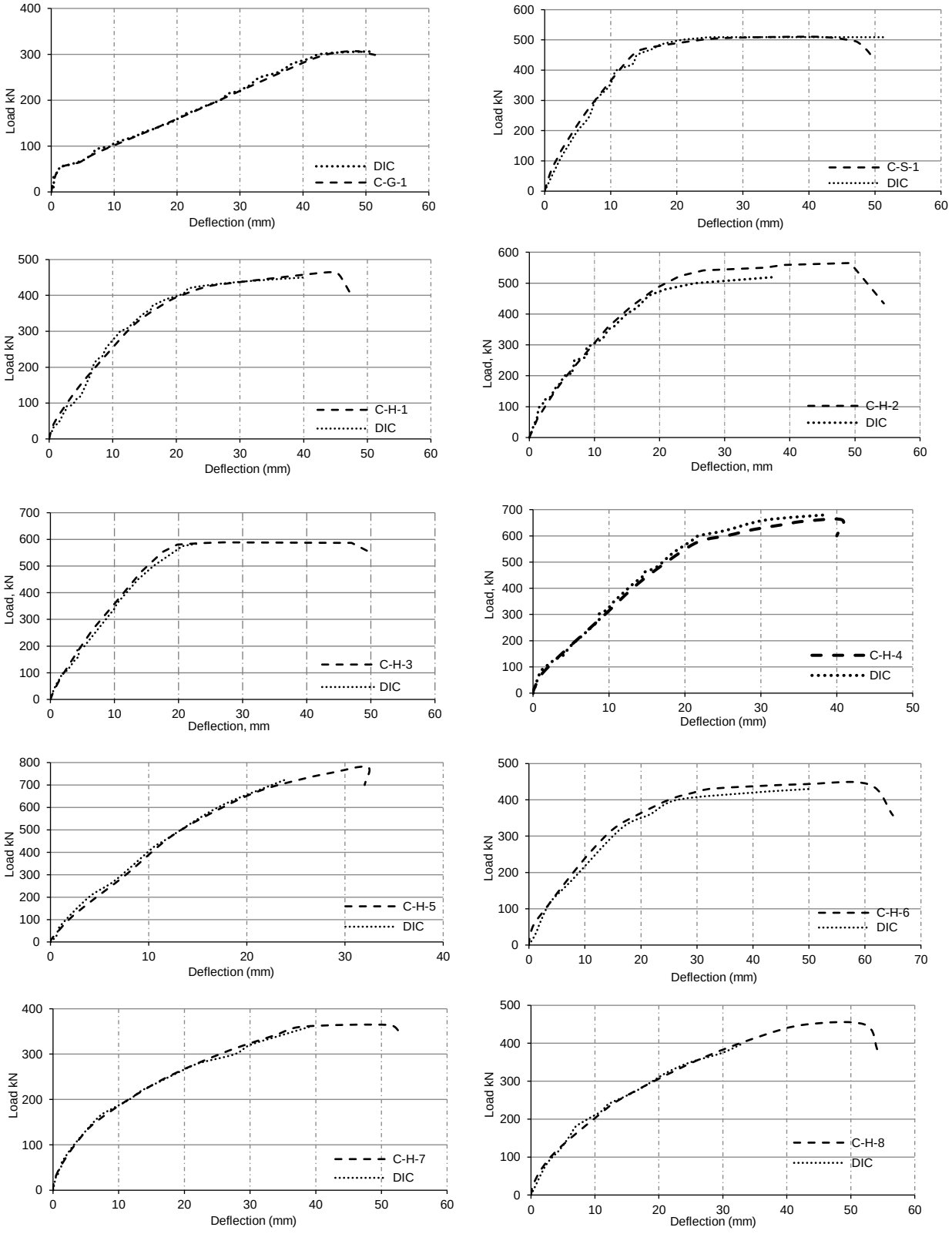

Figure 4.21 Comparison between the experimental and DIC results for specimens tested

4.5 Conclusions

Test results of eleven multi-span continuous concrete beams reinforced with either steel, GFRP or hybrid GFRP/steel bars have been presented in this chapter. The parameters investigated were the longitudinal GFRP reinforcement ratio, the longitudinal steel reinforcement ratio, the area of GFRP bars in sagging and hogging regions, and the hybrid reinforcement ratio in mid-span and middle support sections. Based on the experimental investigation presented in this chapter, the following conclusions are drawn:

- Unlike GFRP reinforced concrete beams, the hybrid and steel reinforced concrete beams failed in a favourable ductile manner due to concrete crushing after yielding of steel reinforcement.
- Beams with hybrid reinforcement ratio in sagging region different from that in hogging regions exhibited more ductile behaviour than beams reinforced with similar hybrid reinforcement ratios in critical sections.
- The lower stiffness and higher deflection of GFRP reinforced concrete beams can be controlled and improved by the use of steel reinforcement in combination with GFRP re-bars. However, the ratio of GFRP to steel reinforcement is a key factor to ensure sufficient ductility and stiffness beyond the first cracking stage.
- The stiffness of hybrid beams increased with either the increase of steel or GFRP reinforcement after the first cracking. However, the stiffness of continuous concrete beams is more reliant on the hybrid reinforcement ratio of mid-span section.

- For beams reinforced with different hybrid reinforcement ratio in critical sections, increasing the area of GFRP bars in either sagging or hogging region had a positive effect on enhancing the load-deflection behaviour.
- For beams with similar hybrid reinforcement ratio at sagging and hogging regions, increasing the amount of steel bars resulted in less load capacity increase after yielding of steel, whereas less ductile behaviour would be achieved by increasing the amount of GFRP bars.
- The GFRP reinforcement in tension side of middle support section was ineffective in enhancing the load capacity of hybrid continuous concrete beams. On the other hand, increasing the bottom GFRP reinforcement ratio of mid-span section has more effect on the load capacity increase.
- Increasing the amount of longitudinal hybrid GFRP-steel re-bars had a clear effect on flexural crack widths.
- Similar hybrid reinforcement ratios at sagging and hogging regions led to limited moment redistribution behaviour. On the other hand, hybrid beams reinforced with different hybrid reinforcement ration in critical section demonstrated a remarkable moment redistribution up to 43%.
- The stiffness of critical sections is a key factor in determining the direction of moment redistribution whether from mid-span to middle support.

CHAPTER FIVE

FLEXURAL ANALYSIS OF HYBRID FRP-STEEL REINFORCED CONCRETE CROSS- SECTIONS

5.1 Introduction

This chapter presents the sectional analysis technique proposed for estimating the moment-curvature relationship and the flexural strength of sections reinforced with hybrid FRP-steel bars. The technique is developed from the strain compatibility and equilibrium of forces. The concrete models take into account the compressive strength decrease after reaching the ultimate strength which was not considered by Kara et al., 2015. In addition, different constitutive model was selected to model concrete in tension. Hence, the influence of design parameters such as the tensile reinforcement ratio, FRP reinforcement type, the position of the steel tensile reinforcement, top reinforcement ratio and the concrete compressive strength on the flexural behavior of aforementioned beams could be studied. The moment capacities obtained by the developed technique will be compared with the experimental results presented in chapter four and experimental results of tests conducted by other authors. Finally, a sample of a design chart and a design procedure to calculate the flexural capacity of hybrid reinforced sections are developed in this chapter.

5.2 Material Models in the Analytical Program

5.2.1 Concrete in Compression

The uniaxial stress-strain relationship of concrete in compression shown in Figure 5-1 developed by Hognestad (1955) and used by Park and Paulay

(1975), is adopted in the current investigation. The equations for different parts of the relationship are as follows:

Region AC ($0 \leq \varepsilon_c \leq \varepsilon_{co}$)

$$f_c = f_c' \left[2\frac{\varepsilon_c}{\varepsilon_{co}} - (\frac{\varepsilon_c}{\varepsilon_{co}})^2\right] \quad (5\text{-}1)$$

Region CD ($\varepsilon_{co} < \varepsilon_c \leq \varepsilon_{cu}$)

$$f_c = f_c'[1 - 0.15(\frac{\varepsilon_c - \varepsilon_{co}}{\varepsilon_{cu} - \varepsilon_{co}})] \quad (5\text{-}2)$$

where f_c and ε_c are the stress and the strain in compressive concrete, respectively, f_c' is the cylinder compressive strength of concrete, $\varepsilon_{co} = 2.4 \times 10^{-4}\sqrt{f_c'}$ is the strain of concrete corresponding to maximum stress, $E_c = 4700\sqrt{f_c'}$ is the elasticity modulus of concrete and ε_{cu} (=0.0035) is the ultimate strain of concrete.

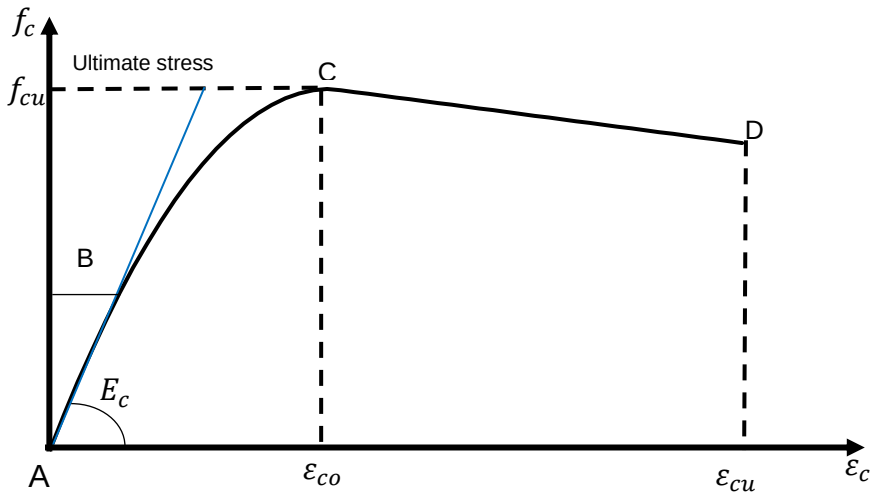

Figure 5.1 Stress-Strain relationship for concrete in compression

5.2.2 Concrete in Tension

A bi-linear stress–strain relationship is adopted to model concrete in tension as shown in Figure 5-2. Before the initiation of vertical cracking due to flexure, the stress strain relationship is assumed to be linear elastic. After cracking of

concrete due to flexure, the tensile force in concrete is assumed to be zero. However, concrete between cracks can still carry tensile stress and thus may increase the stiffness of the member. This is known as tension stiffening (Bischoff and Paixao, 2004). Therefore, the stress-strain relationship shown in Figure 5-2 is adopted in the current investigation and calculated in Eqs (5-3) and (5-4) respectively, as follows (Belarbi and Hsu, 1994) :

Region $A'B'(\ 0 \leq\ \varepsilon_t\ \leq\ \varepsilon_r\ )$ $\quad f_t = E_c\varepsilon_t$ (5-3)

Region $B'C'\ (\ \varepsilon_r \leq\ \varepsilon_t\ )$ $\quad f_t = f_r(\frac{\varepsilon_r}{\varepsilon_t})^{0.4}$ (5-4)

where f_t and ε_t are the tensile stress and strain in concrete, respectively, f_r(=0.62$\sqrt{f_c'}$) and ε_r are the ultimate tensile strength and corresponding tensile strain of concrete, respectively.

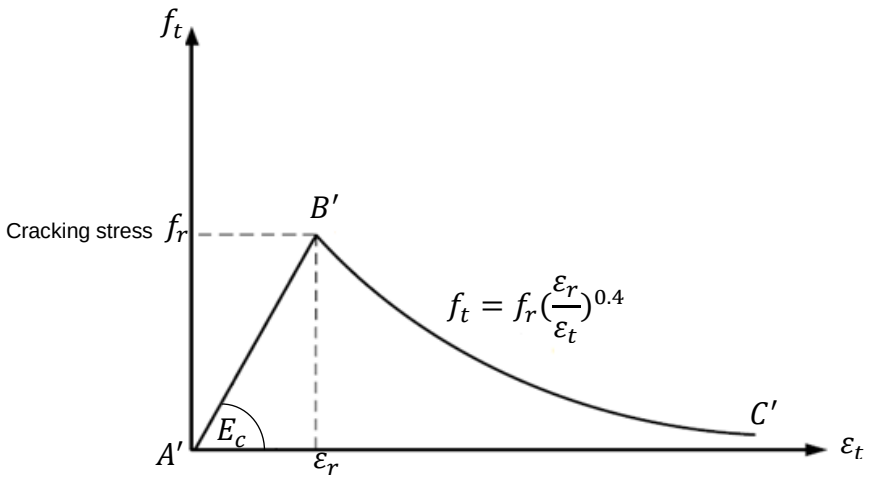

Figure 5.2 Stress-Strain curve of tensile concrete

5.2.3 Steel Reinforcement

Reinforcing steel is modelled as a bilinear elastic-perfectly plastic material with yield stress f_y as shown in Figure 5-3. The equations for different parts of the relationship are:

$$f_s = \varepsilon_s E_s \qquad \varepsilon_s < \varepsilon_y \tag{5-5}$$

$$f_s = f_y \qquad \varepsilon_s \geq \varepsilon_y \tag{5-6}$$

where $\varepsilon_s, f_s, \varepsilon_y, f_y$ and E_s are the strain, stress, yield strain, yield stress and Young's modulus, respectively, of the steel reinforcement.

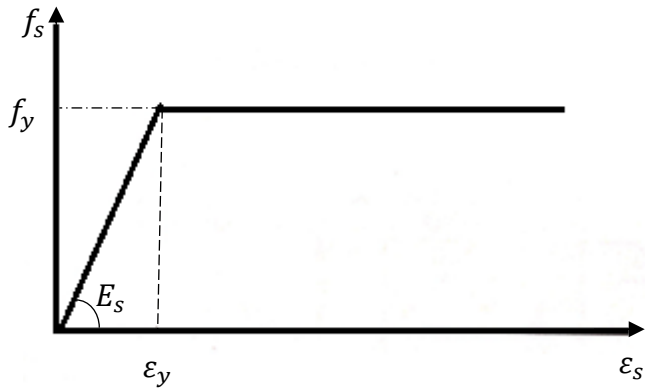

Figure 5.3 Stress-Strain relationship of steel reinforcement (BS EN 1992-1-1:2004)

5.2.4 FRP Reinforcement

The stress–strain relationship of FRP bars in tension is linear elastic up to rupture as shown in Figure 5-4. The equations governing the relationship are as follows:

$$f_f = \varepsilon_f E_f \qquad \varepsilon_f \leq \varepsilon_{fu} \tag{5-7}$$

$$f_f = 0 \qquad \varepsilon_f > \varepsilon_{fu} \tag{5-8}$$

where $\varepsilon_f, f_f, \varepsilon_{fu}, f_{fu}$ and E_f are the strain, stress, rupture strain, rupture tensile strength and Young's modulus, respectively, of the FRP reinforcement.

The compressive strength of FRP bars are not reliable, but test results show far much lower strength for FRP bars in compression than tension, for instance it has been reported that compression stress is 55%, 78% and 20% of the

tensile strength for GFRP, CFRP and AFRP bars respectively. In general, compressive strengths are higher for bars with higher tensile strengths, except in the case of AFRP where the fibres exhibit nonlinear behavior in compression at a relatively low level of stress. (ACI 440.1R-15).

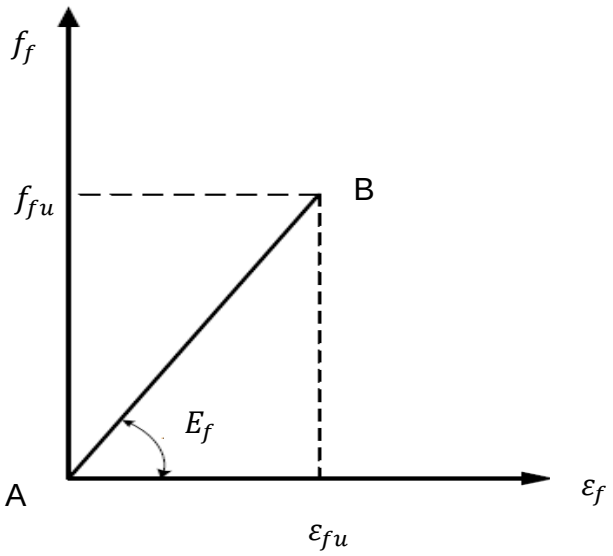

Figure 5.4 Typical stress-strain in tension for FRP reinforcing bars

5.3 Moment-Curvature Relationship

The moment curvature relationship for the rectangular concrete cross-section reinforced with hybrid FRP-steel bars shown in Figure 5-5 (a) is calculated based on the following assumptions:

- Plane sections before bending remain plane after bending.
- Perfect bond exists between hybrid FRP-steel bars and surrounding concrete.

The moment curvature calculation procedure is summarized as follows:

- A small value of strain at the concrete extreme compression fibre, ε_c, is assumed between 0.0 and 0.0035.

- The value of the neutral axis depth, x, is initially assumed within the beam depth. The correct value of neutral axis depth is iteratively obtained when equilibrium of forces is satisfied.
- The concrete cross-section depth is divided into a number of segments, n, as shown in Figure 5-5(a).
- According to the aforementioned assumptions, the strain in each concrete segment, FRP and steel bars are linearly proportional to its distance from the neutral axis as depicted in Figure 5-5(b) and expresses below:

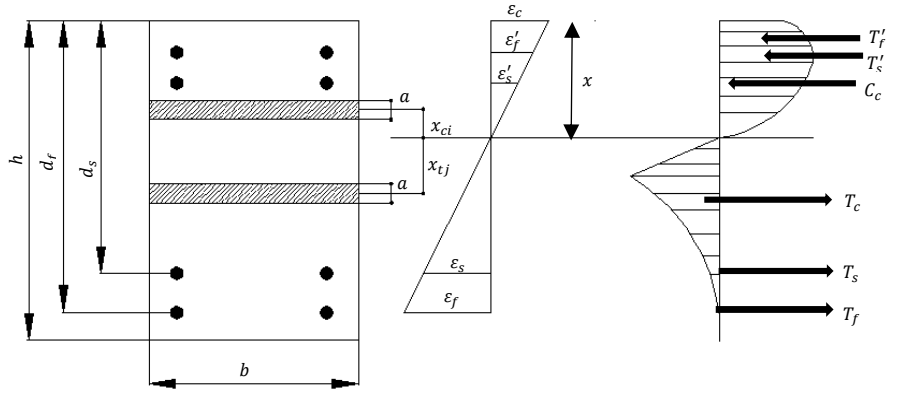

Figure 5.5 Strain, stresses and forces of a reinforced concrete section

$$\varepsilon_{ci} = (\frac{x_{ci}}{x})\varepsilon_c \quad (5\text{-}9)$$

$$\varepsilon_{tj} = (\frac{x_{tj}}{x})\varepsilon_c \quad (5\text{-}10)$$

$$\varepsilon_f = (\frac{d_f - x}{x})\varepsilon_c \quad (5\text{-}11)$$

$$\varepsilon_s = (\frac{d_s - x}{x})\varepsilon_c \quad (5\text{-}12)$$

$$\varepsilon_f' = (\frac{x-d_f'}{x})\varepsilon_c \quad (5\text{-}13)$$

$$\varepsilon_s' = (\frac{x-d_s'}{x})\varepsilon_c \quad (5\text{-}14)$$

where ε_c is the top fibre concrete compressive strain of the reinforced concrete section, ε_{ci} and ε_{tj} are the concrete compressive and tensile strain at mid depth of i and j segments, respectively, x_{ci} and x_{tj} are the distance between the neutral axis and the mid depth of i and j segments, respectively, ε_f, ε_s, indicate the strain in bottom FRP and steel bars, respectively, ε_f' and ε_s' are the strain in top FRP and steel bars, respectively, d_f and d_s are the bottom FRP and steel reinforcement depth, respectively, and d_f' and d_s' are the top FRP and steel reinforcement depth, respectively.

- The corresponding stresses in each concrete segment and tensile and compressive reinforcements can be calculated from the respective stress-strain relationships of concrete, FRP and steel depicted in Figures 5-1, 5-2, 5-3 and 5-4, respectively and by means of equations from (5-1)-(5-8).
- The summation of the internal forces shown in Figure5-5(c), Q, is then calculated:

  $$Q = C_c + (T_f' + T_s') - T_f - T_S - T_c \approx 0 \quad (5\text{-}15)$$

  where

  $$C_c = ab\sum_{i=1}^{n_c} f_{ci} \quad (5\text{-}16)$$

  $$T_c = ab\sum_{i=1}^{n_t} f_{tj} \quad (5\text{-}17)$$

  $$T_f = A_f f_f \quad (5\text{-}18)$$

  $$T_s = A_s f_s \quad (5\text{-}19)$$

$$T_f' = A_f' f_f' \tag{5-20}$$

$$T_s' = A_s' f_s' \tag{5-21}$$

where C_c, T_c are the total compressive and tensile forces in the concrete, respectively, as shown in Figure 5-5(c); T_f, T_S, T_f' and T_s' are the forces of bottom FRP and steel bars and top FRP and steel bars, respectively; $a(=\frac{h}{n})$ is the depth of each concrete segment in compression or tension as depicted in Figure 5-5 (a); n_c and n_t are the number of concrete elements in compression and tension, respectively; f_{ci} and f_{tj} are the concrete compressive stress in element number i and concrete tensile stress in element number j, respectively; A_f, A_s, A_f' and A_s' are the areas of tensile FRP and steel and compressive FRP and steel reinforcements, respectively; f_f' and f_s' are the stresses in compressive FRP and steel bars, respectively.

- The value of the neutral axis depth, x is iteratively adjusted using the bi-section method (see appendix-A) until sufficient equilibrium accuracy is attained as given below:

$$\frac{|C_c+\left(A_f' f_f' + A_s' f_s'\right)-A_f f_f - A_s f_s - T_c|}{|C_c|} \leq 10^{-5} \tag{5-22}$$

- The bending moment,M, is calculated by taking the moments of the internal forces about bottom FRP reinforcements:

  $$M = \sum_{i=1}^{n_c} C_{ci} L_{ci} + T_f'\left(d_f - d_f'\right) + T_s'\left(d_f - d_s'\right) - \sum_{j=1}^{n_t} C_{tj} L_{tj} - T_s(d_f - d_s) \tag{5-23}$$

  where L_{ci} and L_{tj} are the lever arm for the concrete compressive and tensile forces in segment i and j, respectively; C_{ci} and C_{tj} are the compressive and tensile forces in segment i and j, respectively.

- The corresponding curvature, φ, is calculated from the concrete strain and neutral axis depth as given below:

$$\varphi = \frac{\varepsilon_c}{x} \tag{5-24}$$

The strain in the extreme concrete compression fibre is incrementally increased and the above procedure is repeated for each value of strain to obtain further values of M and φ until the maximum concrete compressive strain reaches its ultimate compressive strain (ε_{cu}=0.0035). During such strain increase until concrete crushing, rupture of FRP bars or yielding of steel reinforcement may occur depending on the amount of hybrid FRP/steel reinforcement in the section. The section moment capacity M_u is, therefore, the highest moment attained for various increments considered until failure. Based on the aforementioned procedure, a computer program has been developed for the moment-curvature relationship and moment capacity of FRP, steel and hybrid FRP/steel reinforced concrete sections as shown in Figure 5-6.

5.4 Verification of the Analytical Modelling Program

To validate the present model, comparisons between the predictions from the current technique and flexural capacity of hybrid FRP-steel reinforced concrete beams tested by the author and other authors are presented in table 5-1. In addition, moment curvature diagrams obtained by means of the experimental results in the literature are compared with those of the theoretical model as shown in Figs 5.7 and 5.8. Three modes of failure are recorded in table 5-1, namely tensile rupture of FRP bars, yielding of tensile steel reinforcement

followed by crushing of concrete and crushing of concrete before yielding of steel reinforcement.

The comparison included moment capacities resulted from 64 concrete beams reinforced with hybrid FRP/steel bars from different experimental investigations presented in past researches and current research with details of the tested beams. The average and standard deviation of the ratio between predicted and experimental moment capacities are 96 % and 13 %, respectively. The predictions obtained from the current model are in very good agreement with the tested beams results.

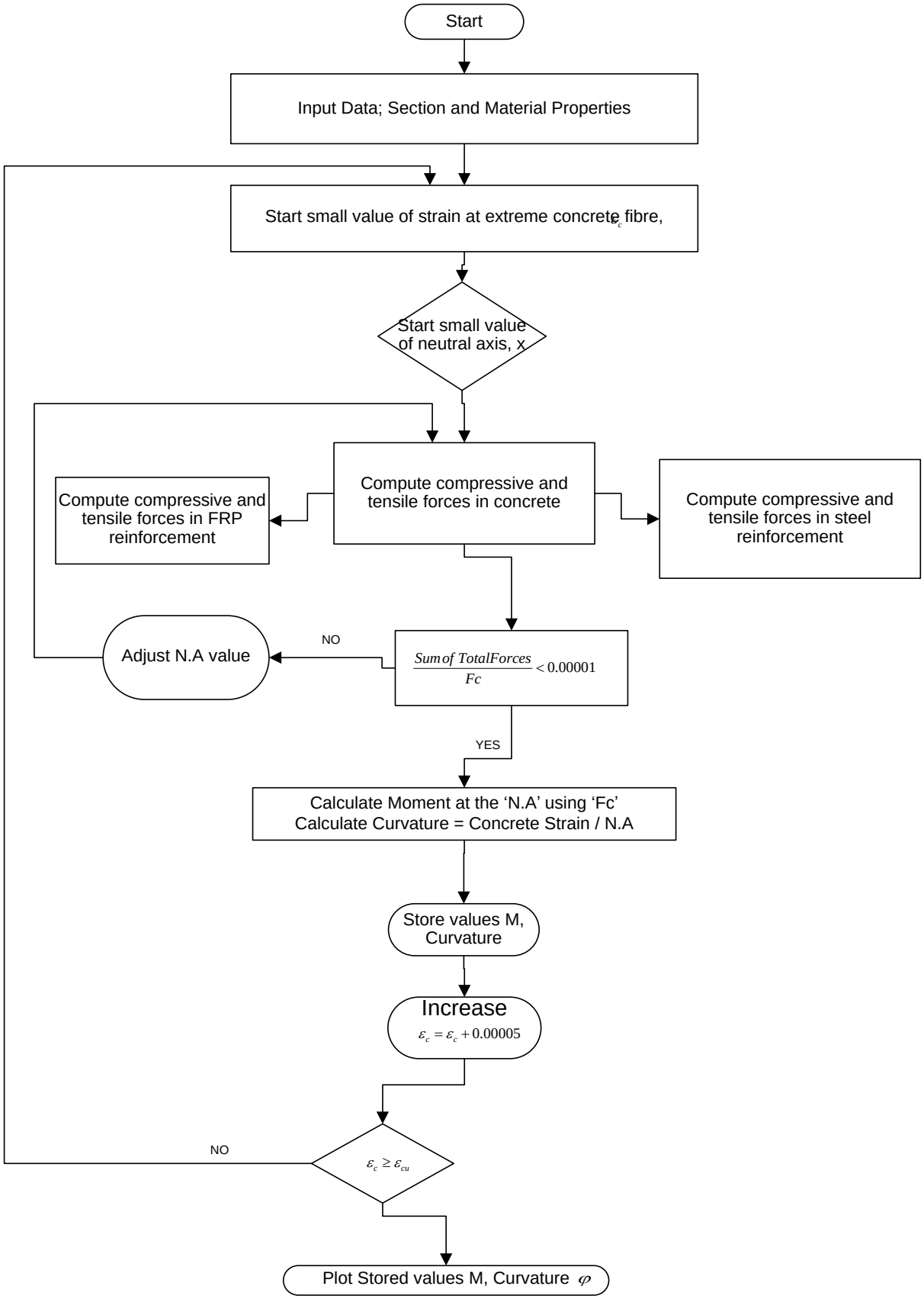

Figure 5.6 Flowchart diagram of the sectional analysis process

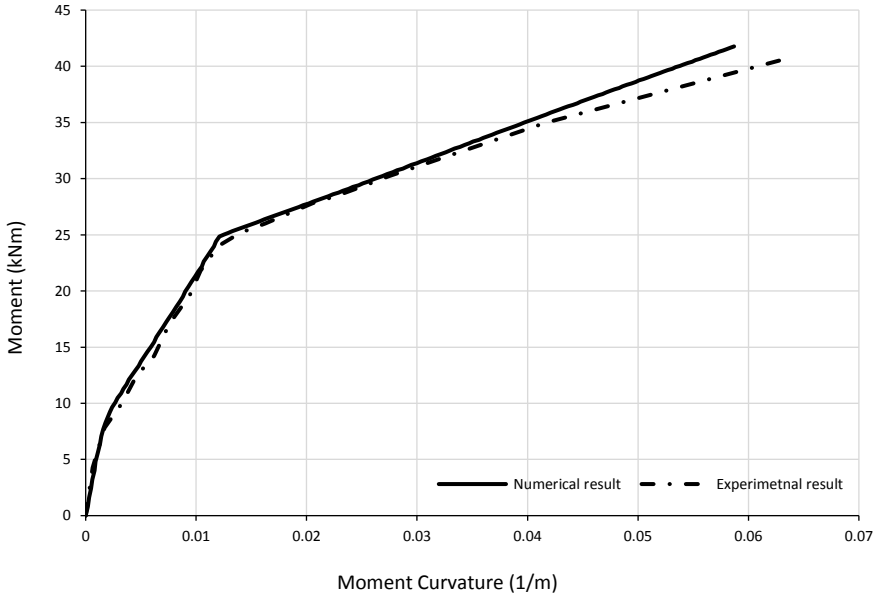

Figure 5.7 Comparison between experimental and numerical moment-curvature relationship for beam B3 (Qu et al., 2009)

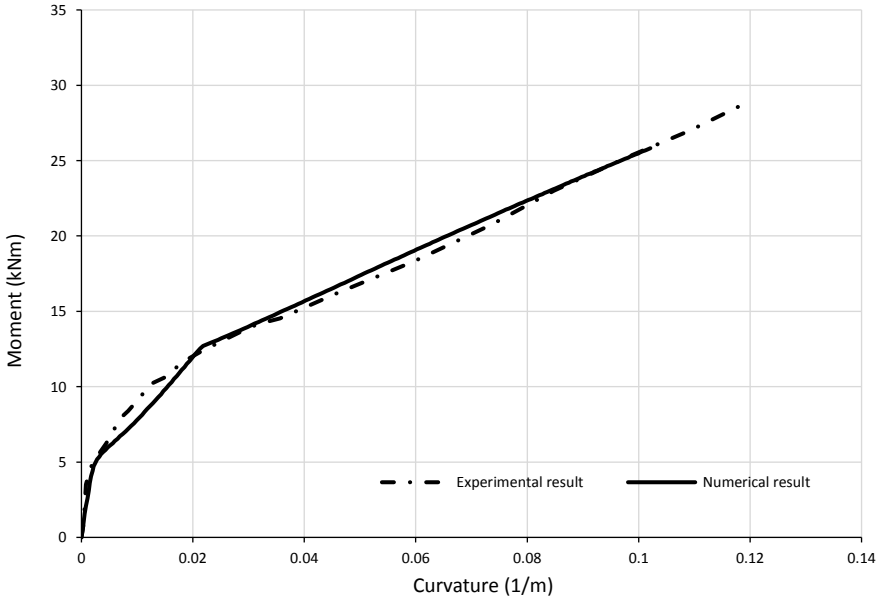

Figure 5.8 Comparison between experimental and numerical moment-curvature relationship for beam A2 (Aiello and Ombres, 2002)

Table 5-1 Comparisons between the theoretical and experimental flexural moment capacities of hybrid steel/FRP reinforced concrete beams

Reference	*Beam Notation*	*Loading type*	*Width (mm)*	*Depth (mm)*	d_f *(mm)*	d_s *(mm)*	*Span (mm)*	f'_c (MPa)	A_f (mm^2)	E_f *(GPa)*	A_s (mm^2)	*Type of FRP*	M_{exp} *kN.m*	M_{the} *kN.m*	*M.F*	$\frac{M_{the}}{M_{exp}}$
Yinghao and Yong, (2013)	S1	Two Points	150	250	225	-	2000	80.1	452.4	75.89	-	GFRP	72.5	66.5	CC	0.9
	S2	Two Points	150	250	225	195	2000	80.1	226.2	75.89	904.8	GFRP	69.9	77	SY-CC	1.1
	S3	Two Points	150	250	195	225	2000	80.1	226.2	75.89	904.8	GFRP	74.8	78.75	SY-CC	0.9
	S4	Two Points	150	250	225	225	2000	80.1	226.2	75.89	904.8	GFRP	82	86.1	SY-CC	0.9
Lau and Pam, (2010)	G0.8-A90	Mid-span	280	380	344	-	4200	36.6	804.2	40	-	GFRP	158.8	136.5	FRPR	1
	G0.3-MD1.0-A90	Mid-span	280	380	342.5	339.5	4200	41.3	283.5	39	981.7	GFRP	147	155.4	SY-FRPR	0.8
	G2.1-A90	Mid-span	280	380	339.5	-	4200	41.3	1963.5	38	-	GFRP	238	225	SY-CC	0.8
	G1.0-T0.7-A90	Mid-span	280	380	339.5	342	4200	39.8	981.7	38	628.3	GFRP	261	240	SY-CC	0.9
	G0.6-T1.0-A90	Mid-span	280	380	342.5	339.5	4200	44.6	567.1	39.5	981.7	GFRP	229	231	SY-CC	1
	G0.4-A135	Mid-span	280	380	346	-	4200	42.3	339.3	40.2	-	GFRP	80.4	68.25	FRPR	0.8
	G0.5-A135	Mid-span	280	380	346	-	4200	42.3	452.4	40.2	-	GFRP	107.3	90	FRPR	1
	G2.1-A135	Mid-span	280	380	339.5	-	4200	33.9	1963.5	38	-	GFRP	236.8	210	CC	0.9
Safan, (2013)	B10-8S	Two Points	100	200	178	136	1220	30	100.6	39	157	GFRP	14.41	13.73	SY-CC	0.8
	B10-6S	Two Points	100	200	179	136	1220	30	56.6	41	157	GFRP	14.09	11.43	SY-CC	0.9
	B12-8S	Two Points	100	200	178	135	1220	30	100.6	39	226	GFRP	16.33	16	SY-CC	0.8
	B12-6S	Two Points	100	200	179	135	1220	30	56.6	41	226	GFRP	14.89	13.7	SY-CC	0.8
Leung and Balendran,2003	L1	Two Points	150	200	160	-	2200	28.5	143	40.8	-	GFRP	11.97	9	FRPR	0.8
	L2	Two Points	150	200	160	130	2200	28.5	143	40.8	157	GFRP	22.3	19	SY-CC	0.9
	L5	Two Points	150	200	160	130	2200	28.5	214	40.8	157	GFRP	23	17.5	SY-CC	0.8
	H1	Two Points	150	200	160	-	2200	48.8	143	40.8	-	GFRP	12.74	10.5	FRPR	0.8
	H2	Two Points	150	200	160	130	2200	48.8	143	40.8	157	GFRP	21.1	21	SY-CC	1
	H5	Two Points	150	200	160	130	2200	48.8	214	40.8	157	GFRP	27	24.5	SF	0.9
Aiello and Ombres, (2002)	A1	Two Points	150	200	175	150	2700	38.8	88.31	49	100.48	AFRP	25.14	18.5	SY-CC	0.7
	A2	Two Points	150	200	175	150	2700	38.8	157	50.1	100.48	AFRP	28.41	25.5	SY-CC	0.9
	A3	Two Points	150	200	175	150	2700	38.8	235	50.1	226.08	AFRP	35.55	29.75	SY-CC	0.8
	B2	Two Points	150	200	175	-	2700	38.8	88.31	49	-	AFRP	20.21	25.5	SY-CC	1.3
	C1	Two Points	150	200	175	175	2700	38.8	88.31	49	100.48	AFRP	25.14	21.25	SY-CC	0.8
Qu et al., (2009)	B2	Two Points	180	250	220	-	1800	26.3	506.4	45	-	GFRP	43.89	42	CC	1
	B3	Two Points	180	250	220	220	1800	28.1	253.23	45	226.08	GFRP	40.7	41.7	SY-CC	1
	B4	Two Points	180	250	220	220	1800	28.1	396.91	41	200.96	GFRP	39.66	45	SY-CC	1.1
	B5	Two Points	180	250	220	220	1800	29.2	141.69	37.7	401.92	GFRP	36.36	42	SY-CC	1.2
	B6	Two Points	180	250	220	220	1800	29.2	253.23	45	401.92	GFRP	42.57	48	SY-CC	1.1
	B7	Two Points	180	250	220	220	1800	34.6	141.69	37.7	113.04	GFRP	23.55	33	SY-CC	1.4
	B8	Two Points	180	250	220	190	1800	34.6	396.91	41	1205.76	GFRP	63.3	75	SY-CC	1.2
Tan 1997	A2	Two Points	175	350	150	150	2300	31.0	50.2	52	150.7	AFRP	36	32.5	SY-FRPR	0.9
	A3	Two Points	175	350	150	150	2300	30.9	25.1	52	301.4	AFRP	43.5	43	SY-FRPR	1
	B2	Two Points	175	350	150	150	2300	30.0	25.1	52	150.7	AFRP	35.25	30	SY-FRPR	0.95
Almusallam et al., (2013)	RW1F	Two Points	150	200	185	157	2000	36.6	78.5	40	157	GFRP	22.5	22	SY-FRPR	0.97
	RW1 Φ12F	Two Points	150	200	185	157	2000	36.6	113	40	157	GFRP	25.2	23	SY-FRPR	0.9
	RW1 Φ14F	Two Points	150	200	185	157	2000	36.6	153	40	157	GFRP	28.1	24.5	SY-FRPR	0.88
	RW1 Φ16F	Two Points	150	200	185	157	2000	36.6	201	40	157	GFRP	31.4	27	SY-FRPR	0.86
	RW2F	Two Points	150	200	185	157	2000	36.6	157	40	78.5	GFRP	22.5	21	SY-FRPR	0.93
	RW2 Φ12F	Two Points	150	200	185	157	2000	36.6	226	40	78.5	GFRP	32.2	28	SY-FRPR	0.87

	RW2 Φ14F	Two Points	150	200	185	157	2000	36.6	306	40	78.5	GFRP	36.6	32	SY-FRPR	0.87
Sharaky et al.,(2015)	F1G2T	Two Points	160	280	270	250	2400	30.5	113	60	226	GFRP	54	50	CC	0.93
Sharaky et al.,(2014)	LB1C1	Two Points	160	280	270	250	2400	32.4	50.24	165	226	CFRP	43.6	43.1	CC	0.99
	LB1G1	Two Points	160	280	270	250	2400	32.4	50.24	60	226	GFRP	39.6	39.1	FRPR	0.99
	LB2C1	Two Points	160	280	270	250	2400	32.4	100.4	165	226	CFRP	46.8	52.5	Cs	1.1
	LB2G1	Two Points	160	280	270	250	2400	32.4	100.4	60	226	GFRP	44.8	47.5	Cs	1.06
	LB1G2	Two Points	160	280	270	250	2400	32.4	113	60	226	GFRP	42	46.3	CC	1.1
Current study (2017)	S-G-B-1	Mid-span	200	300	265	220	2600	62	255	50	-	GFRP	77	70	FRPR	1.1
	S-H-B-1	Mid-span	200	300	265	220	2600	55	142	50	100.5	GFRP	62	60	SY-CC	1.0
	S-H-B-2	Mid-span	200	300	265	220	2600	55	255	50	402	GFRP	110	105	SY-CC	0.96
	C-G-B-1	Mid-span	200	300	265	220	2600	41	255	50	-	GFRP	66	63	CC	0.95
	C-S-B-1	Mid-span	200	300	265	220	2600	43	-	-	603	-	97.3	90	SY	0.92
	C-H-B-1	Mid-span	200	300	265	220	2600	43	255	50	402	GFRP	92.0	88.0	SY-CC	0.96
	C-H-B-2	Mid-span	200	300	265	220	2600	46	255	50	603	GFRP	112.0	103.0	CC-SF	0.92
	C-H-B-3	Mid-span	200	300	265	220	2600	46	255	50	980	GFRP	125.0	129.0	SF	1.03
	C-H-B-4	Mid-span	200	300	265	220	2600	60	595	50	402	GFRP	128.0	135.0	CC-SF	1.05
	C-H-B-5	Mid-span	200	300	265	220	2600	64	993	50	402	GFRP	160.0	165.0	CC-SF	1.03
	C-H-B-6	Mid-span	200	300	265	220	2600	59	255	50	402	GFRP	101.0	99.0	SY-CC	0.98
	C-H-B-7	Mid-span	200	300	265	220	2600	59	142	50	100	GFRP	52.0	62.0	SY-CC	1.19
	C-H-B-8	Mid-span	200	300	265	220	2600	53	255	50	100	GFRP	75.0	79.0	SY-CC	1.05
	C-H-B-9	Mid-span	200	300	265	220	2600	57	255	50	100	GFRP	77.0	81.0	SY-CC	1.05
Notation: M_{exp} and M_{the} are the experimental and theoretical moment capacities of hybrid steel/FRP sections. M.F: Failure modes where SY-CC refers to steel yielding followed by concrete crushing, SY-FRPR indicates steel yielding followed by FRP rupture modes of failure, SF refers to shear failure and Cs indicate concrete splitting. A_f, A_s, E_f, d_f and d_s are the FRP reinforcement area, steel reinforcement area, FRP modulus of elasticity, steel rebar position and FRP bar position.												Average				0.96
												Standard deviation				13%

5.5 Parametric Study

The main aim of the parametric study is to investigate the behavior of hybrid FRP-steel reinforced concrete sections. In particular, the effect of design variables such as the reinforcement ratio, type of FRP rebars, position of tensile reinforcement and compressive strength on flexural capacity of hybrid sections has been investigated using the analytical modelling program described previously. Table 5-2 gives the geometric and mechanical properties of reinforcement used in the parametric study. Table 5-3 illustrates reinforced concrete sections with different types of FRP and steel reinforcements. All sections were 200 mm in width and 300 mm in depth. The beams notation indicated in Table 5.3 includes different characters. The letters B, C, G and S indicate beam, CFRP bars, GFRP bars and steel bars respectively. Whereas the characters Hybrid-1 indicates the reinforcement ratio of CFRP rebars. The numbers 25, 35 and 45 indicate the concrete compressive strength, while 270, 250, 230 and 210 indicate the distance between the top fibre of concrete and tensile steel reinforcement. The numbers that indicate the compressive reinforcement ratio are 0, 1 and 2.

Table 5-2 Geometric and mechanical properties of rebars used in the parametric study (Pultrall Inc)

Bar type	Diameter, mm	Cross sectional area, mm^2	Elastic modulus E_f GPa	Tensile strength f_{fu}MPa	Rupture strain %
GFRP	9.5	71.3	45.4	765	1.68
	12.7	126.7	46.3	708	1.52
CFRP	9.5	71.3	120	1430	1.19
	12.7	126.7	144	1765	1.22
Steel	10	78.5	200	480	-
	16	201	200	480	-

Table 5-3 Parametric studies and reinforcement of hybrid beams

Parametric study	Bean no	FRP type	Bottom reinforcement		d_s mm	d_f mm	Top reinforcement	f_c' MPa
			Steel	FRP				
Tensile reinforcement ratio	B-S	-	2Φ16 mm	-	250	270	-	35
	B-C	CFRP	-	2Φ12.7 mm	250	270	-	35
	Hybrid-1		2Φ16 mm	2Φ9.5 mm	250	270	-	35
	Hybrid-2		2Φ16 mm	2Φ12.7 mm	250	270	-	35
	Hybrid-3		2Φ16 mm	4Φ12.7 mm	250	270	-	35
	B-S	-	4Φ10 mm	-	250	270	-	35
	Hybrid-4	CFRP	4Φ10 mm	2Φ12.7 mm	250	270	-	35
	Hybrid-5		3Φ16 mm	2Φ12.7 mm	250	270	-	35
	Hybrid-6		4Φ16 mm	2Φ12.7 mm	250	270	-	35
Type of FRP reinforcement	B-S-C	CFRP	3Φ16 mm	2Φ12.7 mm	250	270	2Φ9.5 mm	35
	B-S-G	GFRP	3Φ16 mm	2Φ12.7 mm	250	270	2Φ9.5 mm	35
Concrete compressive strength	B-S-C-25	CFRP	3Φ16 mm	3Φ12.7 mm	250	270	2Φ9.5 mm	25
	B-S-C-35		3Φ16 mm	3Φ12.7 mm	250	270	2Φ9.5 mm	35
	B-S-C-45		3Φ16 mm	3Φ12.7 mm	250	270	2Φ9.5 mm	45
Position of the tensile steel reinforcement	B-S-G-270	GFRP	3Φ16 mm	3Φ12.7 mm	270	270	2Φ9.5 mm	35
	B-S-G-250		3Φ16 mm	3Φ12.7 mm	250	270	2Φ9.5 mm	35
	B-S-G-230		3Φ16 mm	3Φ12.7 mm	230	270	2Φ9.5 mm	35
	B-S-G-210		3Φ16 mm	3Φ12.7 mm	210	270	2Φ9.5 mm	35
Compressive reinforcement ratio	B-S-C-0	CFRP	3Φ16 mm	3Φ12.7 mm	250	270	-	35
	B-S-C-1		3Φ16 mm	3Φ12.7 mm	250	270	2Φ9.5 mm	35
	B-S-C-2		3Φ16 mm	3Φ12.7 mm	250	270	2Φ12.7mm	35

5.5.1 Effect of Tensile Reinforcement Ratio

Nine different concrete sections reinforced with different amount of CFRP and steel reinforcement were used to study the effect of the amount of FRP or steel reinforcement on the moment curvature relationship as shown in Figures 5-7 and 5-8.

Figures 5-9 and 5-10 show that the initial slope of moment-curvature curve is similar for all FRP and hybrid reinforced concrete beams investigated, and in general represents the concrete contribution to the moment capacity. An improvement in terms of deformability and ductility can also be observed for all hybrid beams with respect to the FRP R/C (Pure FRP), mainly after cracking. Although there is a sudden drop of moment in specimens Hybrid-1 and Hybrid-4 caused by the rupture of CFRP rebars, some residual ductility could still be maintained as the steel bars were still far below its breaking point.

It is clear from Figures mentioned above that increasing the area of the tensile FRP or steel reinforcement was found to increase the moment capacity of hybrid sections. However, due to the elastic and brittle nature of the CFRP bar material, the ductility of the beam specimens reinforced with larger CFRP reinforcement area was reduced.

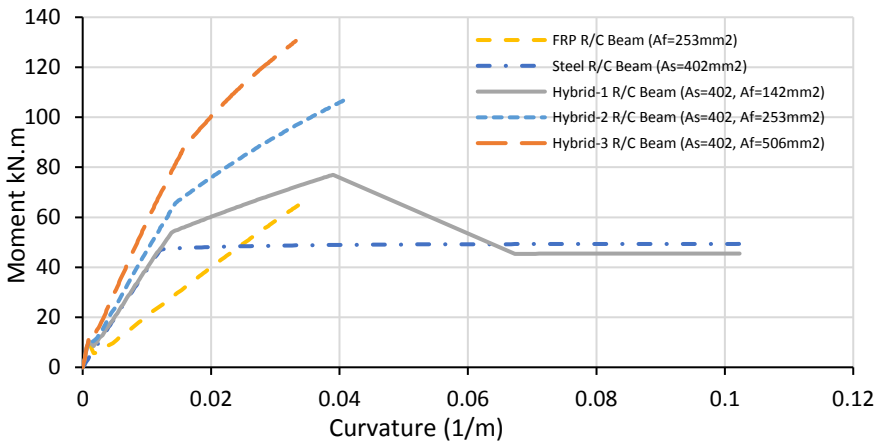

Figure 5.9 Moment vs. curvature for different FRP reinforcement ratio

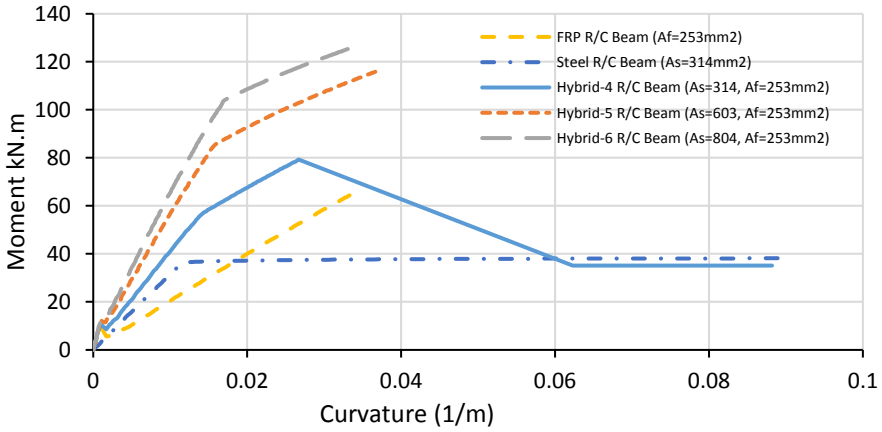

Figure 5.10 Moment vs. curvature for different steel reinforcement ratio

5.5.2 Effect of FRP Reinforcement Type

Figure 5-11 shows the moment curvature relationship of hybrid sections reinforced with different types of FRP rebars as described in Table 5-3. Section reinforced with CFRP exhibited higher moment compared with that reinforced with GFRP after the first crack occurred. Upon concrete cracking, the stress in the tensile reinforcement is utilized to transfer the applied loadings. Hence, a change of slope in the moment-curvature response of the investigated beam with different types of reinforcement is clearly noticeable as shown in Fig 5-11. This behavior is mainly attributed to the lower elastic modulus of GFRP bars than that of CFRP bars leading to a reduced effective moment of inertia and hence large curvature.

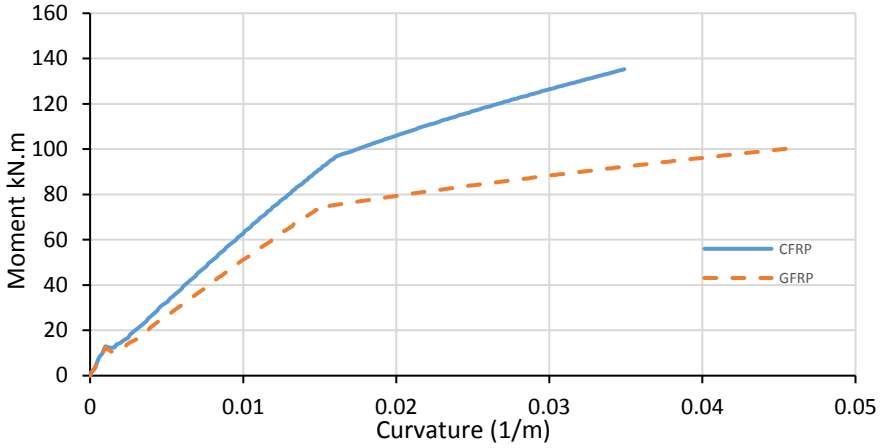

Figure 5.11 Moment-curvature for different type of FRP bars

5.5.3 Effect of Concrete Compressive Strength

In this section, the effect of the concrete compressive strength on the performance of concrete beams reinforced with a hybrid combination of CFRP and steel bars is investigated. Three different specimens, as described in Table 5-3, were used with concrete compressive strengths of 25, 35 and 45 MPa. It can be seen from Figure 5–10 that increasing the concrete compressive strength slightly increased the cracking moment owing to the increase in concrete tensile strength. Figure 5–12 shows that S-C-45 (45MPa) achieved a higher moment capacity than that of specimens S-C-35 and S-C-25 by 14.7% and 34.5%, respectively. Moreover, increasing the concrete compressive strength was found to decrease the curvature of the hybrid reinforced concrete sections at the same value of the bending moment. The figure also shows that the enhanced difference of the curvature increased proportionally as the bending moment increased. Considerable nonlinearity was showed in the moment-curvature response for higher concrete strength. This might be attributed to the fact that concrete elements with higher strength require higher tensile strength in reinforcement to maintain equilibrium in the section.

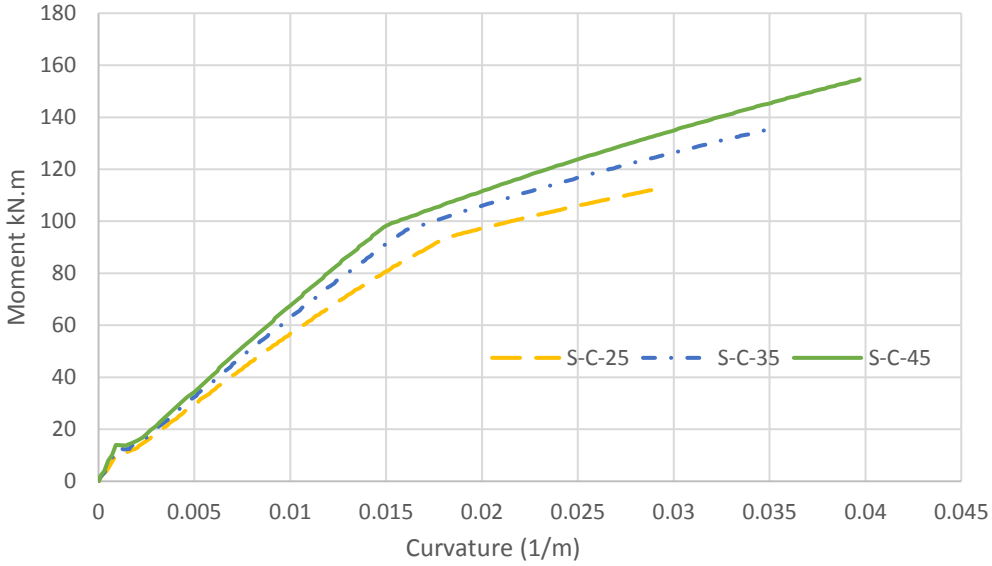

Figure 5.12 Moment-curvature for different concrete compressive strength

5.5.4 Effect of Position of Tensile Reinforcement

Figure 5-13 illustrates the effect of the position of steel tensile reinforcement on the moment-curvature relationship of hybrid reinforced concrete section (B-S-G) reinforced with GFRP and steel bars. The position of steel bars has been increased gradually by decreasing the distance from the top fibre of concrete section from 270 mm to 210 mm.

Figure 5-13 demonstrates that at the same value of curvature, increasing the distance between the steel bars' center and the bottom fibre of concrete section decreased the moment capacity of the hybrid section. This might be attributed to the effect of neutral axis location upon concrete cracking, where steel bars might contribute as compressive reinforcement. The figure also shows that, after the first crack occurred, the reduction of the curvature at the same value of moment increased as the bending moment increased.

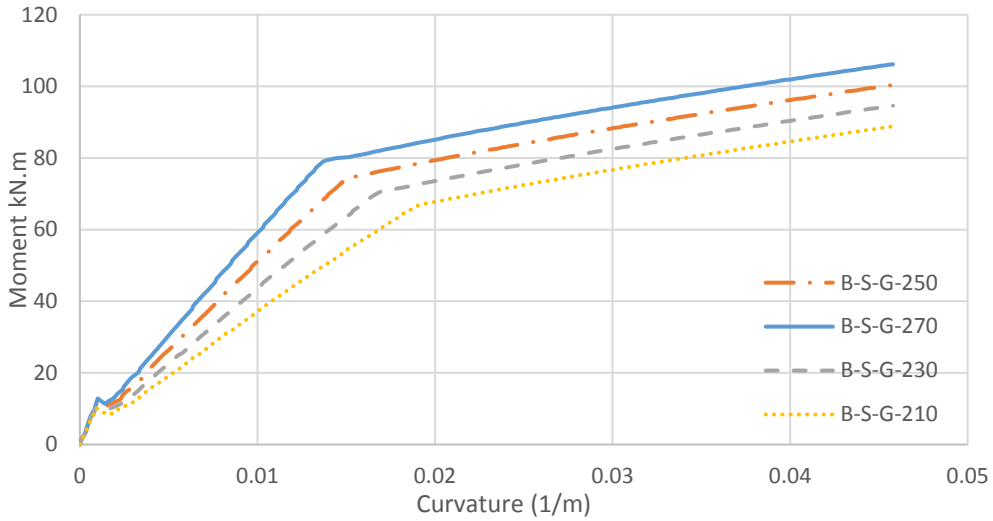

Figure 5.13 Moment-curvature for different positions of steel bars at hybrid section

5.5.5 Effect of Compressive Reinforcement Ratio

The effect of compressive reinforcement ratio on enhancing the flexural capacity of the hybrid sections has been investigated. It is clear from Figure 5-14 that the outcome of this analysis reveals that the increase of the top reinforcement ratio has a minimal effect on the moment capacity improvement, regardless the type of FRP reinforcement, if compared with the influence of the tension reinforcement ratio.

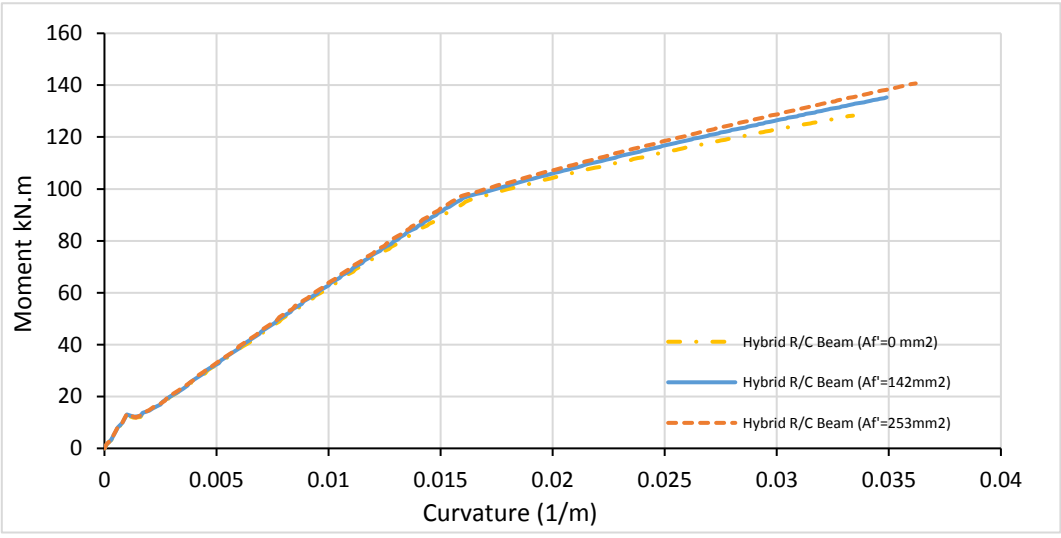

Figure 5.14 Moment-curvature for different compressive FRP reinforcement ratio

5.6 Design Procedure for Flexural Strength of Hybrid FRP-Steel Section

Three flexural modes were observed from the parametric study described in section 5.5: yielding of steel reinforcement followed by concrete crushing, tensile rupture of FRP bars followed by concrete crushing and concrete crushing before tensile rupture of FRP bars and yielding of steel reinforcement. However, Concrete sections reinforced with hybrid FRP-steel rebars can be classified into five different section types according to the flexural failure mode of each section. These are: FRP balanced section, steel balanced section, FRP rupture section, under reinforced section and over reinforced section as shown in Fig 5.15.

Based on these failure modes, a design procedure for concrete sections reinforced with hybrid FRP-steel reinforcement developed. The aim of developing such a design procedure is to form a basis for future design codes. In addition to the assumptions given in section 5.3 for determine the moment-curvature relationship of a hybrid section, concrete strength in tension is ignored (Park and Paulay, 1975). The design procedure for each section is described in Table 5.4.

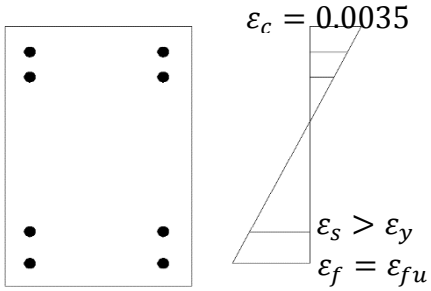

a. FRP balanced section

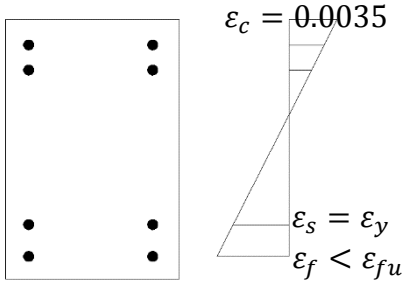

b. Steel balanced section

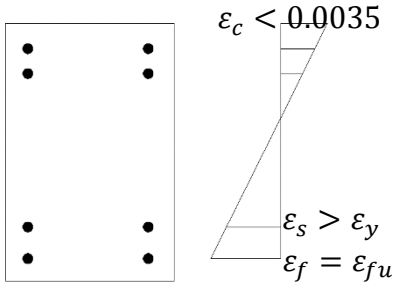

c. FRP rupture section

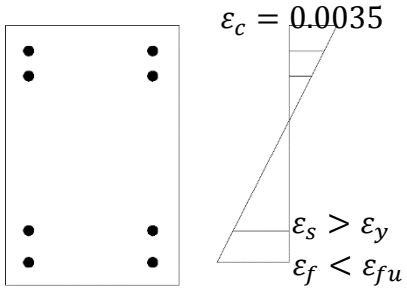

d. Under reinforced section

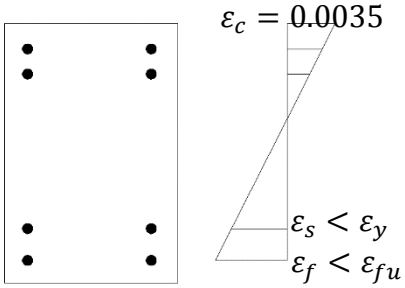

e. Over reinforced section

Figure 5.15 Classification of concrete sections reinforced with hybrid FRP/steel bars

Table 5-4 Moment capacities of different hybrid sections based on mode of failure

Classification of section	Area of FRP bars, A_f	Neutral axis, x	Moment capacity of section, M
FRP balanced section	$\frac{\sum_{i=1}^{n_c} C_{ci}L_{ci} - A_s f_y + A'_f f'_f}{f_{fu}}$	$x = \frac{0.0035}{0.0035 + \varepsilon_{fu}} d_f$	$\sum_{i=1}^{n_c} C_{ci}L_{ci} + \{ T'_f(d_s - d'_f) + T'_s(d_s - d'_s)\} - A_f f_{fu}(d_f - d_s)$
Steel balanced section	$\frac{\sum_{i=1}^{n_c} C_{ci}L_{ci} - A_s f_y + A'_f f'_f}{f_f}$	$x = \frac{0.0035}{0.0035 + \varepsilon_y} d_s$	$\sum_{i=1}^{n_c} C_{ci}L_{ci} + A'_f f'_f (d_f - d'_f) - A_f f_f(d_f - d_s)$
FRP rupture section	-	$x = \frac{\varepsilon_c}{\varepsilon_c + \varepsilon_{fu}} d_f$	$\sum_{i=1}^{n_c} C_{ci}L_{ci} + A'_f f'_f (d_s - d'_f) - A_f f_{fu}(d_f - d_s)$
Under reinforced section	-	$\frac{0.0035}{0.0035 + \varepsilon_y} d_s > x > \frac{0.0035}{0.0035 + \varepsilon_{fu}} d_f$	$\sum_{i=1}^{n_c} C_{ci}L_{ci} + A'_f f'_f (d_f - d'_f) - A_f f_f(d_f - d_s)$
Over reinforced section	-	$x > \frac{0.0035}{0.0035 + \varepsilon_y} d_s$	$\sum_{i=1}^{n_c} C_{ci}L_{ci} + A'_f f'_f (d_f - d'_f) - A_f f_f(d_f - d_s)$

5.7 Design Charts

Figures 5.16 and 5.17 show a sample of design charts for hybrid FRP-steel reinforced section. The design chart were obtained by studying the influence of the tensile FRP reinforcement ratio, ($\rho_f = \frac{A_f}{bd}$), and the tensile steel reinforcement ratio, ($\rho_s = \frac{A_s}{bd}$), on the flexural strength and failure mode of hybrid FRP-steel section with material properties given in table 5.5.

The figures mentioned above show that increasing the ratios of the tensile FRP reinforcement and steel reinforcement increases the flexural strength of the hybrid section but with decreasing the rate of increase of flexural strength.

Figure 5.18 shows how the flexural failure modes are influenced by the different relative amounts of the internal tensile FRP and steel reinforcement for hybrid FRP-steel section with the properties mentioned above in this section. It was found that the boundaries between the different flexural failure modes were linear. Figure 5.18 shows that the higher the tensile FRP reinforcement ratio, the lower the maximum amount of the tensile steel reinforcement ratio required to achieve a ductile flexural failure.

Table 5-5 Section dimensions and material properties used for design charts

$b(mm)$	$h(mm)$	$d_f(mm)$	$d_s(mm)$	f'_c (MPa)	$E_f(GPa)$	$f_f(MPa)$	$E_s(GPa)$	$f_y(MPa)$
150	200	170	140	35	39.5	588	196.4	550

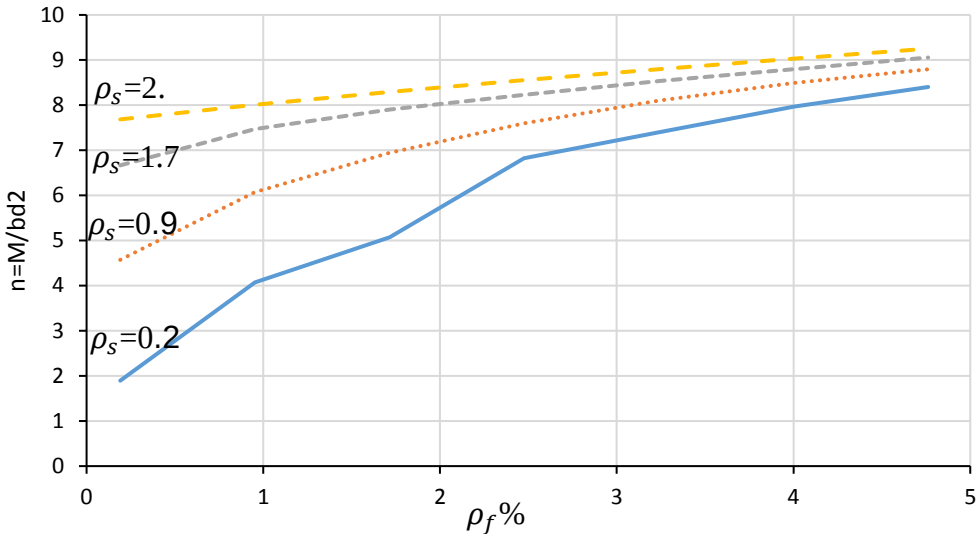

Figure 5.16 Normalized moment vs. steel reinforcement ratio for different FRP reinforcement area

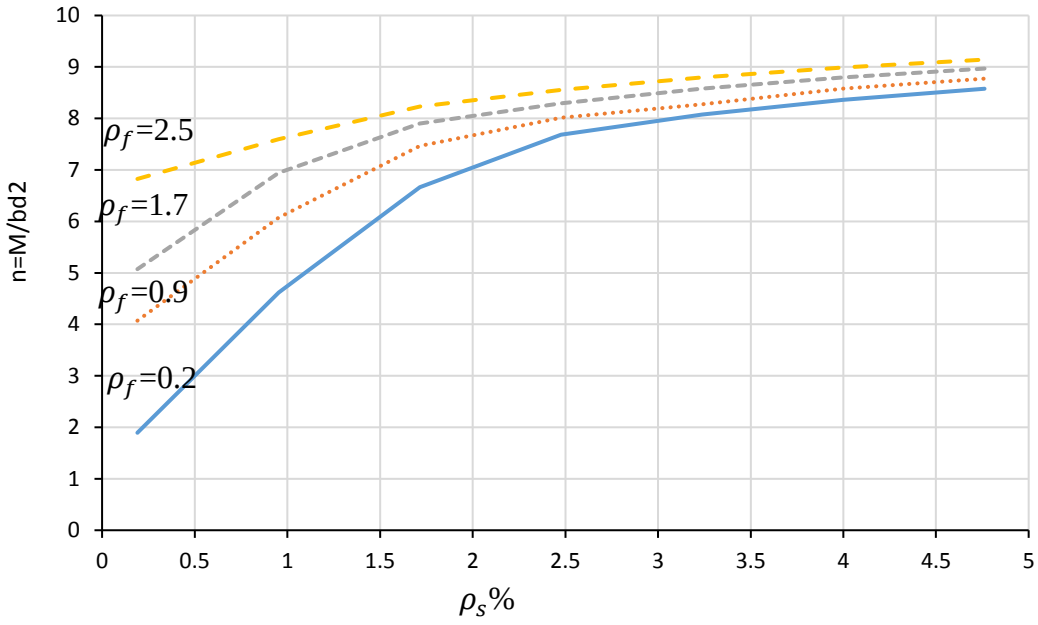

Figure 5.17 Normalized moment vs. FRP reinforcement ratio for different steel reinforcement area

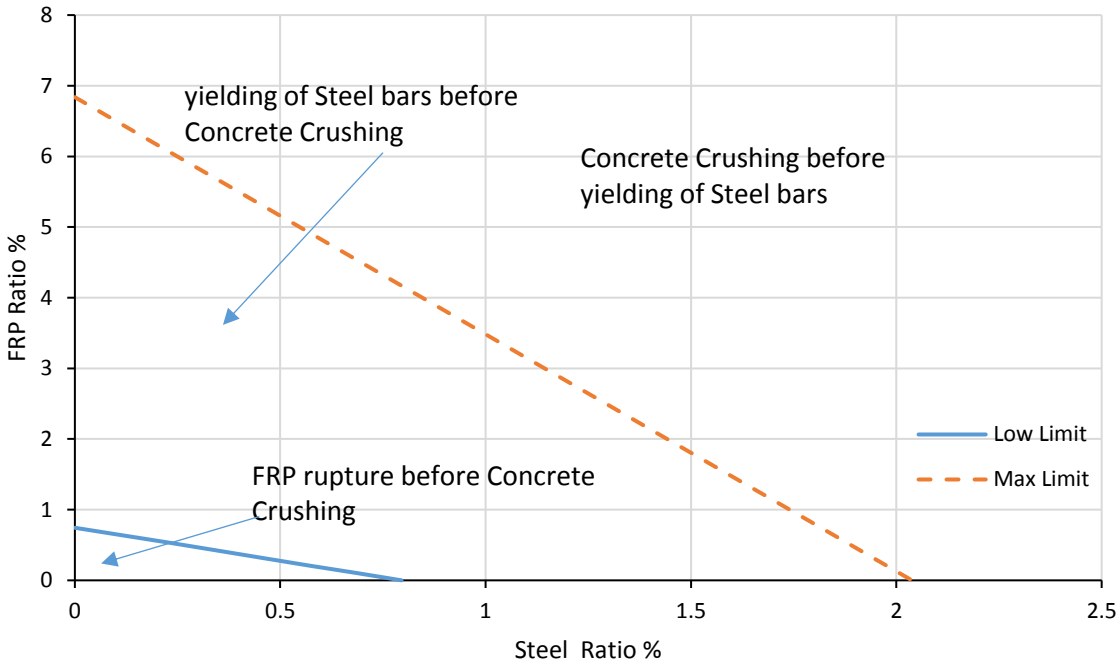

Figure 5.18 FRP reinforcement ratio vs steel reinforcement ratio, indicating the different flexural failures

5.8 Conclusions

The main aim of the analytical modelling program was to investigate the moment capacity and moment curvature relationship of hybrid reinforced concrete sections. The numerical technique has been developed based on equilibrium and compatibility of internal forces and strains.

Comparisons between experimental results available in the literature and presented in chapter four and predicted moment capacity and curvature show good agreement.

The influence of different parameters such as the compressive strength of concrete, amount and type of tensile and compressive FRP reinforcement, the

amount and position of tensile steel reinforcement on the flexural capacity and failure mode of a hybrid reinforced concrete has been investigated by using the developed model.

The main conclusions drawn from the study described in this chapter are summarized below:

- The moment curvature is a valuable tool which can provide an insight of structural response at an individual cross-section level.
- Increasing the concrete compressive strength increased the moment capacity of the hybrid sections and decreased the curvature. However, the failure mode might change accordingly.
- Several flexural failure modes were obtained for a hybrid section reinforced with FRP and steel bars such as: tensile rupture of the FRP re-bars before concrete crushing; steel yielding followed by concrete crushing or FRP rupture; and concrete crushing before FRP rupture or steel yielding.
- The contribution of steel reinforcement to FRP concrete beams provides ductility and stiffness improvement of beams investigated.
- Hybrid GFRP/steel reinforced concrete beams exhibited a significant reduction in stiffness after the initiation of first crack and yielding of steel reinforcement in comparison with CFRP/steel concrete beams.
- Increasing the compressive FRP reinforcement ratio had a relatively marginal influence on enhancing the moment capacity of hybrid reinforced sections.
- Increasing the tensile strength of FRP rods increased the flexural capacity of hybrid section.

- The ratio of FRP reinforcement should lie between upper and lower limits in order to obtain a ductile behaviour of the section. In addition, the higher the tensile FRP reinforcement ratio, the lower the steel reinforcement ratio.

CHAPTER SIX

DESIGN CODES EVALUATION AGAINST EXPERIMENTAL RESULTS OF HYBRID GFRP-STEEL CONCRETE BEAMS

6.1 Introduction

The concept of combining steel bars with FRP bars in reinforcing concrete structures has gained interest in the last decades. The aim is to overcome the lack of ductility; and serviceability limit state becoming the controlling design criteria of purely FRP reinforced structures. However, limited experimental data and theoretical studies on the structural performance of hybrid FRP/steel reinforced concrete beams are available in the literature. Therefore, there are limited recommendations regarding the hybrid FRP/steel reinforced concrete beams.

The main aim of this chapter is to evaluate the use of design codes of practice, mainly those developed for structures reinforced with FRP bars, as well as the formulas suggested by researchers for moment capacity, deflections of hybrid beams against the experimental results of simply and multi-span continuous hybrid GFRP-steel reinforced concrete beams tested. The design codes of practice investigated in this chapter include the ACI 440.2R.08 (for strengthening concrete structures), ACI 440.1R-15 (RC structures with FRP bars), ACI 318-11 (RC structures with steel bars), Euro Code 2 (EC2) and CSA/S608-14. In addition, models suggested by other researchers, namely Pang et al., (2015), Yinghao et al., (2013), and Yoon et al., (2011) to predict flexural strength and deflections of hybrid beams are investigated.

6.2 Moment Capacity Predictions

The moment capacity of hybrid beams is obtained by using different methods as explained in the following sections.

6.2.1 ACI 440.2R.08

The theoretical moment capacities of hybrid beams were calculated based on the procedure provided by ACI 440.2R.08. The reason behind choosing the ACI 440.2R.08 is because strengthening RC structures is one form of hybrid construction in which FRP bars are placed near the external surface of the tensile zone. The calculation procedure used to arrive at the ultimate strength should satisfy strain compatibility and force equilibrium. The iterative procedure involves selecting an assumed depth to the neutral axis *c*; calculating the strain level in each material using strain compatibility; calculating the associated stress level in each material; and checking internal force equilibrium as shown in Fig 6.1. If the internal force resultants do not equilibrate, the depth to the neutral axis should be revised and the procedure repeated. The ultimate moment, M_{pre}, was, therefore, determined using Eq (6.1)

$$M_{pre} = A_s f_s \left(d_s - \frac{\beta_1 c}{2}\right) + A_f f_f \left(d_f - \frac{\beta_1 c}{2}\right) + A'_s f'_s \left(\frac{\beta_1 c}{2} - d'_s\right) \quad (6\text{-}1)$$

where, A_s, A_f and A'_s are the area of tensile steel and GFRP reinforcements and the area of steel bars in compression zone, respectively, d_s, d_f and d'_s are the depth of steel bars, the depth of GFRP bars and the depth of compression steel reinforcement. f_s, f_f and f'_s are the stresses of tensile steel and GFRP bars and stresses of steel bars in compression zone, respectively. c is the

neutral axis depth for balanced failure and β_1 is the strength reduction factor $= 0.85 - 0.05\left(\frac{f_c' - 27.6}{6.7}\right)$.

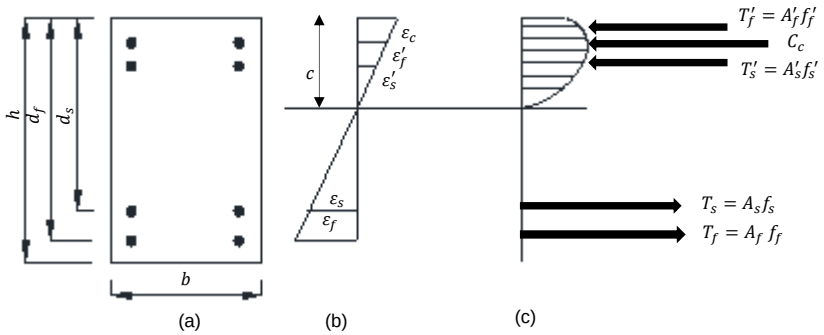

Figure 6.1 Strains, stresses and forces on RC section with hybrid GFRP/steel bars. (a) Hybrid RC section; (b) strain distribution; (c) stresses and forces.

6.2.2 Existing Developed Moment Capacity Formulas for Hybrid Reinforced Concrete Beams

6.2.2.1 Pang et al., (2015)

Pang et al., (2015) suggested to employ Eqs (6.2) -(6.5) in order to predict the failure modes of hybrid FRP/steel reinforced concrete beams as explained below in Table 6.1.

$$\rho_{\text{eff1}} = \frac{E_s A_s + E_f A_f}{E_s bd} = \rho_s + \frac{E_f}{E_s}\rho_f \quad (6\text{-}2)$$

$$\rho_{\text{eff,b1}} = 0.85\,\beta_1 \frac{f_c'}{f_y}\frac{\varepsilon_{cu}}{\varepsilon_{cu} + \varepsilon_y} \quad (6\text{-}3)$$

$$\rho_{\text{eff2}} = \frac{mA_s + A_f}{bd} = \frac{f_y}{f_{fu}}\rho_s + \rho_f \quad (6\text{-}4)$$

$$\rho_{\text{eff,b2}} = 0.85\,\beta_1 \frac{f_c'}{f_{fu}}\frac{E_f \varepsilon_{cu}}{\varepsilon_{cu} E_f + f_{fu}} \quad (6\text{-}5)$$

Table 6-1 Failure modes of the flexural hybrid RC beams (Pang et al., 2015)

Failure mode	Demand reinforcement condition
Mode I (Concrete crushing)	$\rho_{eff1} > \rho_{eff,b1}$
Mode II (Steel yielding followed by concrete crushing)	$\rho_{eff2} < \rho_{eff,b2}$
Mode III (Steel yielding followed by FRP rupture)	$\rho_{eff1} \leq \rho_{eff,b1}$ & $\rho_{eff2} \geq \rho_{eff,b2}$

According to Pang et al., (2015), the moment capacity of hybrid reinforced concrete beams is calculated by applying Eqs. (6.6) and (6.7)

$$M = \left(\rho_f f_f + \rho_s f_y\right)\left(1 - 0.59\frac{\rho_f f_f + \rho_s f_y}{f_c}\right) bd^2 \quad (6\text{-}6)$$

$$f_f = \sqrt{\frac{1}{4}\left(\frac{f_y A_s}{A_f} + \varepsilon_{cu} E_f\right)^2 + \left(0.85\frac{\beta_1 f_c}{\rho_f} - \frac{f_y A_s}{A_f}\right) E_f \varepsilon_{cu}} - \frac{1}{2}\left(\frac{f_y A_s}{A_f} + \varepsilon_{cu} E_f\right) \leq f_{fu} \quad (6\text{-}7)$$

where $\rho_f \left(=\frac{A_f}{bd}\right)$, $\rho_s \left(=\frac{A_s}{bd}\right)$ are the FRP and steel reinforcements ratios, respectively, A_f, A_s are the area of FRP and steel reinforcements, respectively, b and d are the width and effective depth of the GFRP reinforced concrete beam, f_c' is the cylinder compressive strength of concrete, f_{fu} is the ultimate tensile strength of FRP bars, ε_{cu} is the ultimate strain in concrete, E_f is the modulus of elasticity of FRP bars, f_f is the FRP stress at which the concrete crushing failure mode occurs.

6.2.2.2 Yinghao et al., (2013)

In the previous section, the flexural strength of hybrid section at failure is obtained by Eq (6.6) regardless of the failure mode. Yinghao et al., (2013) proposed equations to calculate the moment capacity of hybrid section taking into account failure mode using Eqs. (6.10)- (6.15). In addition, the three kinds of failure can be verified through the two balanced reinforcement ratios for hybrid FRP/steel reinforced concrete beams as follows.

$$\rho_{sb} = \frac{0.85 f'_c \beta_1 \xi_{nsb} - \frac{(h_0 - \xi_{nsb} h)}{(h_1 - \xi_{nsb} h)} E_f \rho_f \varepsilon_y}{f_y} \quad (6\text{-}8)$$

where $\xi_{nsb} = \frac{\varepsilon_{cu}}{\varepsilon_{cu} + \varepsilon_y} \frac{h_0}{h}$

$$\rho_{fb} = \frac{0.85 f'_c \beta_1 \xi_{nfb} - f_y \rho_s}{\varepsilon_{fu} E_f} \quad (6\text{-}9)$$

where $\xi_{nfb} = \frac{\varepsilon_{cu}}{\varepsilon_{cu} + \varepsilon_{fu}} \frac{h_1}{h}$

- Mode I ($\rho_s > \rho_{sb}$)

$$M = \frac{(h_0 - \xi_n h)}{(\xi_n h)} A_s E_s \varepsilon_{cu} (h_0 - 0.5 \beta_1 h \xi_n) + \frac{(h_1 - \xi_n h)}{(\xi_n h)} A_f E_f \varepsilon_{cu} (h_1 - 0.5 \beta_1 h \xi_n)$$

(6-10)

$$\xi_n = \frac{\sqrt{(\varepsilon_{cu} E_s A_s + \varepsilon_{cu} E_f A_f)^2 - 3.4 \beta_1 f_c b \varepsilon_{cu} (E_s A_s h_0 + E_f A_f h_1)} - \varepsilon_{cu} (E_f A_f + E_s A_s)}{2 * 0.85 \beta_1 f'_c b} \quad (6\text{-}11)$$

- Mode II ($\rho_f > \rho_{fb}$ *and* $\rho_s < \rho_{sb}$)

$$M = f_y A_s (h_0 - 0.5 \beta_1 h \xi_n) + \frac{(h_1 - \xi_n h)}{(\xi_n h)} A_f E_f \varepsilon_{cu} (h_1 - 0.5 \beta_1 h \xi_n) \quad (6\text{-}12)$$

$$\xi_n = \frac{f_y A_s - \varepsilon_{cu} E_f A_f + \sqrt{(\varepsilon_{cu} E_f A_f - f_y A_s)^2 + 3.4 \beta_1 f_c \varepsilon_{cu} E_f A_f b h_1}}{2 * 0.85 \beta_1 f'_c} \quad (6\text{-}13)$$

- Mode III ($\rho_f < \rho_{fb}$)

$$M = f_y A_s (h_0 - 0.5 \beta_1 h \xi_n) + A_f E_f \varepsilon_{fu} (h_1 - 0.5 \beta_1 h \xi_n) \quad (6\text{-}14)$$

$$\xi_n = \frac{f_y \rho_s + E_f \varepsilon_{fu} \rho_{fb}}{0.85 \beta_1 f'_c} \quad (6\text{-}15)$$

where h_o, h_1, h and ξ_n are the tensile steel bars depth, the FRP bars depth, the beam depth and the distance from the top of the beam to the neutral axis, respectively.

6.2.3 Moment Predictions for the Hybrid GFRP/Steel Reinforced Concrete Beams

The experimental and predicted moment capacities for the beams tested are presented in Table 6.2 and 6.3. Experimental failure moments at mid-span and middle support regions are calculated from the measured end support reaction and mid-span point load at failure of each beam.

As for hybrid simply and multi-span continuous concrete beams, the predicted results by ACI 440.2R.08 for sagging moments at failure are in a good agreement with the experimental results. The procedure explained above (ACI 440.2R.08) underestimated the hogging moment capacities of hybrid continuous beams except beam C-H-3.

It is noticed from the predicted results that the presence of compression reinforcement has not enhanced the ultimate strength of the hogging sections as much as expected. This is due to the fact that the neutral axis will be smaller at failure because the internal compressive force is shared by the concrete and the compression reinforcement.

As shown in Table 6.2 the equation proposed by Pnag et al., (2015) overestimated the sagging flexural strength of hybrid beams C-H-1, C-H-3 and C-H-7, whereas reasonably predicted the sagging failure moment of other hybrid beams. The predicted hogging moment capacity was underestimated by Eq (6.6) as presented in Table 6.2. On the other hand, It is clear that Yinghao' equations were very conservative in predicting the moment capacity in critical sections of sagging and hogging regions as given in Table 6.2.

The predicted moment capacities of GFRP or steel beams (either simple or continuous beams) were calculated in accordance to the provisions of ACI

440.1R-15 and ACI 318-11, respectively, as shown in Table 6.3. It can be seen from Table 6.3 that the ACI 440.1R-15 equation reasonably predicted the failure moments of beams S-G-1 at mid-span and beam C-G-1 at mid-span and over middle support.

Table 6-2 Comparison between experimental and predicted moment capacity results (hybrid beams)

Beam notation	Experimental results		Predicted results											
			ACI 440.2R.08				Pang et al., (2015)				Yinghao et al., (2013)			
	Failure moments, $M_{exp}(kN.m)$		Failure moments, $M_{pre}(kN.m)$		$\frac{M_{exp}}{M_{pre}}$		Failure moments, $M_{pre}(kN.m)$		$\frac{M_{exp}}{M_{pre}}$		Failure moments, $M_{pre}(kN.m)$		$\frac{M_{exp}}{M_{pre}}$	
	Sagging	Hogging	Sagging	Hogging	Sagging	Hogging	Sagging	Hogging	Sagging	Hogging	Sagging	Hogging	Sagging	Hogging
C-H-1	92.0	118	88	85	1.04	1.38	99.8	99.8	0.92	1.18	78.4	78.4	1.17	1.51
C-H-2	112.0	146	103	102	1.08	1.43	101.5	101.5	1.10	1.44	92.0	92.0	1.22	1.59
C-H-3	125.0	132	129	134	0.96	0.98	163.5	163.5	0.76	0.81	116.9	116.9	1.07	1.13
C-H-4	128.0	174	135	134	0.94	1.29	133	133	0.96	1.31	108.6	108.6	1.18	1.60
C-H-5	160	186	164.5	163	0.97	1.14	156.5	156.5	1.02	1.19	128.0	128.0	1.25	1.45
C-H-6	101	92	99	62	1.02	1.48	109	64.5	0.93	1.43	84.8	55	1.19	1.67
C-H-7	52	132.6	62	99	0.52	1.3	64.5	109	0.81	1.22	54.8	85	0.95	1.56
C-H-8	75	140	79	96	0.95	1.45	74	105	1.01	1.33	67.4	83	1.11	1.69
C-H-9	77	120	81	83	0.95	1.45	76	95	1.01	1.26	68.4	73	1.13	1.64
S-H-1	62	N/A	61.9	N/A	1.0	N/A	63	N/A	0.98	N/A	57	N/A	1.09	N/A
S-H-2	110	N/A	96.8	N/A	1.13	N/A	105	N/A	1.05	N/A	85	N/A	1.29	N/A
Average					0.99	1.33			0.95	1.24			1.15	1.5

Table 6-3 Comparison between experimental and predicted moment capacity results (FRP and steel beams)

Beam notation	Experimental results		Predicted results		$\frac{M_{exp}}{M_{pre}}$	
	Failure moments, $M_{exp}(kN.m)$		Failure moments, $M_{pre}(kN.m)$			
	Sagging	Hogging	Sagging	Hogging	Sagging	Hogging
C-S-1	97.3	137	85[a]	85[a]	1.14	1.6
C-G-1	65.6	69	61[b]	61[b]	1.08	1.13
S-G-1	77	N/A	70[b]	N/A	1.1	N/A

a,b results obtained by using ACI 318-11 and ACI 440.1R-15, respectively.

6.3 Failure Load Predictions for Hybrid GFRP-Steel Reinforced Concrete Beams

The predicted total failure load, P_{pre}, of the simply supported beams is calculated from the load that causes achievement of the moment capacity at mid-span section ($P_{pre} = \frac{4}{L} M_{us}$). While the predicted failure load, P_{pre}, of the continuous concrete beams would be obtained as explained below.

For a fully ductile beam, the flexural load capacity is based on a collapse mechanism with plastic hinges at mid-span and central support sections. Thus, the flexural load capacity P_{pre} on each span would be calculated from:

$$P_{pre} = \frac{2}{L}(M_{uh} + 2M_{us}) \quad (6\text{-}16)$$

where M_{us} and M_{uh} are the ultimate moment capacities at mid span and middle support sections, respectively and L is the span length of concrete member.

For a brittle elastic material, the flexural load capacity, P_{pre}, on each span is the smaller load that causes achievement of the moment capacity at either middle support ($P_{pre} = M_{uh}/0.188L$) or mid-span ($P_{pre} = M_{us}/0.156L$) section.

Table 6.4 presents the experimental failure loads against the computed load capacities based on the above two assumptions. As shown in Table 6.4, the theoretical failure load obtained from Eq. (6.16) based on the moment capacities at

mid-span and middle support sections, where moments obtained by different methods as explained above, gives the closest results for all hybrid beams, with an average and standard deviation between the experimental and predicted load capacities 1.12, 7.9%, 1.1, 11.7%, 1.24 and 12%, respectively. On the other hand, the load capacity computed based on elastic brittle material underestimated the experimental failure load with an average and standard deviation between the experimental and predicted load capacities of 1.29%, 15.1%, 1.2%, 16.9%, 1.48 and 22%, respectively.

Table 6-4 Experimental and predicted failure loads of the tested beams

Beam notation	Experimental Failure load $2P_{exp}: (kN)$	ACI 440.2R.08				Pang.L et al 2015				Yinghao et al 2013			
		Predicted Failure load, $2P_{pre}: (kN)$		$\frac{P_{exp}}{P_{pre}}$		Predicted Failure load, $2P_{pre}: (kN)$		$\frac{P_{exp}}{P_{pre}}$		Predicted Failure load, $2P_{pre}: (kN)$		$\frac{P_{exp}}{P_{pre}}$	
		$2P_{fd}$	$2P_{bem}$	P_{exp}/P_{fd}	P_{exp}/P_{bem}	$2P_{fd}$	$2P_{bem}$	P_{exp}/P_{fd}	P_{exp}/P_{bem}	$2P_{fd}$	$2P_{bem}$	P_{exp}/P_{fd}	P_{exp}/P_{bem}
C-H-1	465	402	348	1.16	1.34	461	408	1.0	1.14	362	321	1.28	1.45
C-H-2	571	474	406	1.21	1.37	468	415	1.2	1.37	425	376	1.34	1.52
C-H-3	589	603	548	0.98	1.07	755	669	0.78	0.88	540	478	1.09	1.23
C-H-4	665	622	548	1.07	1.21	614	544	1.08	1.22	501	444	1.33	1.50
C-H-5	781	757	667	1.03	1.17	722	640	1.08	1.22	591	524	1.32	1.49
C-H-6	452	400	255	1.13	1.78	435	264	1.04	1.7	346	225	1.31	2.01
C-H-7	364	343	306	1.06	1.19	366	318	0.99	1.14	299	270	1.22	1.35
C-H-8	450	391	390	1.15	1.16	389	365	1.16	1.23	335	332	1.34	1.36
C-H-9	423	377	341	1.12	1.25	380	375	1.11	1.13	323	299	1.31	1.41
S-H-1	94	95a	N/A	0.99	N/A	95a	N/A	0.99	N/A	95a	N/A	0.99	N/A
S-H-2	169	146a	N/A	1.15	N/A	146a	N/A	1.15	N/A	146a	N/A	1.15	N/A
Average				1.12	1.29			1.1	1.2			1.24	1.48
Standard deviation				7.9%	15.1%			11.7%	16.9%			12%	22%

P_{fd} and P_{bem} are the predicted failure loads based on fully ductile and brittle elastic materials, respectively.
a Simply supported beam.

6.4 Mid-Span Deflection Models

The immediate deflection Δ of simply and multi-span continuous reinforced concrete beams loaded with a mid-span point load illustrated in chapter four, could be calculated by Eqs. (6.17) and (6.18), respectively, as given below:

$$\Delta = \frac{Pl^3}{48E_cI_e} \quad (6\text{-}17)$$

$$\Delta = \frac{7}{768}\frac{Pl^3}{E_cI_e} \quad (6\text{-}18)$$

where P is the mid-span applied load at which the deflection is computed, l is the span length, E_c is the modulus of elasticity of concrete and I_e is the effective moment of inertia of the beam section. An expression for the effective moment of inertia I_e to be used for predicting the deflection of GFRP reinforced concrete beams is given by ACI 440.1R-15 as follows

$$I_e = \frac{I_{cr}}{1-\gamma\left(\frac{M_{cr}}{M_a}\right)^2\left[1-\frac{I_{cr}}{I_g}\right]} \leq I_g \quad (6\text{-}19)$$

where, M_{cr} is the cracking moment $= 2\frac{f_{cr}I_g}{h}$, M_a is the applied moment, γ is a factor which accounts for the length of the uncracked regions of the member and for the change in stiffness in the cracked regions $= 1.72 - 0.72\left(\frac{M_{cr}}{M_a}\right)$. I_g is the gross moment of inertia $= \frac{bh^3}{12}$, b and h are the width and overall height of the concrete beam, respectively, I_{cr} is the moment of inertia of transformed cracked section $= \frac{bd^3}{3}k^3 + (n_fA_f)\,d^2(1-k)^2$, k is the ratio of the neutral axis depth to reinforcement depth $= \sqrt{(\rho_f n_f)^2 + 2\rho_f n_f} - \rho_f n_f$, $n_f\left(=\frac{E_f}{E_c}\right)$ is the modulus ratio between FRP reinforcement and concrete, $E_c(=4750\sqrt{f_c'})$ is the concrete modulus of elasticity; and f_{cr} $(=0.62\sqrt{f_c'})$ is the modulus of rupture of concrete.

The use of equation (6-19) to predict the continuous change in flexural stiffness in the cracked regions of hybrid GFRP/steel beams is inappropriate, as it does not take into account the change of curve slope after yielding of steel.

To adopt the ACI 440.1R-15 equation for predicting the deflection of hybrid GFRP/steel reinforced concrete beams, steel reinforcement should be taken into account, where I_{cr} should be calculated for the combined GFRP and steel reinforcements by the following Equations (Qu et al., 2009):

$$I_{cr} = \frac{bd^3}{3}k^3 + (n_f A_f + n_s A_s)\, d^2(1-k)^2 \quad (6\text{-}20)$$

$$k = \sqrt{(\rho')^2 + 2\rho'} - \rho' \quad (6\text{-}21)$$

$$\rho' = \rho_f n_f + \rho_s n_s \quad (6\text{-}22)$$

where $n_s \left(= \frac{E_s}{E_c}\right)$ is the elastic modulus ratio between steel reinforcement and concrete and d is the distance from extreme compression fibre to the centroid of the tension reinforcing zone.

More precisely, Yoon et al., (2011) proposed an expression for the effective moment of inertia I_e, which is based on Bischoff's approach, to be used for predicting the deflection of hybrid sections as given in Eq (6.23) below:

$$I_e = \frac{I_{cr1}}{\frac{I_{cr1}}{I_{cr2}} + \frac{M_y}{M_a}\left(1 - \frac{I_{cr1}}{I_{cr2}}\right) - \left(\frac{M_y}{M_a}\right)^2\left(1 - \frac{I_{cr1}}{I_{cr2}}\right)} \leq I_g \quad (6\text{-}23)$$

where M_y is the steel yielding moment, $I_{cr1}\left(= \frac{bd^3}{3}k_1^3 + (n_f A_f)\, d^2(1-k_1)^2\right) + (n_S A_S)\, d^2(1-k_1)^2$ is the moment of inertia of transformed cracked hybrid section, $k_1 (= \sqrt{\left[\rho_f n_f + \rho_s n_s \left(\frac{d_s}{d_f}\right)\right]^2 + 2\left[\rho_f n_f + \rho_s n_s \left(\frac{d_s}{d_f}\right)^2\right]} - \left[\rho_f n_f + \rho_s n_s \left(\frac{d_s}{d_f}\right)\right]$ is the ratio of the neutral axis depth to reinforcement depth before steel yields, $d_s \; and \; d_f$ are the distance between extreme fiber of concrete in compression and

steel and GFRP bars, respectively, I_{cr2} $(= \frac{bd^3}{3} k^3 + (n_f A_f)\, d^2(1-k)^2)$ is the transformed cracked moment of inertia after steel yields.

6.4.1 Deflection Predictions for Hybrid Reinforced Concrete Beams

The comparisons between the experimental and theoretical load-deflection diagrams for the tested beams are shown in Figs 6.2-6.4. The comparison is made between the experimental results and the predictions obtained by ACI 440.1R-15 for FRP beams, Qu's equation and Yoon's model for hybrid beams. The prediction process has shown a good agreement for beam S-G-1 whereas a stiffer trend for beam C-G-1 is predicted by ACI 440.1R-15 equation as presented in Figs 6.2-A and 6.2-B, respectively.

As for hybrid simply supported concrete beams S-H-1 and S-H-2, the curves show that there is a good agreement between the experimental results and predicted deflections values by Yoon's model as shown in Figs 6.2-C and 6.2-D, respectively. On the other hand, it was clear that Qu's equation underestimated the deflections at all stages of loading after cracking. As load increased, this underestimation has progressively increased until failure as Eq (6-20) does not take into account post yielding of steel.

Yoon's model for hybrid continuous concrete beams C-H-1 and C-H-2 has given a closer deflection to experimentally measured deflections for the applied loads up to failure as shown in Figs 6.2-E and 6.2-F. As the steel reinforcement ratio increased (beam C-H-3), Yoon's equation tended to overestimate the mid-span deflections at higher service loads as shown in Fig 6.2-G. It can be seen from Fig 6.2-H that Yoon's model predicted the deflections of beam C-H-4 with a steady overestimation of deflections after cracking. On the other hand, it predicted the deflection of beam

C-H-5 with a steady underestimation of the deflection as shown in Fig 6.2-I. This might be attributed to the high ratio of GFRP to steel bars in beams C-H-4 and C-H-5.

Figures 6.3 and 6.4 show the experimental deflection of hybrid beams C-H-6, C-H-7, C-H-8 and C-H-9 against the predictions obtained by the models explained above (Qu's model and Yoon's model). It is clear that Qu's model predicted stiffer behaviour for beam C-H-6 after formation of cracks as shown in Fig 6.3-A. However, the Yoon's model reasonably predicted the deflection of hybrid continuous beams, with a steady overestimation of the deflection for loads higher than 60kN for beams C-H-7, C-H-8 and C-H-9 as shown in Figs 6.3-B, 6.4-A and 6.4-B, respectively, and accurately predicted the deflection of hybrid beam C-H-6 for high loading levels as shown in Fig 6.3-A.

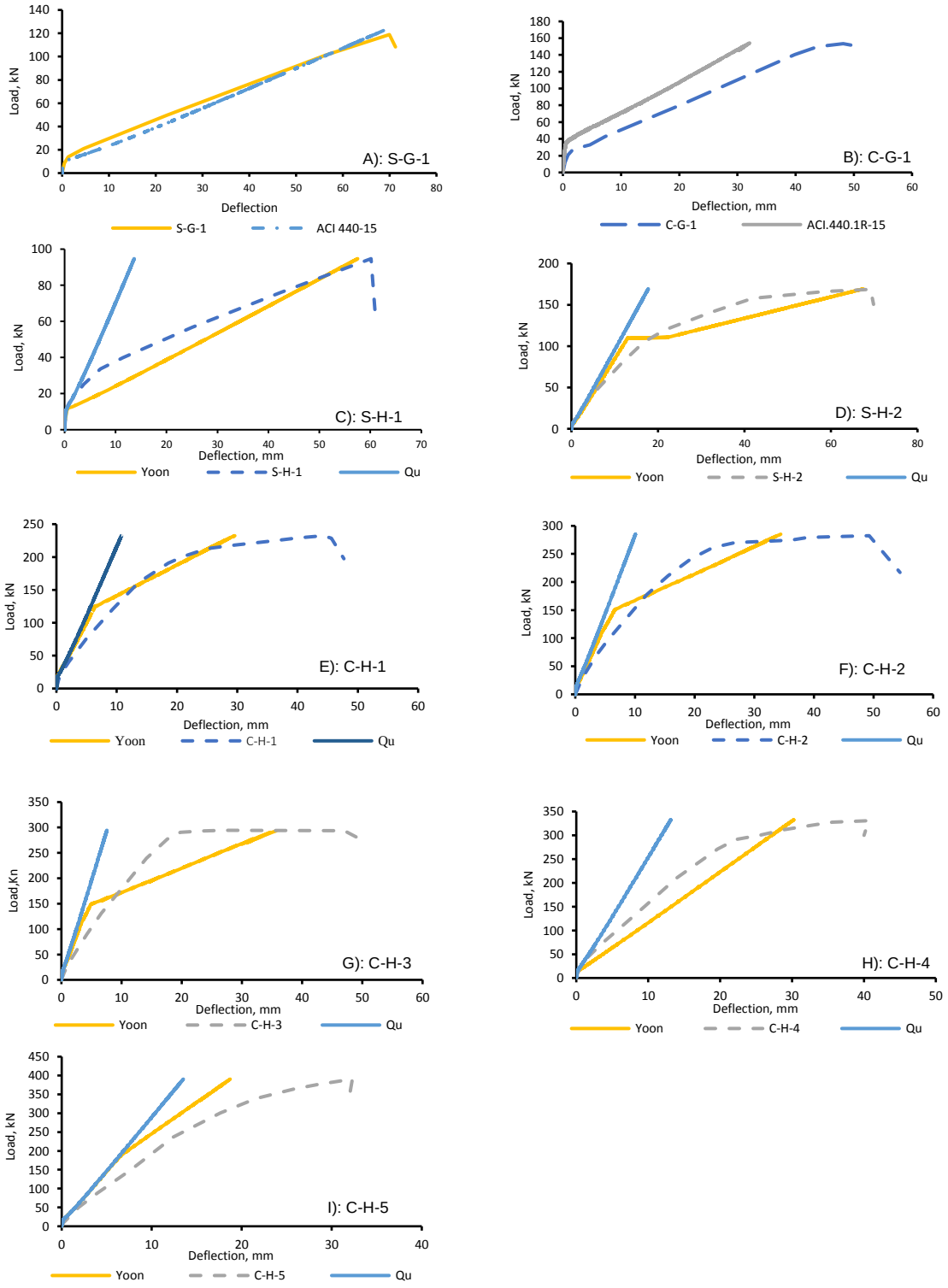

Figure 6.2 Experimental and predicted deflections for beams tested

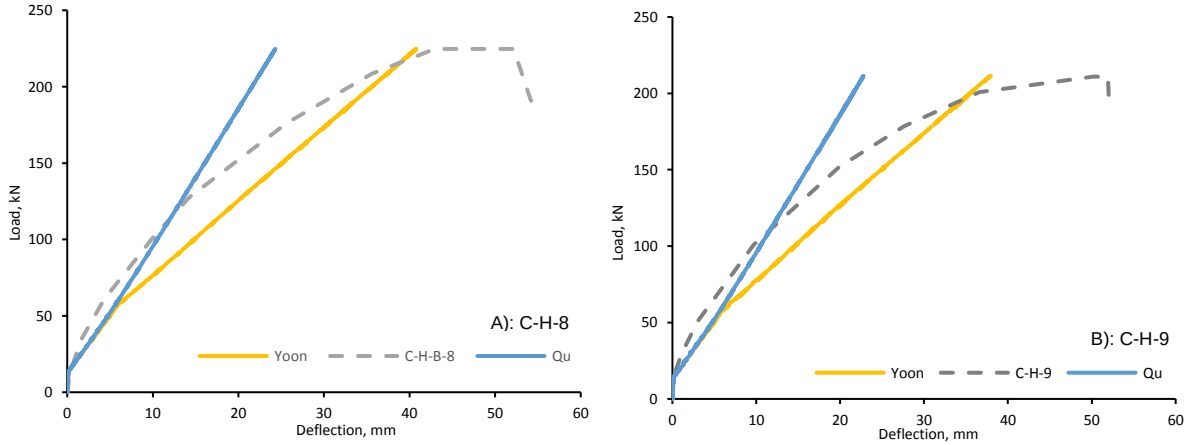

Figure 6.3 Experimental and predicted deflections for beams C-H-6 & C-H-7

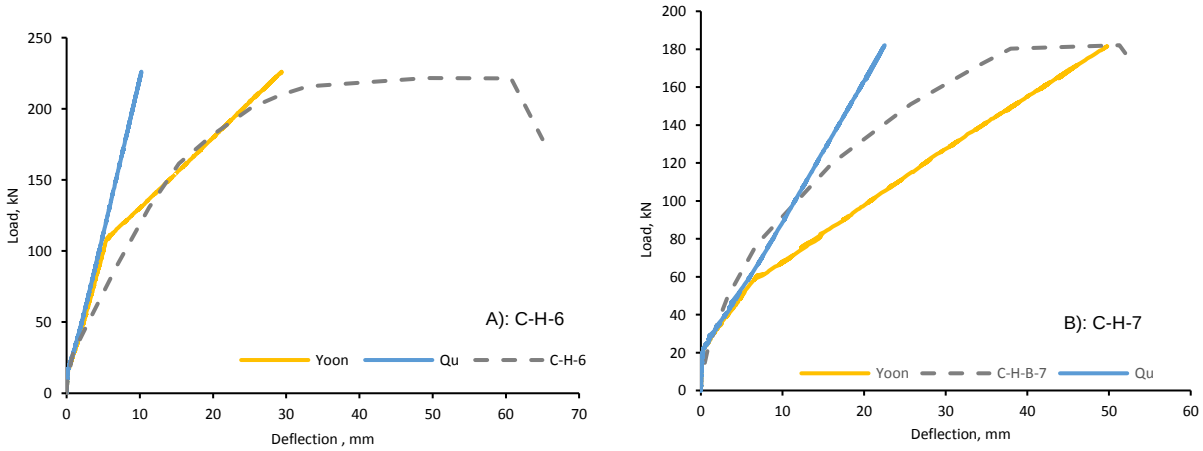

Figure 6.4 Experimental and predicted deflections for beams C-H-8 & C-H-9

6.5 Beam Ductility

The ductility of a beam can be defined as its ability to sustain inelastic deformation without loss in its load carrying capacity prior to failure. For conventional structural elements, ductility can be computed as the ratio of deflection at ultimate load to that at the first yield of steel reinforcement. This is due to the fact that there is clear plastic deformation of steel at yield. The deformation can be expressed as curvature, rotation or displacement (Zou, 2003).

The previous definition of ductility is not applicable for structural elements reinforced with FRP bars due to the linear behaviour of composite materials up to failure. Therefore, two approaches have been employed in the present study, namely, deformation-based methods and energy based methods, in order to evaluate the flexural ductility of specimens test.

6.5.1 Deformation Based Methods

The deflection ductility index, $\mu_{\Delta 1}$, and the displacement ratio, $\mu_{\Delta 2}$, were chosen to assess the ductility index of specimens tested by using Eqs. 6.24 and 6.25.

$$\mu_{\Delta 1} = \frac{\Delta_u}{\Delta_y} \quad (6\text{-}24)$$

$$\mu_{\Delta 2} = \frac{\Delta_u}{L} \quad (6\text{-}25)$$

where Δ_u is the mid span deflection corresponding to ultimate load, Δ_y is the mid span deflection at the second change in in slope of the load-deflection response caused by yielding of tensile steel in either the sagging or the hogging regions and L is the span length.

6.5.2 Energy Based Method

Naaman and Jeong (1995) proposed that ductility can be expressed in terms of the ratio of the total energy to the elastic energy at failure state of a beam as shown in Fig 5.9. The ductility index, μ_{en}, was given by Eq. 6.26.

$$\mu_{en} = 0.5\left(\frac{E_{tot}}{E_{ela}} + 1\right) \quad (6\text{-}26)$$

where E_{tot} is the total energy, computed as the area under the load deflection curve up to the load defined as the failure load, and E_{ela} is the elastic energy, which is a part of the total energy, E_{tot}, as illustrated in Fig 6.5.

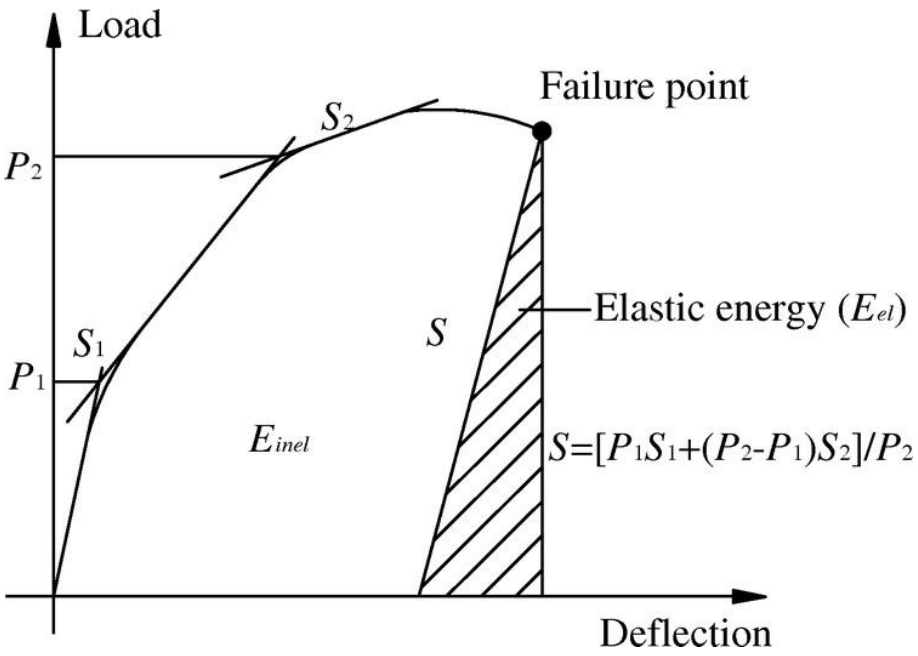

Figure 6.5 Total, elastic and inelastic energies (Naaman and Jeong, 1995)

As shown in Table 6.5, it can be seen that hybrid beams C-H-6 and C-H-7 exhibited higher ductility indexes than that of the control specimens C-H-1 and C-S-1. This is due to the fact that hybrid beams C-H-6 and C-H-7 experienced high percentage of moment redistribution which allowed to undergo a significant deformation after reaching the ultimate load with insignificant reduction in the applied load. As expected, both simply and multi-span continuous beams reinforced with only GFRP

bars featured ductility index values less than that of other beams. This is attributed to the elastic behaviour of GFRP reinforcement and stiffness reduction after formation of first crack. The ductility indexes of specimens C-H-2, C-H-3, C-H-4 and C-H-5, heavily reinforced with either GFRP or steel bars, were lower than that of the specimen C-H-1. This demonstrated that using the same hybrid reinforcement ratios in the sagging and hogging regions resulted in reducing the beam ductility index. There is a good agreement between results obtained by Eqs 6.24 and 6.26, except beams C-H-6 and C-H-9. Generally, the results show that hybrid reinforcement system can improve not only the load capacity but also the ductility.

Table 6-5 Ductility indices of tested beams at failure

Beam no	$\Delta_u\ (mm)$	$\Delta_y\ (mm)$	$\mu_{\Delta 1}$	$\mu_{\Delta 2}$	μ_{en}	Ductility index ratio*	Ductility index ratio**
C-S-1	44	10	4.4	1/59	4.5	1.00	1.00
C-G-1	47	N/A	N/A	1/55	1.9	-	0.42
S-G-1	70	N/A	N/A	1/37	1.8	-	0.40
C-H-1	45	12	3.75	1/58	4.3	0.85	0.96
C-H-2	49	13	3.77	1/53	3	0.86	0.67
C-H-3	47	15	3.13	1/55	3.6	0.71	0.80
C-H-4	40	14	2.86	1/65	3	0.65	0.67
C-H-5	32	12.5	2.56	1/81	2	0.58	0.44
C-H-6	60	14	4.29	1/43	6.7	0.98	1.49
C-H-7	51	7	7.29	1/51	7.9	1.66	1.76
C-H-8	52	14	3.71	1/50	4.9	0.84	1.09
C-H-9	52	8	6.50	1/50	3.8	1.48	0.84
S-H-1	60	7	8.57	1/43	4.5	1.95	1.00
S-H-2	69	16	4.31	1/38	4.3	0.98	0.96

*Relative to ductility index of the control beam C-S-1 obtained by Eq 6.24.
**Relative to ductility index of the control beam C-S-1 obtained by Eq 6.26.

6.6 Shear Capacity

The main aim of this study was to investigate the flexural behaviour of hybrid continuous concrete beams in which an adequate amount of shear reinforcements were provided along specimens tested in order to prevent shear failure. The shear

reinforcement ratio was chosen in accordance to EC2. However, some of test specimens experienced shear failure.

Up to date, there is no research study conducted to investigate the shear behaviour of simply or multi-span continuous beams reinforced with hybrid FRP-steel bars. This section examines the level of reliability delivered by the current design codes, namely, ACI 318-11, CSA/S806-14 and EC2 with regard to predict shear resistance of hybrid GFRP-steel reinforced concrete beams.

Table 6.6 presents the shear capacity expressions employed to predict the shear capacity of test specimens. The aforementioned expressions were originally developed for shear capacity of steel-reinforced concrete member.

It is well known that the principal tensile stress, that cause diagonal cracking at any location near the interior support, depend on the values of bending moments and shear forces at that location. Therefore, discussing the shear strength of continuous beams cannot be separated from the bending moment at critical sections, which depend on the moment redistribution percentage.

Table 6-6 Shear capacity expressions for R.C beams

Approach	Shear strength, V_c,	Shear Strength, V_s
ACI 318-11	$V_c = 0.17\sqrt{f_c'}b_w d$	$V_s = \frac{A_v f_y d}{S}$
CSA/S806-14	$V_c = 2.5\beta\emptyset_c f_{cr} b_w d$	$V_s = \frac{\emptyset_S A_v f_y d_v cot\theta}{S}$
EC-2	$V_c = \left(0.9.\upsilon.\left(\frac{f_c'}{\gamma_c}\right).\frac{1}{(cot\theta + tan\theta)}\right) b_w d$	$V_s = \left(0.9\rho_{sw}\frac{f_y}{\gamma_s}cot\theta\right) b_w d$

Note: f_c'=compressive strength of concrete, b_w and d= beams' width and effective width, respectively, f_y = reinforcement yielding strength, A_v and S = shear reinforcement and its spacing, respectively, $\emptyset_c$ and $\emptyset_S$ = resistance factor for concrete and reinforcing bar in which can be taken as 0.75 and 0.9, respectively, β =factor used to account for the shear resistance of cracked concrete in which can be taken as 0.18, f_{cr}= cracking strength of concrete that shall not be greater than 3.2 MPa , θ= angle of inclination of the principal diagonal compressive stresses to the longitudinal axis of a member, υ = a strength reduction Factor for concrete cracked in shear defined as $0.6\left(1 - \frac{f_c'}{250}\right)$, γ_c and γ_s = partial factors for concrete and steel, respectively equal to1.5 and 1.15, respectively, ρ_{sw} = shear reinforcement ratio (A_v/Sb_w).

6.6.1 Comparison Between Experimental and Code Predicted Shear Strength

Table 6.7 shows the experimental shear strength of the test beams and the predicted shear strength by ACI 318-11, CSA/S806-14 and EC2 as given in Table 6.6. The experimental shear capacity of each beam is the shear force in the interior shear span.

The ACI 318-11 well predicted the shear capacities of continuous concrete beams reinforced with either steel or hybrid GFRP-steel bars, whereas overestimated the shear strengths of beams C-G-1 and S-G-1 that reinforced with only GFRP bars. In addition, the predicted shear strengths of both simply supported hybrid concrete beams S-H-1 and S-H-1 were much higher than the experimental results by 63% and 32%, respectively. It is worth mentioning that hybrid beams C-H-2, C-H-4 and C-H-5 failed due to high shear stress near to interior supports as predicted by ACI 318-11.

The CSA/S806-14 and EC2 equations yield very conservative predictions of the shear capacity of all test specimens where the ratio of the experimental to predicted capacity is 0.56 and 0.59, respectively, as given in Table 6.7.

The test results showed that beams experienced higher moment redistribution namely C-H-6, C-H-7, C-H-8 and C-H-9 were capable of resisting higher loads before failure. On the contrary, small percentage of moment redistribution results in greater moment near the middle support, which cause higher principle tensile stresses that lead to failure of the beam at a lower shear force as occurred in hybrid beams C-H-2, C-H-4 and C-H-5.

Table 6-7 Experimental and predicted shear strength of test specimens

Beam	Shear Capacity, V_{test} , (kN)	ACI 318-11		CSA/S806-14		EU-1992	
		V_{pred}	V_{test} $/V_{pred}$	V_{pred}	V_{test} $/V_{pred}$	V_{pred}	V_{test} $/V_{pred}$
C-S-1	180.5	188.0	0.96	287.8	0.63	241.8	0.75
C-G-1	104	183.9	0.56	286.7	0.36	236.6	0.44
C-H-1	161.5	178.0	0.9	277.6	0.58	242.2	0.67
C-H-2	199.5	180.3	1.1	279.1	0.71	248.5	0.80
C-H-3	199.5	182.9	1.09	279.3	0.71	249.6	0.80
C-H-4	231	185.7	1.24	285.8	0.81	271.8	0.85
C-H-5	268.5	187.7	1.4	287.4	0.93	276.0	0.97
C-H-6	149	185.3	0.8	285.3	0.52	270.6	0.55
C-H-7	140	183.1	0.76	285.4	0.49	270.7	0.52
C-H-8	163	180.7	0.9	282.5	0.58	261.6	0.62
C-H-9	152.5	182.3	0.83	284.2	0.54	267.3	0.57
S-G-1	59	130.9	0.45	189.9	0.31	273.2	0.22
S-H-1	47	125.9	0.37	187.7	0.25	267.3	0.18
S-H-2	84.5	124.9	0.67	186.3	0.45	263.0	0.32
Mean			0.86		0.56		0.59
Standard deviation (%)			29		19		24
Coefficient of variation (%)			33.9		33.7		40.4

6.7 Concluding Remarks

Comparison between the experimental results presented in chapter four and those predicted by a number of design methods suggested by different codes of practice as well as previous research investigations were presented in this chapter. The comparisons aimed to assess the validity of applying these methods to continuous concrete beams reinforced by hybrid reinforcement. Based on the investigation carried out in this chapter, the following conclusions can be drawn:

- The ACI 440.2R-08 and Pang et al., (2015) equations reasonably predicted the sagging failure moment in most continuous hybrid reinforced concrete beams, whereas they underestimated the hogging flexural strength at failure of most hybrid continuous beams. On the other hand, the formulas proposed by Yinghao et al., (2013) were very conservative in predicting the failure moment at the critical sagging and hogging sections.
- The ACI 440.1R-15 design code equation, which were proposed for predicting the deflection of concrete beams reinforced by FRP bars, reasonably predicted the deflection of GFRP simple and continuous beams tested, whereas Qu's model which is based on ACI 440.1R-15 underestimated the deflections of hybrid beams tested at all stage of loading after cracking.
- The Yoon's model seems to be effective in predicting the mid-span deflection of simple and continuous members reinforced by hybrid GFRP/steel bars.
- The energy-based methods seems to be more efficient for estimating ductility index of concrete beams reinforced with hybrid GFRP/steel beams as it is difficult to predict the yield deflection theoretically.

- The CSA/S806-14 and EC2 equations significantly overestimated the shear capacity of all hybrid GFRP/steel beams. On the other hand, ACI 318-11 formulas could mostly reasonably predict the shear capacity of continuous concrete beams reinforced with a combination of GFRP/steel bars.

  It can be concluded that, although the theoretical methods considered in this chapter can reasonably predict the load capacity and load-deflection response of two-span continuous concrete beams reinforced with hybrid GFRP-steel bars, these methods cannot estimate stresses and strains distribution in critical sections of beam and along the member. Therefore, a two-dimensional non-linear finite element analysis will be presented in the next chapter to predict the full behaviour of continuous concrete beams reinforced with hybrid reinforcement. In addition, a parametric study will be carried out to investigate the effect of extended range of parameters on the flexural behaviour of multi-span continuous hybrid RC beams.

CHAPTER SEVEN

FINITE ELEMENT MODELLING OF HYBRID GFRP-STEEL CONTINUOUS CONCRETE BEAMS

7.1 Introduction

The most reliable method to evaluate accurate behavior of concrete structural elements is to experimentally study on actual structures, but because of being expensive and time consuming, usually experiments are not always possible to perform. Therefore, other methods, which models various sources of non-linearity of concrete structures, are required. One method is Finite Element Modeling (FEM), which needs less cost and time to be implemented. Different commercial FEM software has been developed over the past few years and one of them is ABAQUS, which was used in this study.

ABAQUS is a finite element program to evaluate the behavior of structures and solids under external loads. It can analyze both static and dynamic problems and it is capable of modeling a wide range of 2D and 3D shapes and contacts between solids. It has an advanced and extensive library of elements and materials (ABAQUS Inc., 2014).

This chapter presents a FE model using ABAQUS software to analyze and predict the behaviour of simple and continuous concrete beams reinforced with steel, GFRP and hybrid GFRP-steel bars. The model is verified using the experimental results of simply and multi-span continuous concrete beams reinforced with hybrid GFRP/steel bars described in chapter four. Moreover, the proposed model is used to conduct a parametric study in order to investigate the behaviour of continuous

concrete beams with extended parameter variations, both within and outside the range of experiments.

7.2 Constitutive Models for Materials

7.2.1 Constitutive Concrete Material Model

There are three material models for analyzing concrete at low confining pressures in ABAQUS; concrete smeared cracking model in ABAQUS/Standard, concrete damaged plasticity model in both ABAQUS/Standard and ABAQUS/Explicit and brittle cracking model in ABAQUS/Explicit.

The concrete smeared cracking model is suitable for cases that are supposed to describe tensile cracking or compressive crushing. In fact, cracking is the most important aspect of this model. The concrete damage plasticity model considers the stiffness degradation of material as well as stiffness recovery effects under cyclic loading. Therefore, this model is capable of analyzing problems with either monotonic or cyclic loading conditions (ABAQUS Inc., 2014).

The brittle cracking model is applicable for modeling which requires high consideration for tensile cracking. In other words, this model considers anisotropy due to cracking of the material (ABAQUS Inc., 2014).

In this study, for characterizing the mechanical behaviour of concrete, concrete damage plasticity model (CDP) was selected among all the three models available in ABAQUS as it's available in ABAQUS/Explicit which was employed to conduct the analysis as explained in section 7.6.

7.2.1.1 Concrete Damage Plasticity

The concrete damaged plasticity model in the ABAQUS/Standard and ABAQUS/Explicit is capable of modelling concrete and other quasi-brittle materials

in a variety of structures. This model uses concepts of isotropic damaged elasticity together with isotropic tensile and compressive plasticity to represent the inelastic behaviour of concrete. It is designed for applications in which concrete is subjected to arbitrary loading conditions, including monotonic, cyclic and/or dynamic loading under low confining pressures. The model takes into consideration the degradation of the elastic stiffness induced by plastic straining both in tension and compression (ABAQUS Inc, 2014).

In order to define concrete in the damaged plasticity model, initially, it is required defining the elastic modulus and the Poisson's ratio of concrete. Then the damaged plasticity parameters which include five parameters are defined. In this study, the dilation angle was taken as 40º, while default values were assumed for all other plasticity parameters as shown in Table 7.1. After that, the behavior of concrete in compression is defined followed by the behavior of concrete in tension.

Table 7-1 Plasticity parameters for concrete damaged plasticity model

dilation angle, Ψ	Eccentricity, ϵ	σ_{bo}/σ_{co}	K_C	viscosity parameter, μ
40º	0.1	1.16	2/3	0

where (Ψ)is defined in the p-q plane as shown in Fig 7.1 and value is entered in degrees, (ϵ) is flow potential eccentricity which is a small positive number that defines the rate at which the hyperbolic flow potential approaches its asymptote as shown in Fig 7.1, (σ_{bo}/σ_{co}) is the ratio of initial equi-biaxial compressive yield stress to initial uniaxial compressive yield stress, (K_C) is the ratio of the second stress invariant on the tensile meridian, $\boldsymbol{q}(\boldsymbol{TM})$, to that on the compressive meridian, $\boldsymbol{q}(\boldsymbol{CM})$ as shown in Fig 7.2, at initial yield for any given value of the pressure invariant *p* such that the maximum principal stress is negative, $\sigma_{max} < 0$. It must satisfy the condition $0 < K_C \leq 1.0$ and μ is used for the visco-plastic regularization

of the concrete constitutive equations in ABAQUS/Standard analyses. This parameter is ignored in ABAQUS/Explicit.

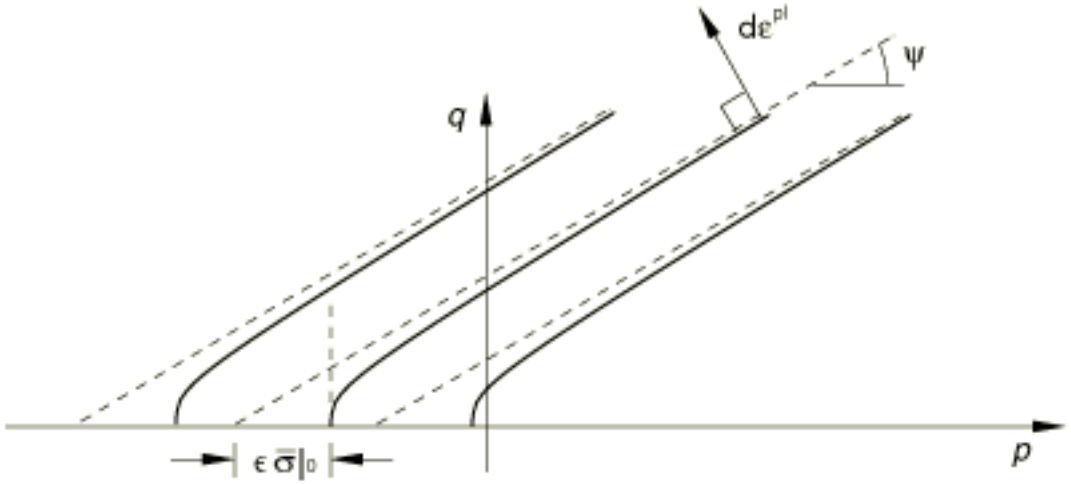

Figure 7.1 Hyperbolic plastic flow rule (ABAQUS Inc, 2014)

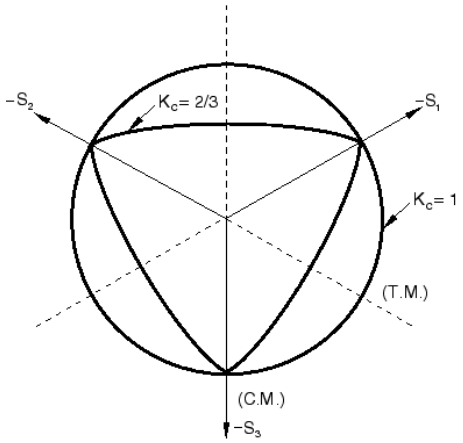

Figure 7.2 Yield surfaces in the deviatoric plane, corresponding to different values of K_C

In the concrete damage plasticity model, to define the compressive behavior of concrete, two input values should be defined, yield stress as a function of plastic strain, given in a tabular form. In the first row, the first point has plastic strain equal to zero and is where the first nonlinear behavior of concrete has been observed with equivalent stress of approximately 40% of the ultimate compressive strength, f_c'.

For compression behaviour, stress-strain model provided by Hognestad et al., (1955) and used by Park and Paulay, (1975); and presented in chapter five was adopted in this chapter.

The post failure behavior for direct straining is modeled with tension stiffening, which allows to define the strain-softening behavior of cracked concrete. This behavior also allows for the effects of the reinforcement interaction with concrete to be simulated in a simple manner. Tension stiffening is required in the concrete damaged plasticity model in which can be modeled by means of post failure stress-strain relation or by applying a fracture energy cracking criterion (ABAQUS Inc, 2014). In The proposed FE model, the post failure stress as a function of cracking strain was selected and defined by using Eq (5.4) in chapter five.

7.2.2 Reinforcement Materials

In ABAQUS, reinforcement can be modeled with different methods including smeared reinforcement in concrete, cohesive element method, discrete truss or beam elements with the embedded region constraint or built-in rebar layers. In this study, truss element has been used for reinforcement modeling of which the only required input is the cross-sectional area of bars. The material of the reinforcement was defined based on the stress-strain relationships of steel and FRP rebars as shown in Figures 7.3 and 7.4, respectively, and presented in chapter five.

The elastic part of the behavior was defined by the longitudinal elastic modulus (E_s, E_f) and Poisson's ratio (v). The plastic part of steel and FRP reinforcements was defined by (stress, plastic strain) data pairs. The rupture of the FRP reinforcement was defined by specifying a plastic part where the rupture stress drops to zero at a negligible plastic strain.

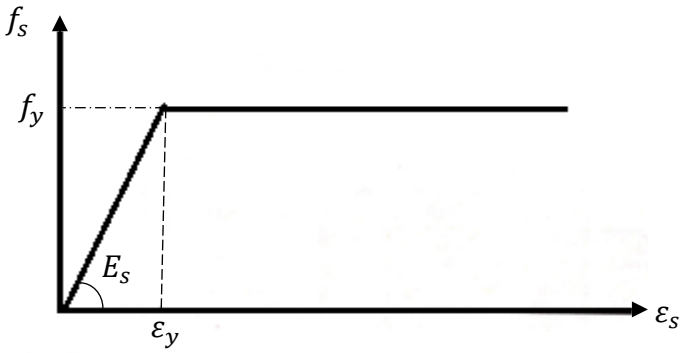

Figure 7.3 Stress-Strain relationship of steel reinforcement (BS EN 1992-1-1:2004)

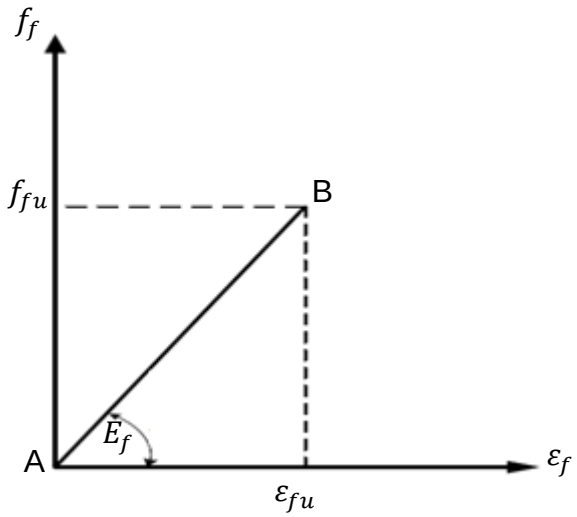

Figure 7.4 Stress-strain in tension for GFRP reinforcing bars

7.3 Model Geometry and Boundary Conditions

All tested beams are symmetrical in geometry, loading and internal reinforcement in the longitudinal direction about the middle support location. In order to achieve computational efficiency, only half of each specimen was modelled in ABAQUS taking advantage of symmetry about one axis in which appropriate symmetry boundary conditions were applied. The geometrical model with mesh is shown in Figure 7.5, including the symmetry plane and applied loads. The boundary

conditions at the axis of symmetry were set to represent the effect of continuity. The end-support was modelled as a roller whereas the middle support was modelled to simulate a hinge. This was achieved at the end support by restricting the vertical movement only, while restricting both vertical and horizontal movements at the middle support. The load was defined as a displacement at the middle of the loading plate. An increment of deformation in y-direction was applied to the reference point at the centre node of the loading plate. Fig 7.5 shows the geometry of the 2-D model whereas the longitudinal reinforcement and transverse stirrups are illustrated in Fig 7.6.

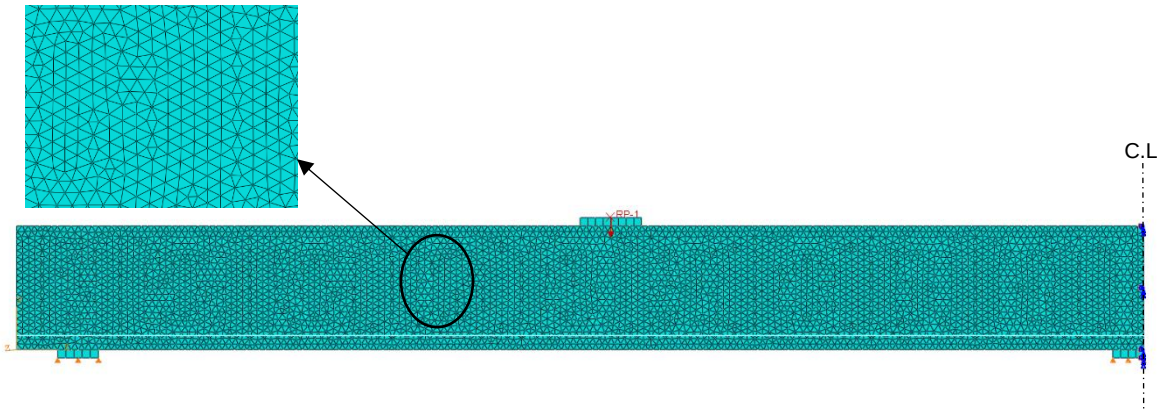

Figure 7.5 Model geometry and concrete elements

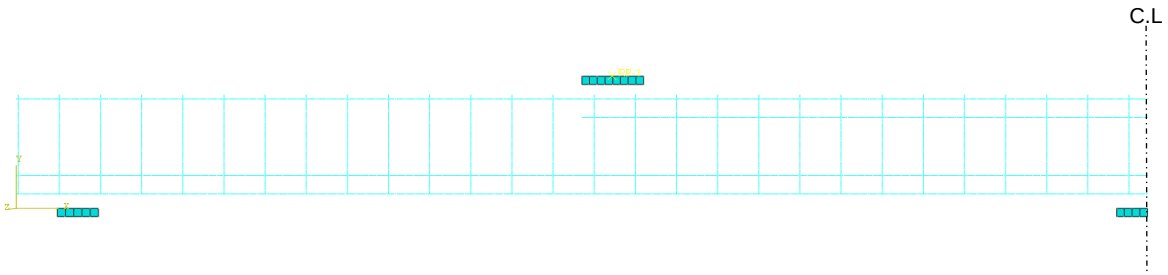

Figure 7.6 Longitudinal and transverse reinforcement configuration

7.4 Element Types and Meshes Density

The selection of the element type for each part of the model is important due to its clear effect on the accuracy of the results and computational time. In the proposed finite element model, the concrete was modelled using a 3-node linear plane stress triangle element (CPS3) which has six degrees of freedom at connections.

As for the steel and GFRP reinforcements, they were modelled using a 2-node linear 2-D truss elements (T2D2) which has one translation degree of freedom in the x direction. The truss element can be used to represent a slender structural element that resists and transfers only axis forces. The advantage of using a truss element is that the perfect-bond can easily be defined by embedding the reinforcements into a host region (concrete beam). The loading and rigid steel supports were modelled using the plane stress element (CPS4R) with elastic steel material properties to avoid any major stress concentration problems on the concrete material.

A mesh size sensitivity study was conducted to determine the most suitable finite element mesh size. The mesh size should be fine enough to achieve accuracy. However, excessively fine mesh should be avoided as it requires more processing time and desk usage. Element sizes ranging from 5 mm to 25 mm were considered in the study to obtain a suitable mesh size that would produce accurate results while remaining computationally efficiency.

The sensitivity study conducted on beam C-H-1 suggested that mesh size of 5 mm to 20 mm gives an acceptable degree of accuracy compared with experimental results as shown in Fig. 7.7. It is clear that the coarse mesh with element size of 25 mm led to a significant difference in the predicted load capacity of the beam. On the other hand, using smaller mesh size improved the accuracy of the model and

reduced the difference in results, however, required large number of nods. The choice of the appropriate mesh size was performed with respect to the load-deflection response as shown in Fig 7.7 and the load-tensile steel strains which presented in section 7.7. As a result, the element size that was selected for the proposed model is 15 mm for concrete and 10 mm for reinforcing bars. As the microcracks behaviour is out of the study scope, therefore the small element size will have no effect on the results accuracy (Bencardino et al., 2015).

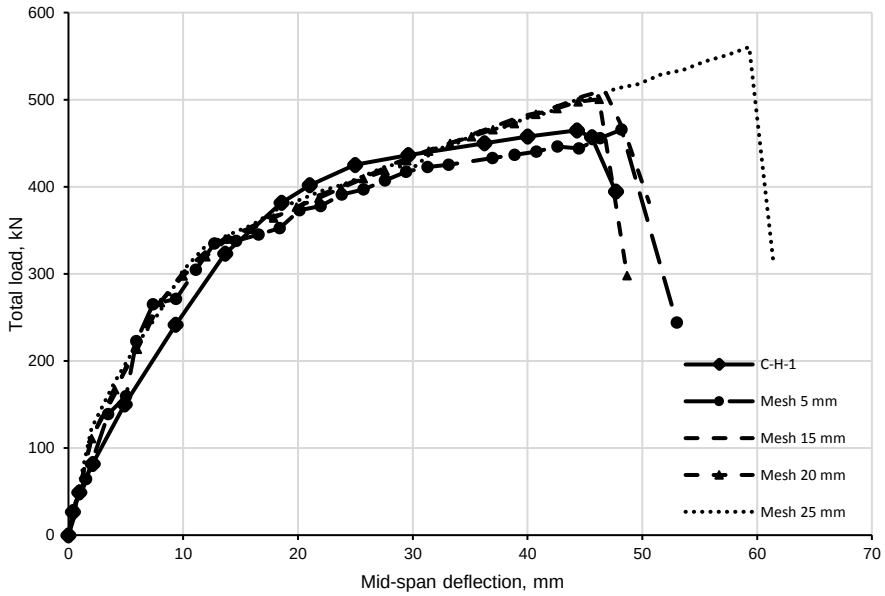

Figure 7.7 Effect of mesh size on the load-deflection response and comparison with experimental results of Beam C-H-1

7.5 Interaction between Concrete and Reinforcement

As the main objective of this study is to investigate the overall structural performance rather than the local behaviour at concrete reinforcement interface, proper modelling of the bond behavior between the internal GFRP or steel bars and concrete is important in some cases, but not in all cases. The bond-slip behavior of GFRP/steel-concrete has limited influence on the structural response of beam internally reinforced with GFRP/steel bars as the failure of GFRP-RC is caused by

concrete crushing or rupture of GFRP bars instead (Bencardino et al., 2015; Hawileh, 2015; Alkhalil and El-Maadddawy, 2016; Qin et al., 2017). In addition, this effect is considered in analysis by definition of the tension stiffening behavior of concrete (ABAQUS Inc., 2014). Therefore, a perfect bond between GFRP-concrete and steel-concrete is assumed here with an appropriate tensile behaviour of concrete after cracking.

7.6 Numerical Solution Method

Material degradation and failure often lead to severe convergence difficulties in an implicit analysis programs, such as ABAQUS/standard. However, ABAQUS/Explicit is well suited for modelling such materials. It is an effective tool for solving a wide variety of nonlinear solid and structural mechanics problems. Explicit methods are independent of type and duration of the loading and require a smaller time increment size as compared to implicit methods (ABAQUS Inc., 2014).

The proposed FE model is solved using a dynamic approach in order to overcome convergence difficulties and to perform a quasi-static analysis of RC beams. The computational efficiency in the quasi-static analysis using dynamic explicit procedure is ensured by either increasing the time increment or by introducing mass scaling in the model. In either case, the ratio of the kinetic energy to the internal energy (ALLKE/ALLIE) must always be checked and should be less than 10% (ABAQUS Inc., 2014). The variable mass scaling is used at the beginning of each step with a fixed time increment equal to 0.00005 in all regions of the model. For this time increment the kinetic energy was a small fraction of the internal energy of the model and hence the simulations were quasi-static as shown in Fig. 7.8.

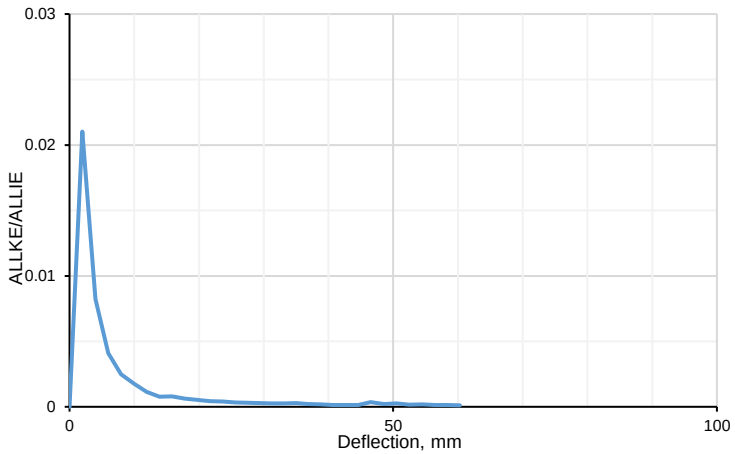

Figure 7.8 The ratio of kinetic over internal energy versus deflection for dynamic analysis (beam C-H-1)

7.7 Validation of FE Model

With the aim of achieving accurate simulation for the behavior of continuous concrete beams reinforced with hybrid GFRP-steel reinforcements, the proposed FE model using ABAQUS version 6.14 described in this chapter was verified against the experimental results obtained from the specimens tested in this study. The comparison was performed with respect to the load-deflection response, load capacity, mode of failure and tensile strain in longitudinal steel bars.

Comparisons between the load-deflection responses predicted by the proposed FE model against the experimental results is shown in Fig 7.9. It can be seen that the FEM was able to demonstrate a similar response to the tested beams. The reduction of stiffness after cracking as well as the effect of steel yielding prior to failure was predicted by the model with a reasonable accuracy. However, after the occurrence of the first crack, some differences can be noticed between both curves; possibly, due to the initial micro cracks generated by shrinkage and temperature effect which are not included in the FE model. With the reasonable accuracy, it can

be concluded that the developed FE models in this study can well predict the structural behavior of continuous concrete beams reinforced with GFRP, steel and hybrid GFRP-steel bars.

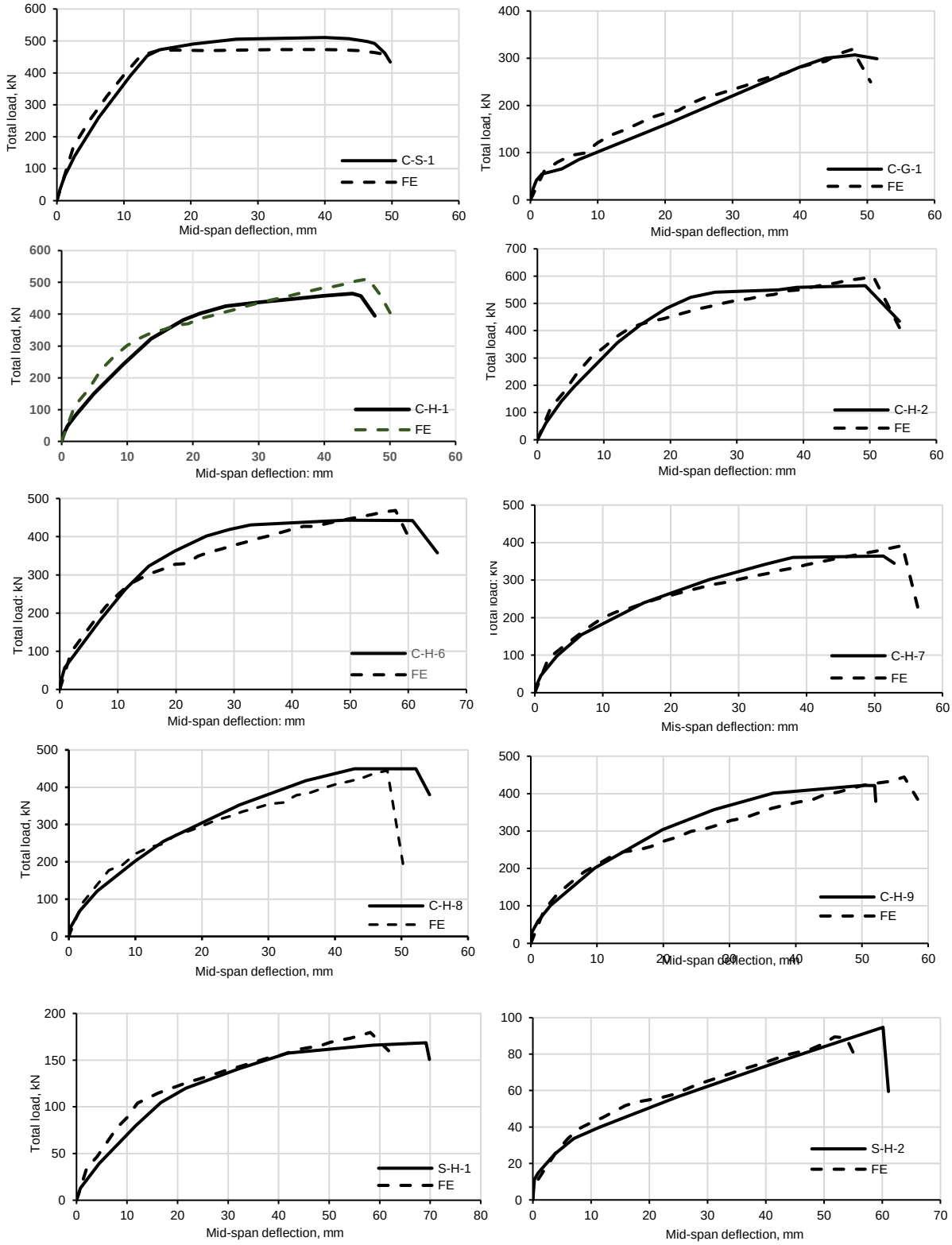

Figure 7.9 Validation of the proposed FE model against the current experimental results

Table 7.2 summarises the load capacity of the specimens, measured in the experiments and those predicted by the FE models. The means, standard deviation and coefficient of variation for the ratio between the predicted and experimental failure load are 0.99, 5% and 5.3%, respectively. It can be clearly concluded that the predictions from the proposed FE model show good agreement with the experimental results.

Table 7-2 Comparison of load capacity predicted by ABAQUS and obtained from experiments

Beam notation	Experimental Failure load $(2P_{exp}, kN)$	Predicted Failure load, $(2P_{pre}, kN)$	$\frac{P_{exp}}{P_{pre}}$
C-S-1	510	473	1.08
C-G-1	306	318	0.96
C-H-1	465	504	0.92
C-H-2	571	597	0.96
C-H-6	443	468	0.95
C-H-7	364	391	0.93
C-H-8	450	444	1.01
C-H-9	423	440	0.96
S-H-1	169	173	0.98
S-H-2	94	88	1.01
Average			0.99
Standard deviation (%)			5
Coefficient of variation (%)			5.3

As discussed in chapter four, the two major failure modes of continuous concrete beams were yielding of steel reinforcement followed by crushing of concrete and concrete crushing combined with shear failure. Therefore, beams C-H-1 and C-G-1 were chosen to discuss the predicted failure mode obtained by the proposed FE model against that observed from the experimental results. The predicted failure modes of beam C-H-1 is in agreement with the test observation reported in chapter four and shown in Figs 7.10-7.12. Figures 7.10 and 7.11 show that the ultimate strain of the GFRP bars (21300 micro-strain) in sagging and hogging regions was

not reached when the tensile steel bars yielded at a load of 300 kN as the beam was designed for yielding of tensile steel bars followed by concreter crushing while GFRP bars are far behind rupture which agrees well with that observed from the experimental results. The predicted crack pattern is also in close agreement with the test results as shown in Fig 7.12.

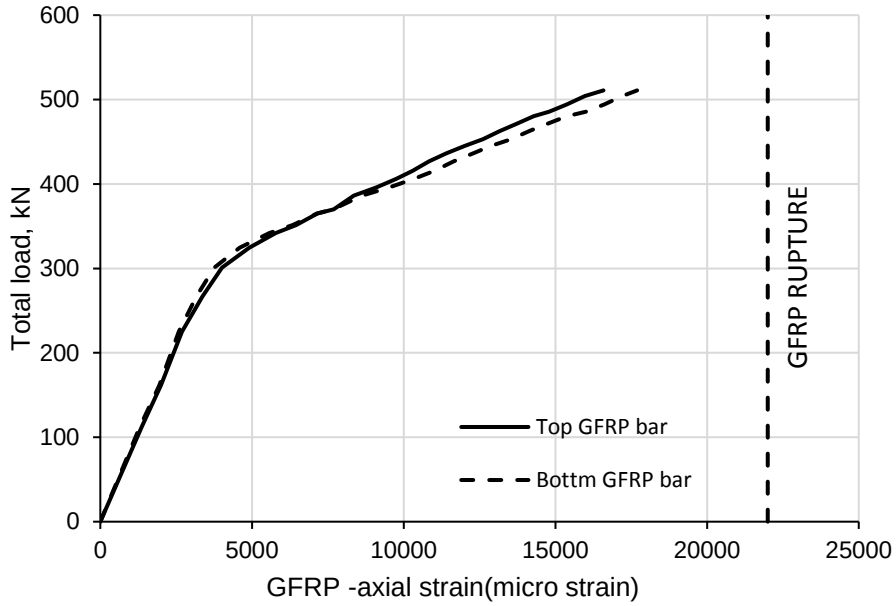

Figure 7.10 Predicted load-GFRP strains response in beam C-H-1

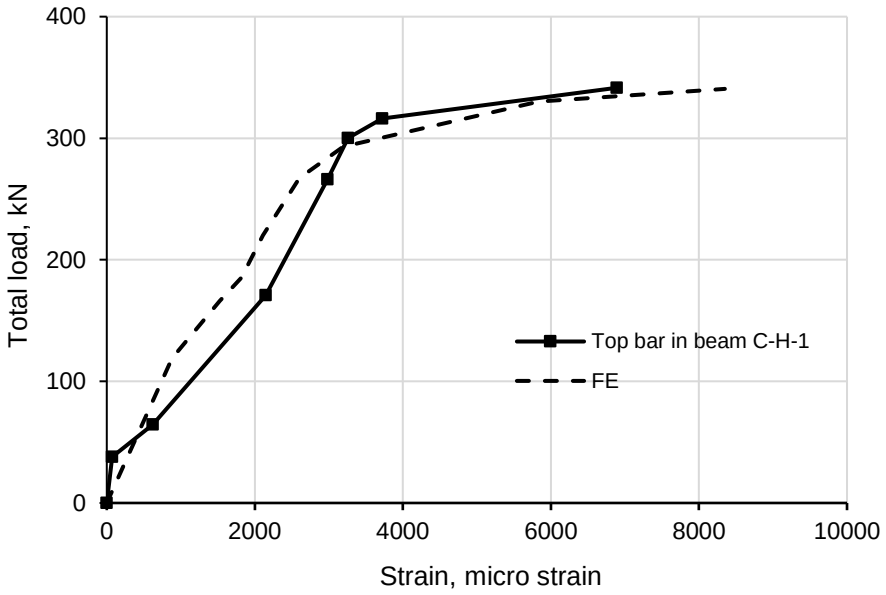

Figure 7.11 Load-steel strain response in beam C-H-1 (FE-experimental results)

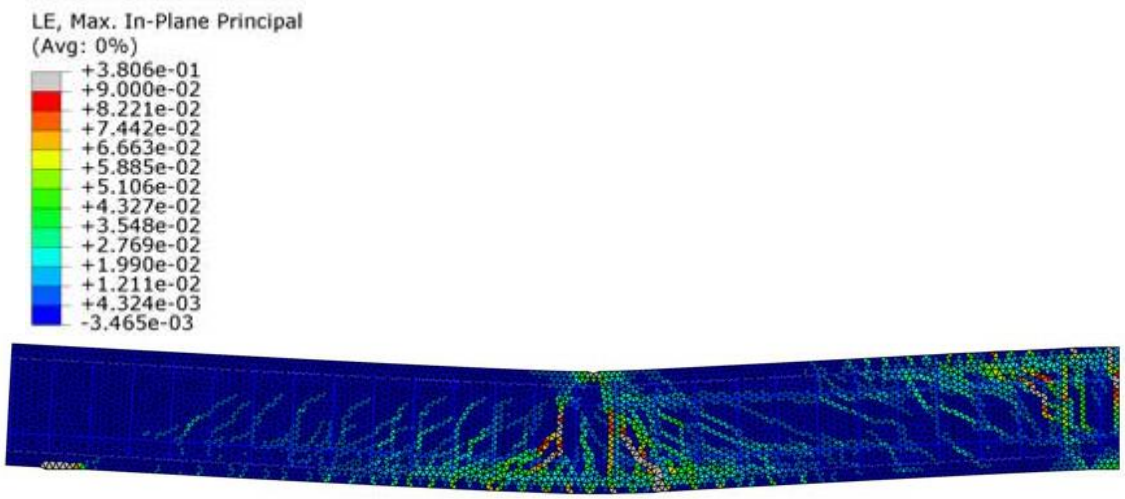

(a)

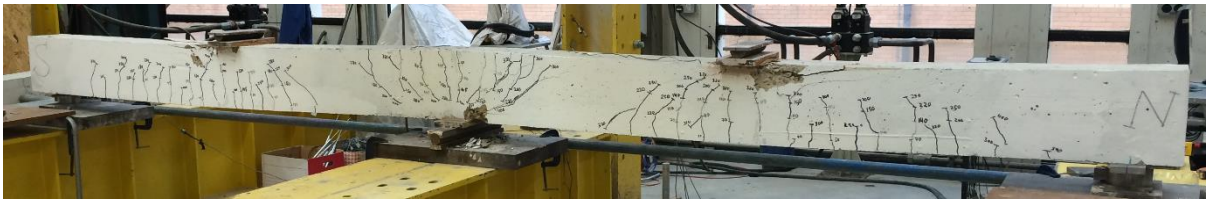

(b)

Figure 7.12 Crack patterns at ultimate state for beam C-H-1

(a) FE results; (b) Experimental results

Figure 7.13 shows the predicted and observed failure of beam C-G-1. It can be observed that cracking in the finite element model and experiment occurred at the same location near to the middle support section. The highest strain (highest stresses) led to the development of a major diagonal crack causing the failure of the beam.

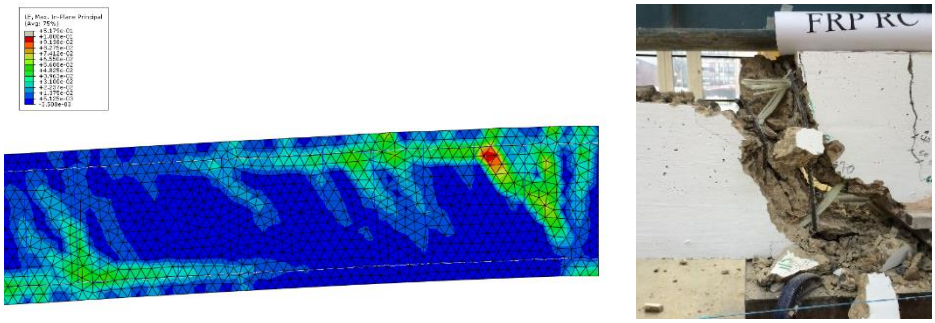

Figure 7.13 Crack patterns at ultimate state for beam C-G-1

FE results vs Experimental results

Figure 7.14 shows the predicted and experimental tensile stains in reinforcement at middle support sections of beams C-H-1, C-H-2, C-H-7, C-H-8 and C-H-9 and mid-span section of beam C-H-6. It can be seen that strains calculated by ABAQUS are in good agreement with those measured experimentally. The experimental tensile steel strain response was either not captured or incomplete due to malfunction of the corresponding strain gauges. The good agreement between the predicted and experimental strain measurements strengthen the confidence in the capability of the program to simulate the response of continuous concrete beams reinforced with hybrid GFRP-steel bars.

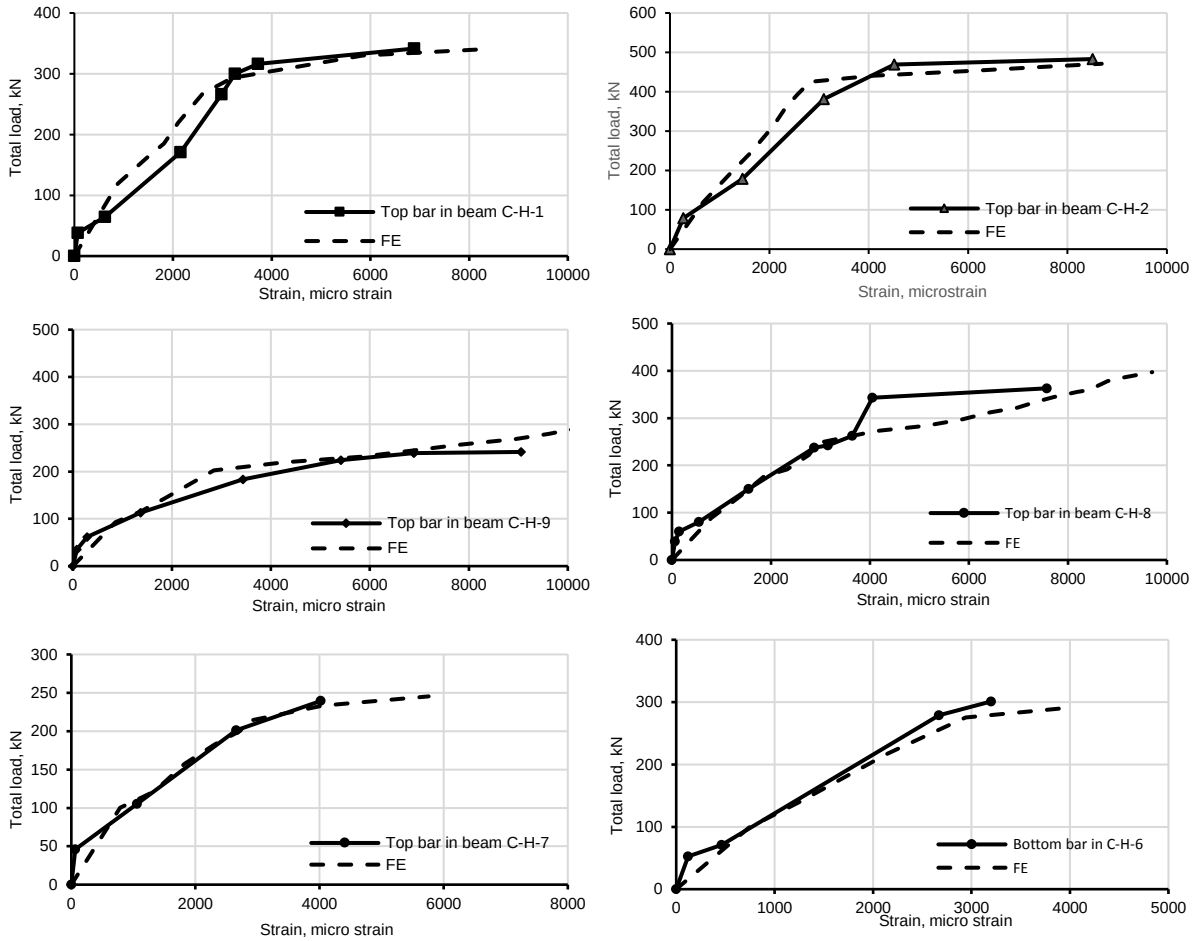

Figure 7.14 Tensile stains in steel reinforcement (FE-experimental results)

7.8 Parametric Study

The used FEM was based on the same geometry, material properties and assumptions used in modelling beam C-H-1 in the verification section of the previous sections. The reasons behind choosing this beam are the similarity in reinforcement configuration in sagging or hogging section with most of the tested beams as it was considered as the control beam and the reasonable predicted results obtained from FE model in comparison with test results. The key parameter included in the parametric studies are concrete compressive strength, steel reinforcement ratio at critical sections, hybrid reinforcement ratio at critical sections, FRP reinforcement type and transverse reinforcement type.

7.8.1 Concrete Compressive Strength

In this section, the effect of the concrete compressive strength on the performance of continuous concrete beams reinforced with hybrid GFRP-steel bars is investigated. In this study the, the compressive strength of concrete in the selected FEM (based on hybrid beam C-H-1) was chosen to vary between 30 and 60 MPa with an increment of 10 MPa.

Figure 7.15 shows the change in load-deflection relationship with the studied range of concrete compressive strength. For all the considered compressive strength values, increasing the compressive strength of concrete led to similar behaviour in all beams, irrespective of the values of other parameters. The general behaviour during the loading process can be divided into three stages, pre-cracking stage, post-cracking stage and post-yielding of steel stage. It can be mentioned that increasing the concrete compressive strength slightly increased the cracking load owing to the increase in concrete tensile strength as it could be seen in Figure 7.15. In addition, it led to an increase in the load corresponding to yielding of tensile steel reinforcement. The same figure also revealed that after yielding of tensile steel bars at the same value of loading, increasing the concrete compressive strength has a remarkable effect on reducing the deflections.

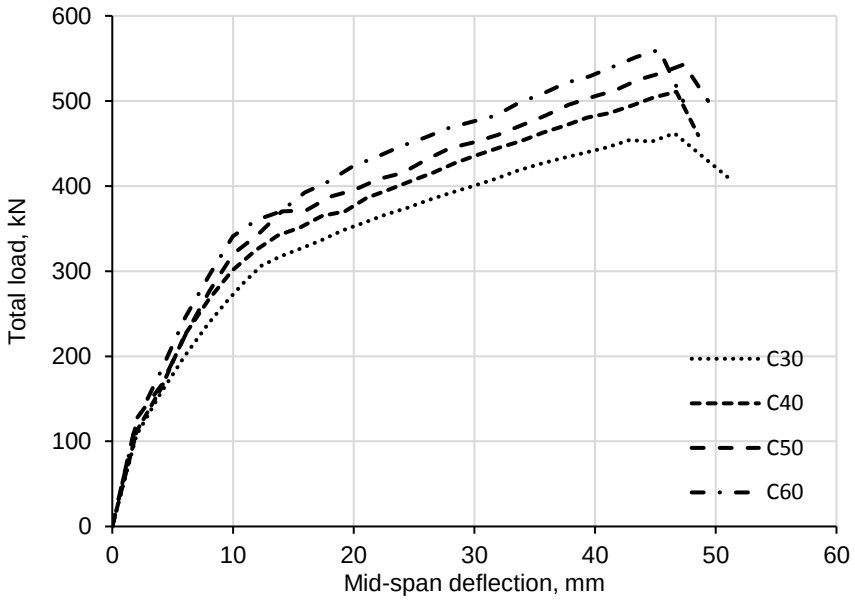

Figure 7.15 Variation in load-deflection relationship with concrete strength

The relationship between concrete strength and ultimate load capacity was found to be approximately linear as illustrated in Fig. 7.16. However, this relationship would significantly change with any change in geometry, reinforcement or material properties.

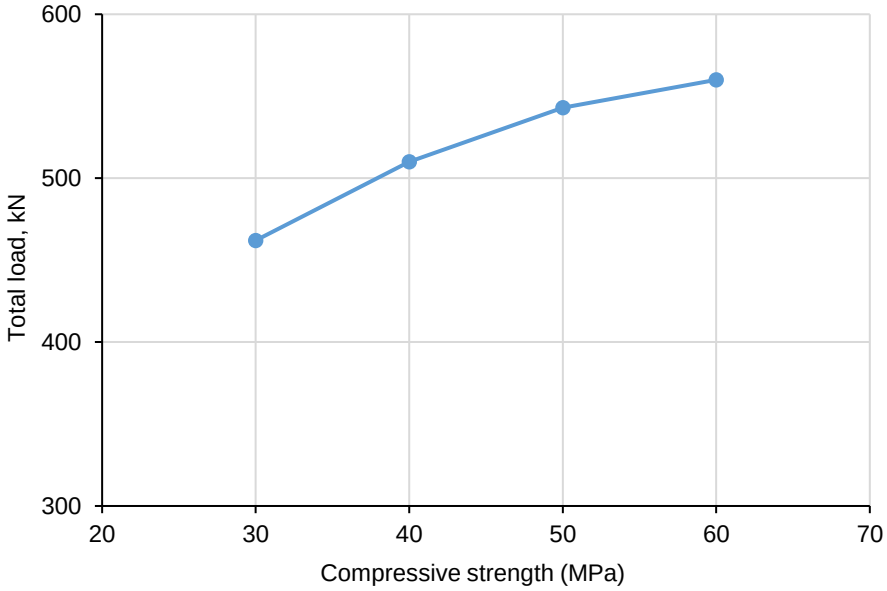

Figure 7.16 Effect of concrete strength on ultimate load capacity

Table 7.3 shows the effect of concrete strength on the ductile behaviour of beam studied. The ductility index was calculated using Eq (6.24) presented in chapter six based on the deflection ductility index $\mu_{\Delta 1}$. The beam with lower compressive strength showed slightly more ductile behavior than that with higher compressive strength.

Table 7-3 Effect of concrete strength on ductility index

Compressive strength (MPa)	$\Delta_u\ (mm)$	$\Delta_y\ (mm)$	$\mu_{\Delta 1}$
C30	46.5	12	3.8
C40	46.7	13.7	3.4
C50	47.3	13.9	3.4
C60	45.3	13.9	3.2

7.8.2 Steel Reinforcement Ratio at Critical Sections

As the aim of this research is to study the effect of combining GFRP bars with steel bars in continuous concrete beams to overcome the brittle failure of continuous concrete beams reinforced with only FRP bars. It is not clear whether both sagging and hogging regions should be reinforced with tensile steel bars in order to obtain a ductile behaviour. In this parametric study, the proposed FE model was used to study the effect of the presence of longitudinal steel bars in only one of the critical sections, namely sagging or hogging region. To investigate the effect of steel reinforcing bars in the critical sections of continuous beams reinforced with hybrid GFRP-steel bars, the longitudinal tensile steel bars in the FEM was changed three times and the analysis was run each time to determine the response of the model. Again, the model was based on the geometry, reinforcement and material properties of hybrid beam C-H-1. The hybrid reinforcement at the middle support and mid-span sections was kept constant as hybrid beam C-H-1 and designated as ‘’sagging and hogging’’. While the two specimens with only tensile steel

reinforcement in either sagging or hogging region were designated as only sagging and only hogging, respectively, as shown in Fig. 7.17.

As illustrated in Fig. 7.17, the specimen reinforced with tensile steel bars in both critical sections demonstrated the highest stiffness and ultimate load capacity whereas the opposite in the case of specimen reinforced with longitudinal steel bars only in hogging region. The stiffness of specimen reinforced with tensile steel bars only in mid-span section lies between the other two beams. It is obvious from the load-deflection results that stiffness of hybrid cross section after cracking is proportional to the amount of steel reinforcement, hence, stiffer mid-span section than middle support one will most probably result in significant improvement in the flexural stiffness and ultimate load. This observation was also confirmed by the experimental investigation conducted in this study.

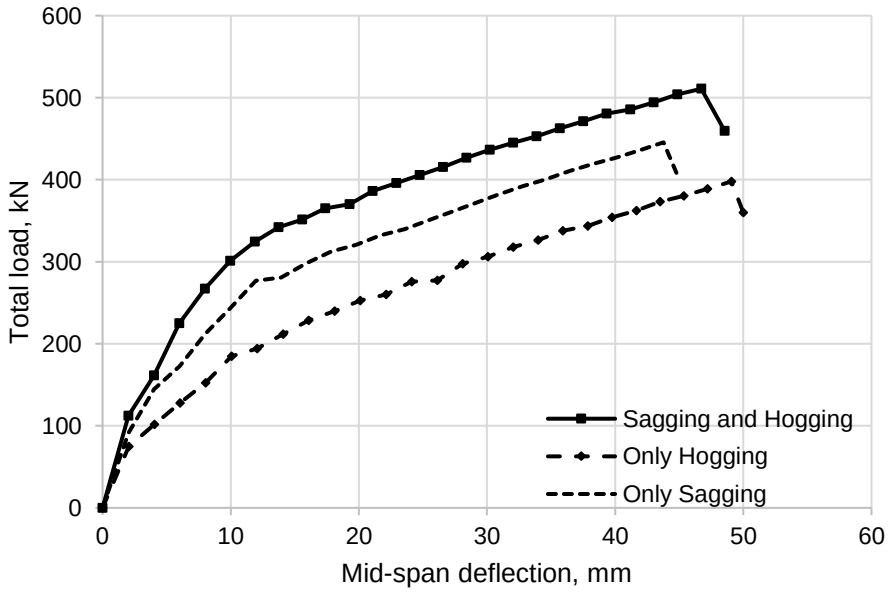

Figure 7.17 Effect of tensile steel bars in sagging and hogging regions

7.8.3 Hybrid Reinforcement Ratio at Critical Sections

In this section, the effect of hybrid reinforcement ratio between GFRP and steel (Af/As) on the flexural behavior of continuous concrete beam reinforced with hybrid

reinforcement is investigated. To achieve this, nine FE models were used based on specimen C-H-1 with different hybrid reinforcement ratios at sagging and hogging regions as shown in Tables 7.4a and 7.4b. The specimens were divided into two groups, namely group A and group B. In group A, the effect of using Af/As equal to or less than 1 in sagging and hogging regions is investigated. While in group B, the effect of using Af/As equal to or greater than 1 in sagging and hogging regions is investigated. The results were compare in terms of the load-deflection response and moment redistribution based on end reactions.

Table 7-4a Hybrid reinforcement ratio of FE beam specimens (Group A)

Beam No	Sagging			Hogging		
	GFRP, mm^2	Steel, mm^2	Af/As	GFRP, mm^2	Steel, mm^2	Af/As
H1	379	339	1	379	339	1
H2	379	339	1	253	402	0.63
H3	379	339	1	142	402	0.35
H4	253	402	0.63	379	339	1
H5	142	402	0.35	379	339	1

Note: Af/As is the area of GFRP bars to the area of steel bars

Table 7-4b Hybrid reinforcement ratio of FE beam specimens (Group B)

Beam No	Sagging			Hogging		
	GFRP, mm^2	Steel, mm^2	Af/As	GFRP, mm^2	Steel, mm^2	Af/As
H1	379	339	1	379	339	1
H6	379	339	1	142	100	1.42
H7	379	339	1	253	100	2.53
H8	142	100	1.42	379	339	1
H9	253	100	2.53	379	339	1

Note: Af/As is the area of GFRP bars to the area of steel bars

7.8.3.1 Load Deflection Response

Figures 7.18 and 7.19 show the change in the load-deflection relationship with different Af/As ratios for group A and B, respectively. The general behavior of the model is similar to that described in the ‘’ Concrete Compressive Strength’’ section. It can be seen that the specimens with a higher Af/As ratio in the sagging region demonstrated the highest flexural stiffness. This reflects the effect of increasing the axial stiffness of the longitudinal reinforcement ratio. For example, H4 and H5 show that increasing the area of GFRP bars at sagging region reduced the deflection at mid-span by approximately 33% at the failure load of H5 as shown in Fig 7.18. Also, the deflections of beam H8 and H9 at a load level of 300 kN was reduced by approximately 30% when the GFRP reinforcement ratio in sagging region was increased by 43% in beam H9 as shown in Fig 7.19. This observation was also confirmed by the experimental investigation conducted in this this study.

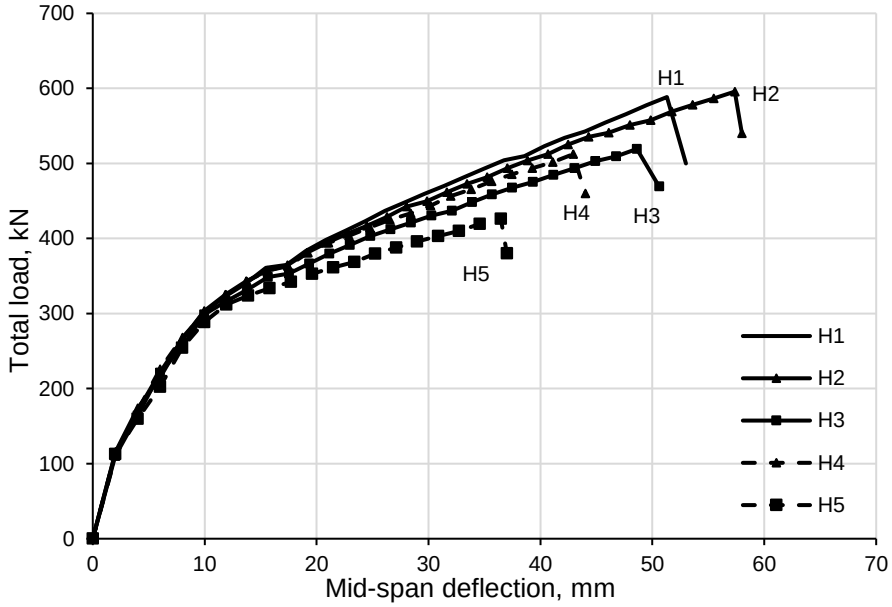

Figure 7.18 Variation in load-deflection relationship with different Af/As ratio (Group A)

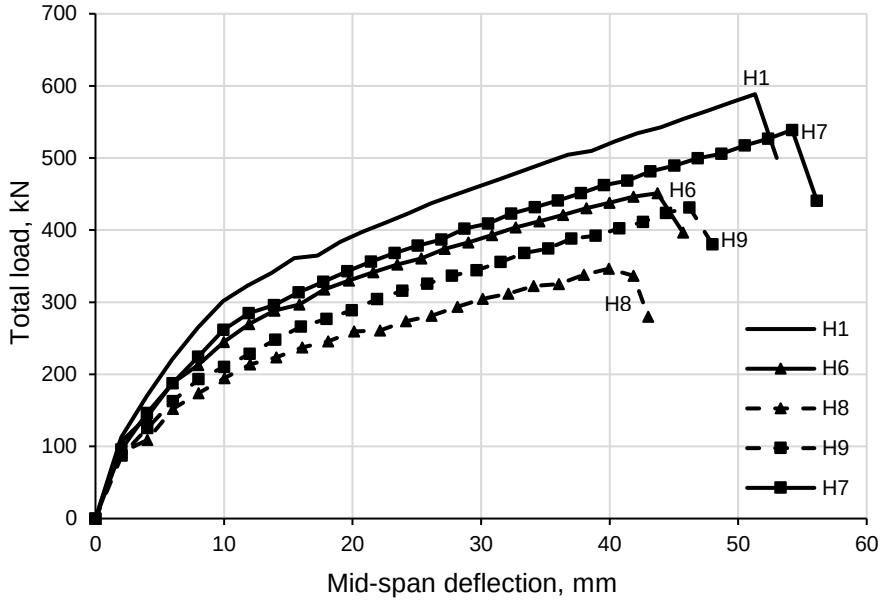

Figure 7.19 Variation in load-deflection relationship with different Af/As ratio (Group B)

7.8.3.2 Load Capacity

The relationship between the ultimate load capacity and the hybrid reinforcement ratio is illustrated in Figures 7.20 and 7.21. Figure 7.20 shows that increasing the area of GFRP bars in hogging region from 142 mm^2 to 253 mm^2 increased the ultimate load capacity by approximately 12% and 16%, respectively, for area of steel bars in hogging region of 402 mm^2 and 100 mm^2. The same figure also shows that increasing the area of steel bars in hogging region from 100 mm^2 to 402 mm^2 increased the ultimate load capacity by approximately 9% and 13%, respectively, for area of steel bars in hogging region of 253 mm^2 and 142 mm^2 , respectively. This result shows that the GFRP reinforcement ratio in hogging region is a key factor in enhancing the load capacity.

Figure 7.21 shows that increasing the area of GFRP bars in sagging region from 142 mm^2 to 253 mm^2 increased the ultimate load capacity by approximately 16% and 19%, respectively, for area of steel bars in hogging region of 402 mm^2 and 100

mm^2. The same figure also shows that that increasing the area of steel bars in sagging region from 100 mm^2 to 402 mm^2 increased the ultimate load capacity by approximately 15% and 18%, respectively, for area of steel bars in hogging region of 253 mm^2 and 142 mm^2. This result also shows that GFRP reinforcement ratio in sagging region is a key factor in enhancing the load capacity.

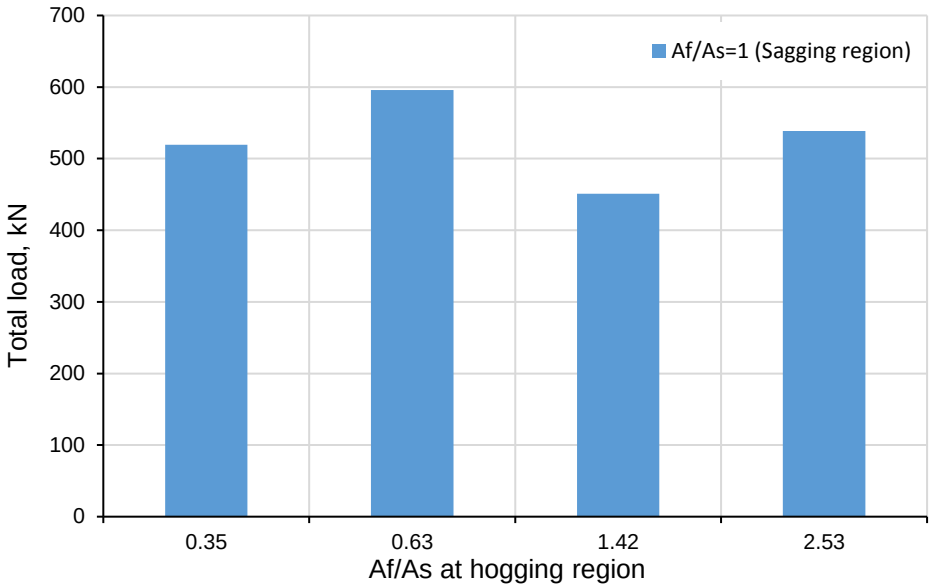

Figure 7.20 Effect of Af/As at hogging region on load capacity for Af/As=1 at sagging region

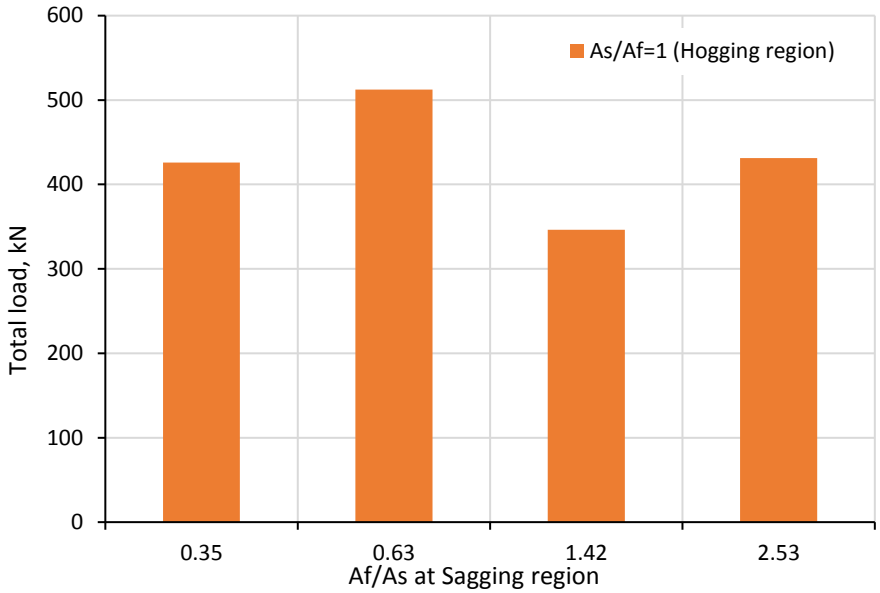

Figure 7.21 Effect of Af/As at sagging region on load capacity for As/Af=1 at hogging region

7.8.3.3 Moment Redistribution

Figures 7.22 and 7.23 show the relationship between the Af/As ratio in mid-span and middle support sections on the moment redistribution at critical regions, respectively. The exterior reactions corresponding to the failure loads were used to calculate the achieved moment redistribution at failure. It can be seen that there was no constant trend when the hybrid ratio increased from 0.35 to 2.53 in sagging or hogging regions.

As illustrated in Figs 7.22 and 7.23, there is no correlation between the hybrid reinforcement ratios in mid-span section to that in middle support section on moment redistribution ratio in both sagging and hogging regions. However it is noticed that the beams reinforced with Af/As=1.4 in either mid-span (H6) or middle support (H8) section demonstrated the largest moment redistribution in both critical section as shown in Figs. 7.22 and 7.23, respectively. Beam H6, which have opposite reinforcement configuration to that used in beam H8, demonstrated the largest moment redistribution in both sagging and hogging regions in groups A as

shown in Fig 7.22. While beam H8 demonstrated the largest moment redistribution in both sagging and hogging regions in groups B as shown in Fig 7.23.

Comparisons between the results show that decreasing area of GFRP bars or area of steel bars in either sagging or hogging section resulted in an increase in moment redistribution except if the Af/As in sagging region was 0.35 (H5). The effect of decreasing reinforcement ratio of one type of reinforcing material was also confirmed by the experimental investigation conducted in this study.

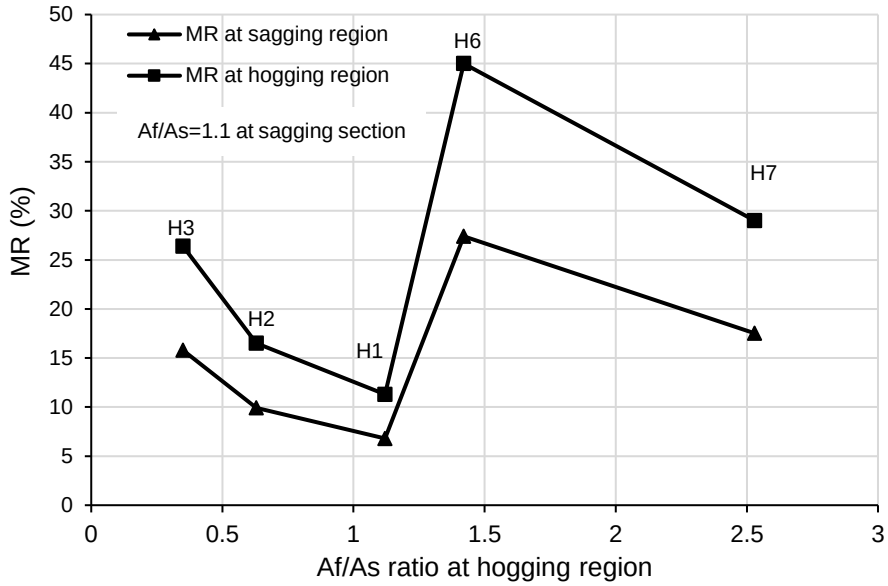

Figure 7.22 Effect of Af/As ratio at hogging region on moment redistribution

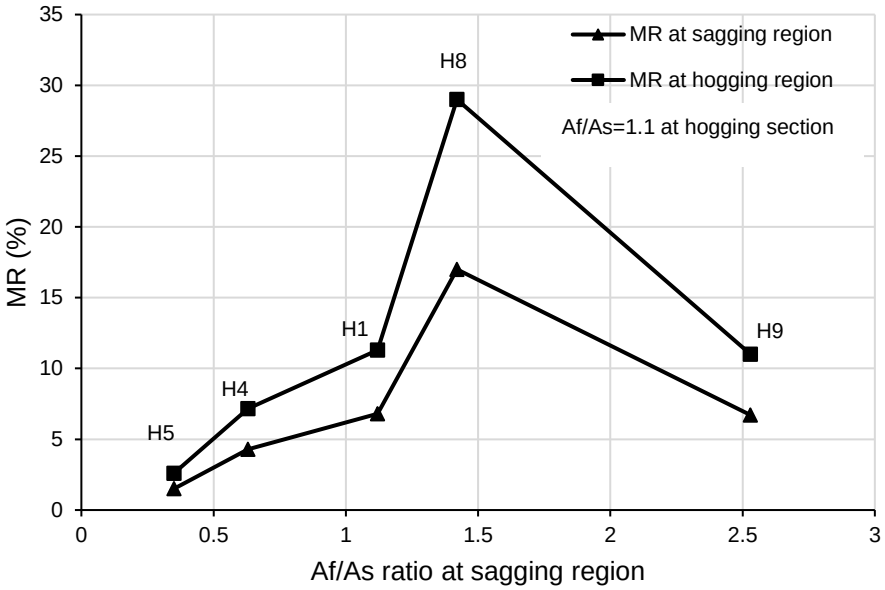

Figure 7.23 Effect of Af/As ratio at sagging region on moment redistribution

7.8.4 FRP Reinforcement Type

The proposed FE model has also been employed to study the effect of type of FRP reinforcement (GFRP or CFRP) on the load-deflection relationship of hybrid FRP/steel reinforced concrete continuous beams. The model was based on the geometry, reinforcement and material properties of hybrid beam C-H-1. However, in case of using CFRP bars instead of GFRP bars, the assumed elastic modulus and tensile strength of the CFRP bar were 120GPa and 1300 MPa, respectively.

Figure 7.24 shows the response of the different RC continuous beams reinforced with GFRP, CFRP and steel bars. It is clear that the initial slope of the load-deflection curve of the investigated beams is quite similar and represents the contribution of concrete contribution to the load-carrying capacity. Fig 7.24 indicates that hybrid GFRP/steel reinforced concrete continuous beam exhibited a significant reduction in stiffness after yielding of steel in comparison with hybrid CFRP/steel specimen. This behaviour is mainly attributed to the lower elastic modulus of GFRP bars than that of CFRP bars leading to a reduced axial stiffness and hence a larger deflection.

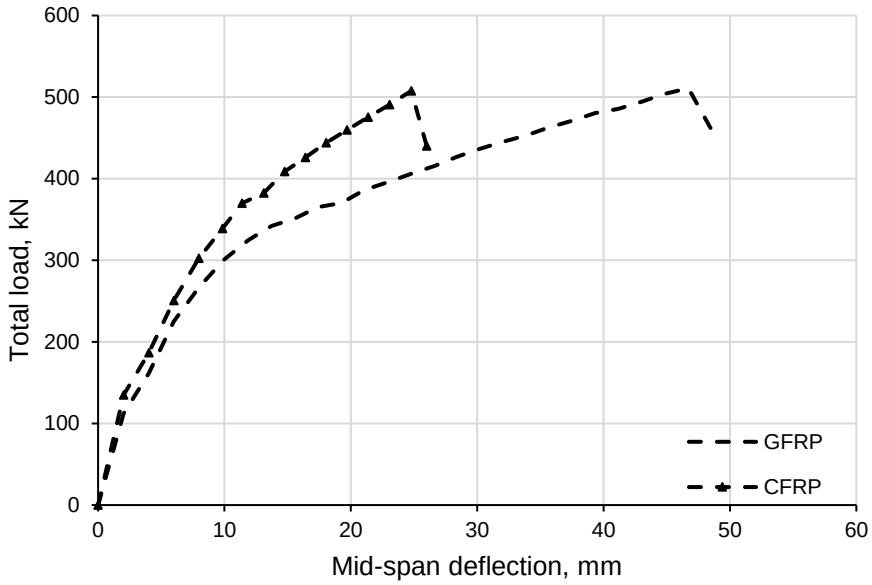

Figure 7.24 Effect of longitudinal FRP reinforcement type

7.8.5 Transverse Reinforcement Type

As reported in the literature that the presence of the transverse reinforcement in beams improved the shear capacity and also provided better confinement for the concrete in the compression regions. In the current experimental study, the test beam C-H-1 was provided with 10 mm @ 100 mm steel stirrups, which provided enough shear capacity to prevent shear failure. A finite element model with similar geometry, reinforcement and material properties to this beam was used to evaluate the effect of type of transverse reinforcement on continuous concrete beams reinforced with hybrid GFRP/steel bars. The main spacing was the one used in the test beam C-H-1.

The relationship between the applied load at each span and the measured deflection at mid-span is shown in Figure 7.25. Up to approximately 60% of its failure load, hybrid beam with GFRP stirrups had similar load deflection behaviour as hybrid beam with steel stirrups, which had identical flexural reinforcement and same spacing of stirrups. Using GFRP stirrups did not change beam performance during loading, however, beam with GFRP stirrups demonstrated less stiffness than

beam with steel stirrups after yielding of steel bars. This is due to the lower modulus of elasticity of GFRP stirrups compared to steel.

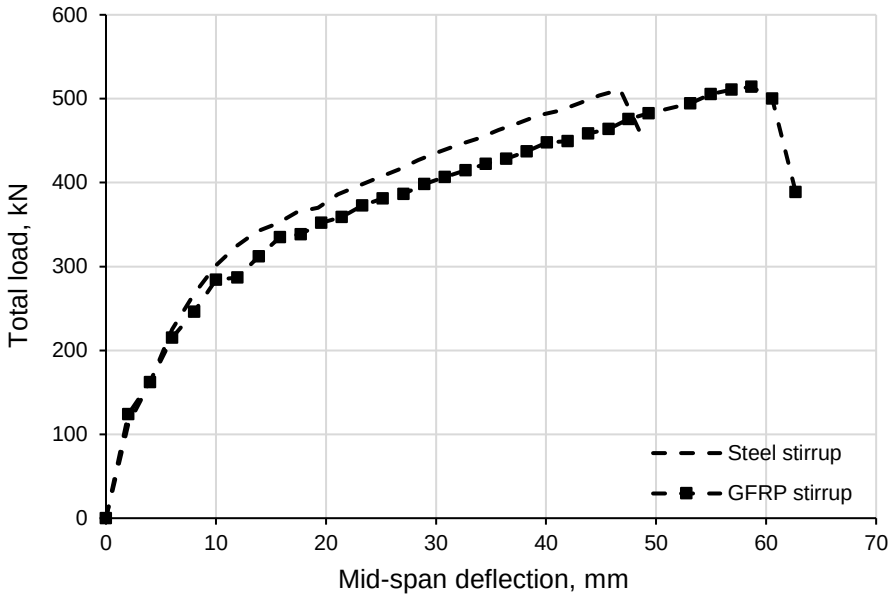

Figure 7.25 Effect of transverse reinforcement type

7.9 Conclusions

In this chapter, a two-dimensional non-linear finite element model for assessing the behavior of continuous concrete beams reinforced with hybrid GFRP/steel bars has been presented. The developed FE model was implemented in ABAQUS version 6.14, a nonlinear finite element program. Only one half of the continuous beam was modelled taking advantage of the symmetry in the geometry and boundary conditions. The proposed FE model was validated against the experimental results of ten continuous concrete beams and two simply supported beams presented in chapter four.

The proposed FE model was used to conduct a parametric study in order to investigate the effect of key parameters on the flexural performance of continuous concrete beams reinforced with GFRP/steel bars. The parametric study included an

extended range of parameters in addition to those investigated experimentally. The parameters investigated included the compressive strength, the presence of tensile steel bars in critical sections, hybrid reinforcement ratio (Af/As) in sagging and hogging regions, type of FRP material and the effect of vertical stirrups type. Based on the results of the present study, the following conclusions can be drawn:

- The failure loads predicted from the proposed FE model were very close to those obtained experimentally with a mean of 0.99, a standard deviation of 5 and a coefficient of variation of 5.3.
- Dynamic Explicit technique can be used to solve the static problem by ensuring that the ratio of the kinetic energy to the internal energy (ALLKE/ALLIE) less than 10%.
- The load-deflection curves predicted by the proposed FE model showed a reasonable agreement with that obtained from experimental results. The initial stiffness of the predicted curves was similar to experiments.
- The concrete compressive strength had a mild effect on the performance of hybrid continuous beams.
- The presence of longitudinal steel reinforcement in both sagging and hogging regions has a considerable effect on enhancing the flexural stiffness of continuous concrete beams reinforced with hybrid reinforcement.
- The GFRP reinforcement in either sagging or hogging section was found to play an important role on resisting loading after yielding of steel.
- There is no correlation between the ratio of GFRP area to steel area in mid-span and middle support sections and moment redistribution. However, it was noticed that the beams reinforced with Af/As=1.4 in either mid-span or

middle support section demonstrated the largest moment redistribution in both critical sections.

- Decreasing area of GFRP bars or area of steel bars in either sagging or hogging section resulted in an increase in moment redistribution except if the Af/As in sagging region was 0.35. The effect of decreasing reinforcement ratio of one type of reinforcing material was also confirmed by the experimental investigation conducted in this study.
- It has been found that hybrid GFRP/steel reinforced concrete continuous beams exhibit a significant reduction in stiffness after the initiation of first crack and yielding of steel reinforcement in comparison with that reinforced with hybrid CFRP/steel bars.
- Type of transverse reinforcement has a small effect on the overall behaviour of continuous concrete beams reinforced with hybrid GFRP/steel bars.

CHAPTER EIGHT

CONCLUSIONS AND RECOMMENDATIONS FOR FUTURE WORK

8.1 Summary

The flexural and shear behaviour of multi-span continuous concrete beams reinforced with hybrid GFRP/steel bars were studied in this thesis. The research consisted of four phases, an experimental investigation, evaluation of the predictability of available developed equations against the experimental results of this research, the development of sectional analysis and FE modelling.

The experimental phase contained the construction and testing of nine continuously and two simply supported concrete beams reinforced with hybrid GFRP/steel bars. In addition, two control concrete continuous beams reinforced with steel and GFRP bars and one simply supported beam reinforced with GFRP bars were also tested for comparison purposes. All simple and continuous reinforced concrete beams were loaded at their midpoints up till failure. The combination and number of reinforcing bars were the main parameters investigated in this study. Hence, cracking patterns, failure modes, redistribution of support reactions, crack width, deflections and ultimate load capacity of reinforced concrete beams were experimentally investigated.

The analytical phase included the sectional analysis of concrete sections reinforced with GFRP, steel or hybrid GFRP/steel bars. The performance of the developed model was validated against the moment capacity results obtained from the experimental phase in this project and elsewhere. Afterwards, the influence of design parameters such as the internal reinforcement type, longitudinal reinforcement ratio, and concrete compressive strength could be investigated.

The final part of the research included the numerical simulation. A two-dimensional nonlinear finite element model was proposed using ABAQUS package. The proposed model was validated against the experimental results of the beams tested in the present research.

The main aim of this chapter is to summarize the principal findings of the research carried out in this study and provide a number of recommendations and suggestions for future work.

8.2 Conclusions

The principal findings drawn from the current investigation can be summarised below:

- The hybrid reinforcement system is a promising method of construction to overcome the shortcomings of the individual use of a single type of reinforcement. However, the hybrid reinforcement ratio and area of FRP to steel bars are a key factor to ensure sufficient ductility and stiffness beyond the first cracking stage.
- Brittle behaviour of continuous concrete beams reinforced with FRP bars was avoided which, in turn, a more ductile behaviour was exhibited by multi-span continuous beams reinforced with a hybrid combination of GFRP and steel bars; in which failed in a favourable ductile manner with warnings before collapse.
- The tested hybrid continuous beams demonstrated narrow cracks and smaller deflections compared to the GFRP-reinforced control beam due to the presence of steel bars. Increasing the amount of longitudinal hybrid

GFRP-steel re-bars had a clear effect on flexural crack widths and deflection reduction.

- Increasing the area of GFRP bars in either the sagging or hogging region contributes significantly in improving the stiffness of hybrid continuous concrete beams and in return reducing deflections.
- Increasing the reinforcement ratio of GFRP in the middle support section of multi-span continuous hybrid reinforced concrete beams does not contribute in improving load capacity whereas increasing the bottom GFRP reinforcement ratio of mid-span section has more effect on load capacity increase.
- The tested hybrid reinforced continuous beams demonstrated redistribution of moment from the mid-span to the middle support sections and adversely from the middle support to the mid-span due to yielding of steel reinforcement.
- The extent of moment redistribution in hybrid reinforced continuous beams depends mainly on the amount of hybrid reinforcement ratio in critical sections. Similar area of steel and GFRP bars in critical sections leads to limited moment redistribution whereas different amount of steel and FRP bars in critical sections leads to a remarkable moment redistribution.
- The ACI 440.2R-08 and Pang et al., (2015) equations reasonably predicted the sagging failure moment of continuous hybrid reinforced concrete beams, whereas they underestimated the hogging flexural strength at failure of most hybrid continuous beams. On the other hand, the formulas proposed by Yinghao et al., (2013) were very conservative in predicting the failure moment at the critical sagging and hogging sections.

- The ACI 440.1R-15 design code equation, which were proposed for predicting the deflection of concrete beams reinforced by FRP bars, reasonably predicted the deflection of GFRP simple and continuous beams tested, whereas it underestimated the deflections of hybrid beams tested at all stage of loading after cracking.
- The Yoon's model seems to be effective in predicting the mid-span deflection of simple and continuous members reinforced by hybrid GFRP/steel bars.
- The energy-based method is more efficient for estimating ductility index of concrete beams reinforced with hybrid GFRP/steel beams as it is difficult to predict the yield deflection theoretically.
- The CSA/S806-14 and EC2 equations significantly overestimated the shear capacity of hybrid GFRP/steel beams. On the other hand, ACI 318-11 formulas could mostly reasonably predict the shear capacity of continuous concrete beams reinforced with a combination of GFRP/steel bars.
- Comparisons between the predicted moment capacities of hybrid FRP/steel reinforced concrete members using the developed numerical technique and experimental results available in the literature indicate very good agreement.
- The two-dimensional nonlinear finite element model proposed in chapter seven accurately predicted the failure modes, the load capacity and the load-deflection response of multi-span continuous hybrid GFRP/steel concrete beams described in chapter four.
- The parametric study conducted using the proposed FE model showed that there is no correlation between the ratio of GFRP area to steel area in mid-span and middle support sections and moment redistribution. Moreover, type

of transverse reinforcement has a small effect on the overall behaviour of continuous concrete beams reinforced with hybrid GFRP/steel bars

8.3 Recommendations for Future Work

The following important areas are recommended for further investigations:

- As the present research was carried out using hybrid GFRP/steel reinforcement, it is recommended to investigate more experiments on concrete beams reinforced with other types of fibres such as CFRP and BFRP reinforcement due to the difference in material properties.
- Further to the current research, it is recommended to investigate the effect of use of hybrid GFRP/steel reinforcing bars on the shear behaviour of multi-span continuous concrete beams reinforced with hybrid reinforcement. This is to investigate the effect of longitudinal hybrid reinforcement on dowel action contribution to shear capacity.
- The present experimental study was carried out using equal spans and one loading configurations. However, in practice, live load intensity is most likely to vary from one span to another of the continuous beam depending on the type and distribution of occupancy on the floor system. Therefore, more variables need to be studied such as the effect of unequal spans, different loading configurations.
- From the geometrical perspective, it is expected that beams with T-sections behave differently from beams with rectangular sections. This is due to the fact that the section over the middle support behaves as a rectangular section while the section at the mid-span region behaves as a T-section. Therefore, there is a need to investigate the effect of different cross-sections,

such as T-shaped sections on the structural performance of continuous concrete beams reinforced with hybrid FRP/steel bars.

- Further experimental researches are required to validate available developed equations for moment capacity and deflection of multi-span continuous hybrid FRP/steel reinforced concrete beams.
- Further work is needed to consider the influence of the bond characteristics between FRP bars and surrounding concrete in predicting the deflection of indeterminate hybrid FRP/steel reinforced concrete members.

REFERENCES

ABAQUS. (2014) A finite Element Computer Program, Version 6.14. User's and Theory Manuals, Vélizy-Villacoublay, Inc.

ACI Committee 440, 2004. "Guide test methods for fiber reinforced polymers FRPs for reinforcing or strengthening concrete structures." *ACI 440.3R-04*, Farmington Hills, Mich.

ACI Committee 440, 2006. "Guide for the design and construction of concrete reinforced with FRP bars." *ACI 440.1R-06*, Farmington Hills, Mich.

ACI Committee 440, 2008, Guide for the design and construction of externally bonded FRP systems for strengthening concrete structures. (ACI 440.2R-08), Farmington Hills, Mich. USA American Concrete Institute.

ACI Committee 318, 2011. Building code requirements for structural concrete and commentary. (ACI 318-11), Farmington Hills, Mich. USA American Concrete Institute.

ACI Committee 440, 2015, Guide for the Design and Construction of Concrete Reinforced with FRP Bars, (ACI 440.1R-15), Farmington Hills, Mich. USA American Concrete Institute.

British Standards Institution (BSI) (2004) Design of concrete structures-Part 1-1: General rules and rules for buildings, BS EN 1992-1-1: 2004. British Standards (BSi).

AHMED, E. A., EL-SALAKAWY, E. F. & BENMOKRANE, B. 2010. Performance evaluation of glass fiber-reinforced polymer shear reinforcement for concrete beams. ACI structural Journal, 107 (1), 53.

AHMED, E. A., SETTECASI, F. & BENMOKRANE, B. 2014. Construction and testing of GFRP steel hybrid-reinforced concrete bridge-deck slabs of sainte-catherine overpass bridges. Journal of Bridge Engineering, 19 (6), 04014011.

AIELLO, M. A. & OMBRES, L. 2002. Structural performances of concrete beams with hybrid (fiber-reinforced polymer-steel) reinforcements. *ASCE* Journal of Composites for Construction, 6 (2), 133-140.

AKIEL, M. S. M. 2016. Performance of Continuous Concrete Slabs Reinforced with Hybrid Steel-Basalt Bars. Master of Science in Civil Engineering (MSCE), United Arab Emirates University.

ALKHALIL, J. & EL-MAADDAWY, T. 2016. Nonlinear Flexural Response of Continuous Concrete Slab Strips Strengthened with Near Surface–Mounted Composites. *ASCE* Journal of Composites for Construction, 21 (1), 04016071.

ALMUSALLAM, T. H., ELSANADEDY, H. M., AL-SALLOUM, Y. A. & ALSAYED, S. H. 2013. Experimental and numerical investigation for the flexural strengthening of RC beams using near-surface mounted steel or GFRP bars. Construction and Building Materials, 40, 145-161.

ALSAYED, S. H. & ALHOZAIMY, A. M. 1999. Ductility of concrete beams reinforced with FRP bars and steel fibers. Journal of composite materials, 33 (19), 1792-1806.

ASHOUR, A. 2006. Flexural and shear capacities of concrete beams reinforced with GFRP bars. Construction and Building Materials, 20 (10), 1005-1015.

ASHOUR, A. F. & HABEEB, M. N. 2008. Continuous Concrete Beams Reinforced with CFRP Bars. Proceeding of the institution of Civil Engineers-Structures and Building, 161(6), 349-357.

Beeby, A.W., 1997. Ductility in reinforced concrete: why is it needed and how is it achieved?. Structural Engineer, 75(18).

BEHNAM, B. & EAMON, C. 2014. Analysis of alternative ductile fiber-reinforced polymer reinforcing bar concepts. Journal of Composite Materials, 48 (6), 723-733.

BELARBI, A. & HSU, T. T. 1994. Constitutive laws of concrete in tension and reinforcing bars stiffened by concrete. Structural Journal, 91 (4), 465-474.

BENCARDINO, F., CONDELLO, A. & OMBRES, L. 2016. Numerical and analytical modeling of concrete beams with steel, FRP and hybrid FRP-steel reinforcements. Composite Structures, 140, 53-65.

BENMOKRANE, B. & TIGHIOUART, B. 1996. Bond strength and load distribution of composite GFRP reinforcing bars in concrete. Materials Journal, 93 (3), 254-259.

BISCHOFF, P. H. 2007. Deflection calculation of FRP reinforced concrete beams based on modifications to the existing Branson equation. *ASCE* Journal of Composites for Construction, 11 (1), 4-14.

BISCHOFF, P. H. & PAIXAO, R. 2004. Tension stiffening and cracking of concrete reinforced with glass fiber reinforced polymer (GFRP) bars. Canadian Journal of Civil Engineering, 31(4), 579-588.

BRANSON, D. E. 1977. Deformation of concrete structures, McGraw-Hill Companies. ISBN-13:978-0070072404.

Canadian Standards Association (CSA). 2002. “Design and construction of building components with fibre-reinforced polymers.” *CSA Standard S806-02*, Rexdale, Ont., Canada.

Canadian Standards Association (CSA). 2006. “Canadian Highway Bridge Design Code.” *CSA Standard S06-06*, Rexdale, Ont., Canada.

Canadian Standards Association (CSA). 2012. “Design and construction of building components with fibre-reinforced polymers.” CSA Standard S806-12, Rexdale, Ont., Canada.

CHEUNG, M. M. & TSANG, T. K. 2010. Behaviour of concrete beams reinforced with hybrid FRP composite rebar. Advances in Structural Engineering, 13(1), 81-93.

CUI, Y., CHEUNG, M. M., NORUZIAAN, B., LEE, S. & TAO, J. 2008. Development of ductile composite reinforcement bars for concrete structures. Materials and structures, 41 (9), 1509-1518.

EL-MOGY, M., EL-RAGABY, A. & EL-SALAKAWY, E. 2010. Flexural behavior of continuous FRP-reinforced concrete beams. *ASCE* Journal of Composites for Construction, 14 (6), 669-680.

EL-NEMR, A., AHMED, E. A. & BENMOKRANE, B. 2013. Flexural behavior and serviceability of normal-and high-strength concrete beams reinforced with glass fiber-reinforced polymer bars. ACI Structural Journal, 110 (6), 1077.

EL-SAYED, A. K., EL-SALAKAWY, E. F. & BENMOKRANE, B. 2006. Shear strength of FRP-reinforced concrete beams without transverse reinforcement. ACI Structural Journal, 103(2), 235.

EL REFAI, A., ABED, F. & AL-RAHMANI, A. 2015. Structural performance and serviceability of concrete beams reinforced with hybrid (GFRP and steel) bars. Construction and Building Materials, 96, 518-529.

ETMAN, E. E.-S. 2010. Innovative hybrid reinforcement for flexural members. *ASCE* Journal of Composites for Construction, 15(1), 2-8.

HABEEB, M. & ASHOUR, A. F. 2008. Flexural behavior of continuous GFRP reinforced concrete beams. *ASCE* Journal of Composites for Construction, 12(2), 115-124.

HARRIS, H. G., SOMBOONSONG, W. & KO, F. K. 1998. New ductile hybrid FRP reinforcing bar for concrete structures. *ASCE* Journal of composites for construction, 2 (1), 28-37.

HAWILEH, R. 2015. Finite element modeling of reinforced concrete beams with a hybrid combination of steel and aramid reinforcement. Materials & Design (1980-2015), 65, 831-839.

HOGNESTAD, E., HANSON, N. W. & MCHENRY, D., 1955 Concrete stress distribution in ultimate strength design. ACI Journal Proceedings, 52(12). 455-480.

HOLLAWAY, L. 2003. The evolution of and the way forward for advanced polymer composites in the civil infrastructure. Construction and Building Materials, 17(6-7), 365-378.

ISSA, M. S., METWALLY, I. M. & ELZEINY, S. M. 2011. Influence of fibers on flexural behavior and ductility of concrete beams reinforced with GFRP rebars. Engineering Structures, 33(5), 1754-1763.

KARA, I. F. & ASHOUR, A. F. 2012. Flexural performance of FRP reinforced concrete beams. Composite Structures, 94(5), 1616-1625.

KARA, I. F. & ASHOUR, A. F. 2013. Moment redistribution in continuous FRP reinforced concrete beams. Construction and Building Materials, 49, 939-948.

KARA, I. F., ASHOUR, A. F. & KÖROĞLU, M. A. 2015. Flexural behavior of hybrid FRP/steel reinforced concrete beams. Composite Structures, 129, 111-121.

KASSEM, C., FARGHALY, A. S. & BENMOKRANE, B. 2011. Evaluation of flexural behavior and serviceability performance of concrete beams reinforced with FRP bars. *ASCE* Journal of Composites for Construction, 15(5), 682-695.

LAU, D. & PAM, H. J. 2010. Experimental study of hybrid FRP reinforced concrete beams. Engineering Structures, 32(12), 3857-3865.

LEUNG, H. & BALENDRAN, R. 2003. Flexural behaviour of concrete beams internally reinforced with GFRP rods and steel rebars. Structural Survey, 21(4), 146-157.

LI, V. C. & WANG, S. 2002. Flexural behaviors of glass fiber-reinforced polymer (GFRP) reinforced engineered cementitious composite beams. Materials Journal, 99 (1), 11-21.

MAHMOUD, K. & EL-SALAKAWY, E. 2013. Shear strength of GFRP-reinforced concrete continuous beams with minimum transverse reinforcement. *ASCE* Journal of Composites for Construction, 18 (1), 04013018.

MAHROUG, M., ASHOUR, A. F. & LAM, D. 2014a. Experimental response and code modelling of continuous concrete slabs reinforced with BFRP bars. Composite Structures, 107, 664-674.

MAHROUG, M., ASHOUR, A. F. & LAM, D. 2014b. Tests of continuous concrete slabs reinforced with carbon fibre reinforced polymer bars. Composites Part B: Engineering, 66, 348-357.

MATOS, B., CORREIA, J. R., CASTRO, L. M. & FRANÇA, P. 2012. Structural response of hyperstatic concrete beams reinforced with GFRP bars: Effect of increasing concrete confinement. Composite Structures, 94 (3), 1200-1210.

NAAMAN, A. & JEONG, S. 1995,'Structural Ductility of Concrete Beams Prestressed with FRP Tendons,' Non-Metallic(FRP) Reinforcement for Concrete Structures, Proceedings of the Second International RILEM Symposium(FRPRCS-2), E & FN Spon, London.

NANNI, A., DE LUCA, A. & ZADEH, H. J. 2014. Reinforced concrete with FRP bars: mechanics and design, CRC Press. ISBN-13:978-0415778824.

NANNI, A., HENNEKE, M. J. & OKAMOTO, T. 1994. Tensile properties of hybrid rods for concrete reinforcement. Construction and Building Materials, 8(1), 27-34.

PANG, L., QU, W., ZHU, P. & XU, J. 2015. Design propositions for hybrid FRP-steel reinforced concrete beams. *ASCE* Journal of Composites for Construction, 20 (4), 04015086.

PARK, R. & PAULAY, T. 1975. Reinforced concrete structures, John Wiley & Sons.

QIN, R., ZHOU, A. & LAU, D. 2017. Effect of reinforcement ratio on the flexural performance of hybrid FRP reinforced concrete beams. Composites Part B: Engineering, 108, 200-209.

QU, W., ZHANG, X. & HUANG, H. 2009. Flexural behavior of concrete beams reinforced with hybrid (GFRP and steel) bars. *ASCE* Journal of Composites for construction, 13 (5), 350-359.

RAFI, M. M. & NADJAI, A. 2011. Behavior of hybrid (steel-CFRP) and CFRP bar-reinforced concrete beams in fire. Journal of Composite Materials, 45(15), 1573-1584.

RAHMAN, S. H., MAHMOUD, K. & EL-SALAKAWY, E. 2016. Behavior of Glass Fiber–Reinforced Polymer Reinforced Concrete Continuous T-Beams. *ASCE* Journal of Composites for Construction, 21(2), 04016085.

RAZAQPUR, A. & MOSTOFINEJAD, D. 1999. Experimental study of shear behavior of continuous beams reinforced with carbon fiber reinforced polymer. Special Publication, 188, 169-178.

RAZAQPUR, A. G., SHEDID, M. & ISGOR, B. 2010. Shear strength of fiber-reinforced polymer reinforced concrete beams subject to unsymmetric loading. *ASCE* Journal of Composites for Construction, 15(4), 500-512.

SAFAN, M. A. 2013. Flexural Behavior and Design of Steel-GFRP Reinforced Concrete Beams. ACI Materials Journal, 110(6). 677-686.

SAIKIA, B., THOMAS, J., RAMASWAMY, A. & RAO, K. N. 2005. Performance of hybrid rebars as longitudinal reinforcement in normal strength concrete. Materials and structures, 38(10), 857-864.

SANTOS, P., LARANJA, G., FRANÇA, P. M. & CORREIA, J. R. 2013. Ductility and moment redistribution capacity of multi-span T-section concrete beams reinforced with GFRP bars. Construction and Building Materials, 49, 949-961.

SHARAKY, I. A., TORRES, L., COMAS, J. & BARRIS, C. 2014. Flexural response of reinforced concrete (RC) beams strengthened with near surface mounted (NSM) fibre reinforced polymer (FRP) bars. Composite Structures, 109, 8-22.

SHARAKY, I. A., TORRES, L. & SALLAM, H. 2015. Experimental and analytical investigation into the flexural performance of RC beams with partially and fully bonded NSM FRP bars/strips. Composite structures, 122, 113-126.

SI-LARBI, A., FERRIER, E. & HAMELIN, P. 2006. Flexural behaviour of MRBC beams (multi-reinforcing bars concrete beams), promoting the use of FRHPC. Composite structures, 74(2), 163-174.

SOMBOONSONG, W., KO, F. K. & HARRIS, H. G. 1998. Ductile hybrid fiber reinforced plastic reinforcing bar for concrete structures: design methodology. Materials Journal, 95(6), 655-666.

TAN, K., 1997 Behaviour of hybrid FRP-steel reinforced concrete beams. Proc., 3rd Int. Symposium, FRPRCS, 3, 487-494.

TEPFERS, R., TAMUŽS, V., APINIS, R., VILKS, U. & MODNIKS, J. 1996. Ductility of nonmetallic hybrid fiber composite reinforcement for concrete. Mechanics of composite materials, 32(2), 113-121.

THERIAULT, M. & BENMOKRANE, B. 1998. Effects of FRP reinforcement ratio and concrete strength on flexural behavior of concrete beams. *ASCE* Journal of composites for construction, 2(1), 7-16.

VIJAY, P. & GANGARAO, H. V. 2001. Bending behavior and deformability of glass fiber-reinforced polymer reinforced concrete members. Structural Journal, 98(6), 834-842.

WANG, H. & BELARBI, A. 2011. Ductility characteristics of fiber-reinforced-concrete beams reinforced with FRP rebars. Construction and Building Materials, 25(5), 2391-2401.

WU, Y.-F., JIANG, J.-F. & LIU, K. 2010a. Perforated SIFCON blocks–An extraordinarily ductile material ideal for use in compression yielding structural systems. Construction and Building Materials, 24(12), 2454-2465.

WU, Y.-F., ZHOU, Y.-W. & HE, X.-Q. 2010b. Performance-based optimal design of compression-yielding FRP-reinforced concrete beams. Composite Structures, 93(1), 113-123.

YINGHAO, L. & YONG, Y. 2013. Arrangement of hybrid rebars on flexural behavior of HSC beams. Composites Part B: Engineering, 45(1), 22-31.

YOON, Y. S., YANG, J. M., MIN, K. H. & SHIN, H. O. Flexural strength and deflection characteristics of high-strength concrete beams with hybrid FRP and steel bar reinforcement. 10th International Symposium on Fiber-Reinforced Polymer Reinforcement for Concrete Structures 2011, FRPRCS-10, in conjunction with the ACI Spring 2011 Convention, 2011.

ZHOU, Y., WU, Y., TENG, J. & LEUNG, A. 2009. Ductility analysis of compression-yielding FRP-reinforced composite beams. Cement and Concrete Composites, 31(9), 682-691.

ZOU, P. X. 2003. Flexural behavior and deformability of fiber reinforced polymer prestressed concrete beams. *ASCE* Journal of composites for Construction, 7(4), 275-284.

APPENDIX A

Interval halving (bisection) method

The developed numerical technique sets three limits for the neutral axis depth, upper limit, x_1(=0), average limit, $x_2(=\frac{h}{2})$, and lower limit, x_1(=h) as shown in Figures A.1 and A.2. This technique calculates both compressive and tensile forces, and then these values will be compared. According to the results of the comparison, one of the cases will be taken as bellow:

Case 1: Total Compressive Force, $F_C >$ Total Tensile Force, F_T

In such case the neutral axis depth is overestimated and is required to be declined according to decrease the value of the compressive force of the section. To decrease the natural axis depth the upper limit, x_1 remains unchanged and the new neutral axis depth is $x_2 = (x_1 + x_2)/2$ but the lower limit x_3 moves to the old position of the neutral axis (see Figure A.1)

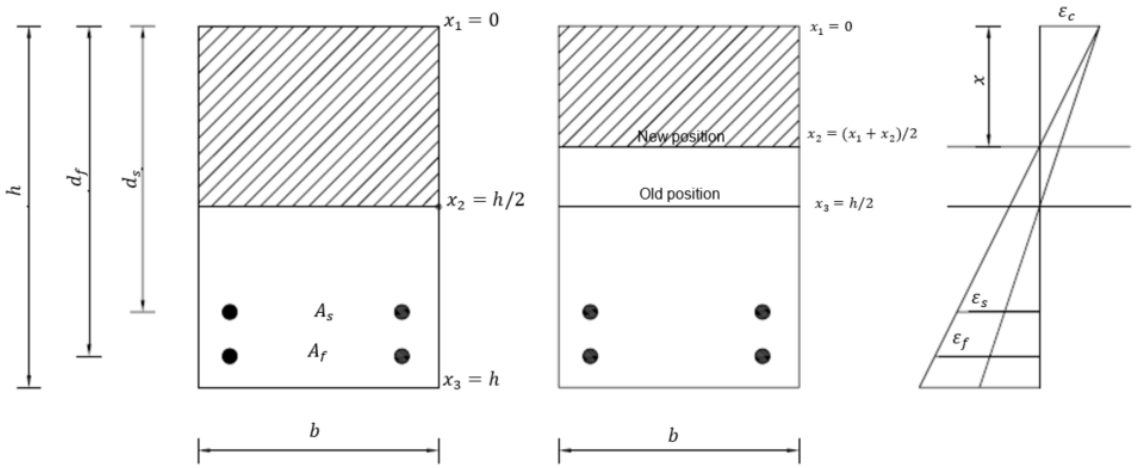

Figure A.1 Bi-section method for adjusting the neutral axis depth in case of $F_C > F_T$

Case 1: Total Compressive Force, $F_C <$ Total Tensile Force, F_T

The neutral axis depth is underestimated and is required to be increased according the value of the compressive force of the examined section to achieve the equilibrium condition of the internal force. In such case the new neutral axis depth x_2 is the average of the previous neutral axis depth and the lower limit x_3;($x_2 = (x_2 + x_3)/2$). The upper limit x_1 moves to the previous position of the neutral axis where the lower limit remains in the same position (see Figure A.2).

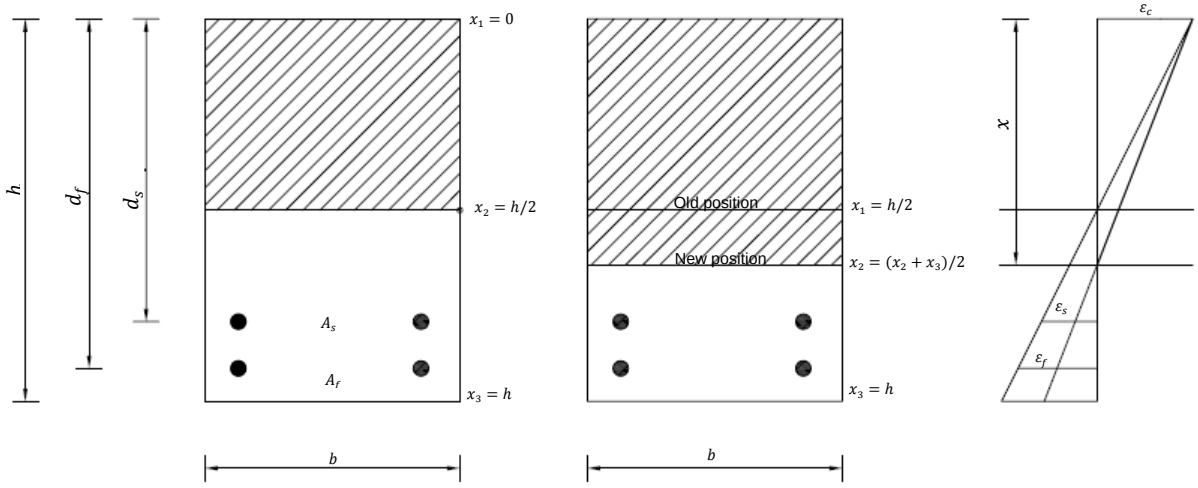

Figure A.2 Bi-section method for adjusting the neutral axis depth in case of $F_T > F_C$